Supporting Information

Light-Induced Conformational Variability Enabling [2+2] Cycloaddition Beyond Schmidt's Criteria: Unlocking New Horizons for Photomechanical Molecular Crystals

Jiangbin Zhong, Jingbo Sun, Tingting Feng, Liping Zhou, Chao Chen, Xiqiao Yang, Kaiqi Ye, Ran Lu*

State Key Laboratory of Supramolecular Structure and Materials, College of Chemistry, Jilin University, Changchun, 130012, P. R. China

E-mail: luran@mail.jlu.edu.cn

Video S1: Photoinduced bending, peeling, cracking of the ribbon-like crystal of **35ClSPyL**.

Video S2 Photoinduced bending, peeling, wriggling and unbending of needle-like crystal of 3**5ClSPyL**.

Video S3 Photosalient behavior of needle-like crystal of **35ClSPyL**.

Video S4: Photoinduced cracking of the ribbon-like crystal of **35BrSPyL**.

Video S5: Photoinduced exfoliation and cracking of the bulk crystal of **35FSPyL**.

Video S6: Photoinduced exfoliation and cracking of the bulk crystal of **2FSPyL**.

Video S7: Photoinduced jumping of the rod-like crystal of **3FSPyL**.

Video S8: Photoinduced breaking of the rod-like crystal of **2ClSPyL**.

1. Materials and General Methods

The solvents and reagents were commercially available and used as received without further purification. 2-Fluorobenzaldehyde (98%), 3-fluorobenzaldehyde (98%), 4-fluorobenzaldehyde (98%), 2-chlorobenzaldehyde (99%), 3-chlorobenzaldehyde (97%), 4-chlorobenzaldehyde (97%), 2-bromobenzaldehyde (98%), 3-bromobenzaldehyde (97%), 4-bromobenzaldehyde (98%), 2,4-difluorobenzaldehyde (98%), 2,4-dichlorobenzaldehyde (98%), 2,4-dibromobenzaldehyde (98%), 3,5-difluorobenzaldehyde (98%), 3,5-dichlorobenzaldehyde (98%), 3,5-dibromobenzaldehyde (97%), 3,4,5-trifluorobenzaldehyde (98%), benzaldehyde (99%), pivaloyl chloride (98%), 2-chloro-2-methylpropane (99%), tin tetrachloride (99%) and tetrafluoroboric acid (48 wt. % in H_2O) were purchased from *Energy Chemical*. 2,6-Di-*tert*-butyl-4-methylpyrylium tetrafluoroborate was prepared by a modified procedure reported by Lange and Balaban.[1-2]

^{1}H NMR (400 MHz) and ^{13}C NMR (100 MHz) spectra were recorded on *Bruker-Avance* III spectrometer and using $CDCl_3$, DMSO-d_6, TFA-*d* as solvents. The chemical shifts for references in ^{1}H NMR spectra: 7.26 ppm for $CDCl_3$, 2.50 ppm for DMSO-d_6, and 11.50 ppm for TFA-*d*. The chemical shifts for references in ^{13}C NMR spectra: 77.16 ppm for $CDCl_3$, 40.00 ppm for DMSO-d_6. The data were processed with Mestrenova suite of software program. High resolution mass spectra (HRMS) were measured on an Agilent 1290 Infinity LC system coupled with Bruker micro TOF QII mass spectrometer. FT-IR spectra were obtained with a Nicolet-360 FT-IR spectrometer by the incorporation of samples into KBr disks. The UV-vis absorption spectra were obtained by using a Shimadzu UV-2700 spectrophotometer. Powder X-Ray Diffraction (PXRD) patterns were obtained on Empyrean XRD equipped with graphite monochromatized Cu-Kα radiation (λ =1.5418 Å), employing a scanning rate of 0.00267 $^o \cdot s^{-1}$ in the 2θ range of 5º-40º. The samples were coated on wafers for PXRD measurements. The single crystal X-ray diffraction (SCXRD) was measured on a Rigaku RAXIS-RAPID diffractometer using graphite-monochromated MoKα radiation (λ = 0.71073 Å), and the crystals were kept at 100 K during data collection. And the

structures were solved by the direct methods and refined on F2 by full-matrix least-square using the SHELXTL-97 program.[3] The structure models were examined and confirmed to be correct. The structure data were examined by PLATON and the symmetries of the structures were confirmed to be correct and their space groups were proved to be correct. The crystals of **35FSPyL**, **3FSPyL**, **35ClSPyL**, **35BrSPyL**, **2BrSPyL**, **4BrSPyL**, **3ClSPyL**, **3BrSPyL**, **4FSPyL**, **24FSPyL**, **345FSPyL** and **SPyL** were obtained by slow evaporation from the solutions in the mixed solvents of dichloromethane and petroleum ether (V/V = 1/2) and the crystals of **4ClSPyL**, **2ClSPyL** and **2FSPyL** were recrystallized from acetic acid (Tables S1-S4). The morphologies were simulated by Bravais-Friedel Donnay-Harker (BFDH) method on Mercury software.[4] The Hirshfeld surfaces and atomic contacts contributions were calculated using *CrystalExplorer* software.[5]

2. Synthesis and Characterizations

(*E*)-2,6-di-*tert*-butyl-4-styrylpyrylium tetrafluoroborate (**SPyL**)

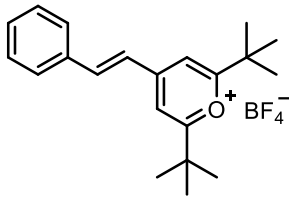

According to the literatures,[1-2] 2,6-Di-*tert*-butyl-4-methylpyrylium tetrafluoroborate (882 mg, 3.0 mmol) and benzaldehyde (382 mg, 3.6 mmol) were condensed to synthesize **SPyL**, which was obtained as ribbon-like yellow crystals (920 mg, 80%). m.p.: 230.0−231.2 ℃. ^{1}H NMR (400 MHz, $CDCl_3$) δ (ppm) 8.32 (d, *J* = 16.0 Hz, 1H), 7.92 (s, 2H), 7.88 (d, *J* = 7.2 Hz, 2H), 7.48 (d, *J* = 16.3 Hz, 1H), 7.43 – 7.37 (m, 3H), 1.51 (s, 18H) (Figure S36). ^{13}C NMR (100 MHz, $CDCl_3$) δ (ppm) 184.26, 165.65, 151.58, 134.59, 132.59, 130.65, 129.15, 123.37, 114.24, 38.71, 28.10 (Figure S37). FT-IR (KBr, cm^{-1}) 1638, 1603, 1596, 1588, 1572, 1521, 1449, 1412, 1371, 1347, 1316, 1285, 1242, 1213, 1204, 1192, 1099, 1058, 1052, 986, 945, 904, 874, 763, 751, 691, 531, 485. HRMS (ESI), m/z of $C_{21}H_{27}O^+$ calcd.: 295.2056, found: 295.2051 $[M]^+$ (Figure S38).

(*E*)-2,6-di-*tert*-butyl-4-(2-fluorostyryl)pyrylium tetrafluoroborate (**2FSPyL**)

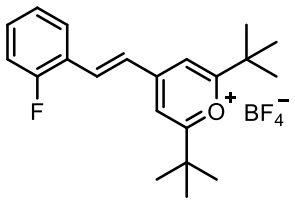

The condensation of 2,6-di-*tert*-butyl-4-methylpyrylium tetrafluoroborate (882 mg, 3.0 mmol) and 2-fluorobenzaldehyde (446 mg, 3.6 mmol) afforded **2FSPyL** (yellow crystals, 1.20 g, ~100%). m.p.: 209.1−210.2 ℃. ^{1}H NMR (400 MHz, DMSO-d_6) δ (ppm) 8.59 (d, *J* = 16.3 Hz, 1H), 8.36 (s, 2H), 7.95 (t, *J* = 7.6 Hz, 1H), 7.74 (d, *J* = 16.3 Hz, 1H), 7.65 (q, *J* = 7.0 Hz, 1H), 7.44 (td, *J* = 8.4 Hz, 3.6 Hz, 2H), 1.49 (s, 18H) (Figure S39). ^{13}C NMR (100 MHz, DMSO-d_6) δ (ppm) 185.31, 164.56, 161.78 (d, *J* = 255.3 Hz), 141.44, 134.80 (d, *J* = 9.1 Hz), 130.75, 126.72 (d, *J* = 6.9 Hz), 125.99, 123.01 (d, *J* = 11.4 Hz), 117.18 (d, *J* = 21.4 Hz), 115.56, 39.05, 28.21 (Figure S40). FT-IR (KBr, cm^{-1}) 1638, 1602, 1522, 1217, 1119, 1060, 979, 949, 888, 857, 796, 767, 637, 574, 548, 520. HRMS (ESI): m/z of $C_{21}H_{26}FO^+$ calcd.: 313.1968, found: 313.1956 $[M]^+$ (Figure S41).

(*E*)-2,6-di-*tert*-butyl-4-(2-chlorostyryl)pyrylium tetrafluoroborate (**2ClSPyL**)

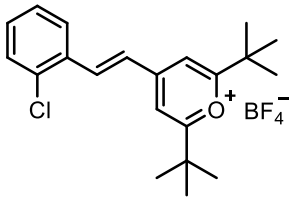

2,6-Di-*tert*-butyl-4-methylpyrylium tetrafluoroborate (588 mg, 2.0 mmol) and 2-chlorobenzaldehyde (338 mg, 2.4 mmol) were condensed to synthesize **2ClSPyL**, which was obtained as block yellow crystals (750 mg, 90%). m.p.: 200.5−202.2 ℃. ^{1}H NMR (400 MHz, $CDCl_3$) δ (ppm) 8.33 (d, *J* = 16.2 Hz, 1H), 8.11 (d, *J* = 6.6 Hz, 1H), 7.98 (s, 2H), 7.71 (d, *J* = 16.1 Hz, 1H), 7.41 – 7.33 (m, 3H), 1.54 (s, 18H) (Figure S42). ^{13}C NMR (100 MHz, $CDCl_3$) δ (ppm) 185.31, 165.36, 144.08 (d, *J* = 11.7 Hz), 136.23, 133.41 (d, *J* = 11.5 Hz), 132.01, 130.18, 129.95 (d, *J* = 11.6 Hz), 128.10 (d, *J* = 12.3 Hz), 126.03, 114.79, 38.92, 28.16 (Figure S43). FT-IR (KBr, cm^{-1}) 1636, 1601, 1523, 1465, 1443, 1369, 1329, 1292, 1239, 1203, 1122, 1054, 979, 948, 764, 712, 541, 519. HRMS (ESI): m/z of $C_{21}H_{26}ClO^+$ calcd.: 329.1672, found: 329.1665 $[M]^+$ (Figure S44).

(*E*)-2,6-di-*tert*-butyl-4-(2-bromostyryl)pyrylium tetrafluoroborate (**2BrSPyL**)

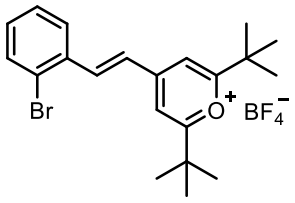

2,6-Di-*tert*-butyl-4-methylpyrylium tetrafluoroborate (588 mg, 2.0 mmol) and 2-bromobenzaldehyde (444 mg, 2.4 mmol) were condensed to synthesize **2BrSPyL**, which was obtained as sheet-like yellow crystals (811 mg, 88%). m.p.: 185.1−186.5 ℃. ^{1}H NMR (400 MHz, $CDCl_3$) δ (ppm) 8.30 (dd, *J* = 16.2, 3.8 Hz, 1H), 8.15 (t, *J* = 7.3 Hz, 1H), 8.00 (d, *J* = 2.6 Hz, 2H), 7.77 – 7.70 (m, 1H), 7.62 (ddd, *J* = 7.6, 5.4, 1.9 Hz, 1H), 7.45 (q, *J* = 7.3 Hz, 1H), 7.35 – 7.30 (m, 1H), 1.55 (d, *J* = 2.2 Hz, 18H) (Figure S45). ^{13}C NMR (100 MHz, $CDCl_3$ δ (ppm) 185.35, 165.32, 146.66, 133.59, 133.50, 130.08, 128.69, 127.01, 126.24, 114.80, 38.92, 28.15 (Figure S46). FT-IR (KBr, cm^{-1}) 1636, 1609, 1561, 1527, 1463, 1440, 1432, 1369, 1336, 1260, 1241, 1200, 1119, 1095, 1054, 1031, 970, 951, 911, 849, 770, 688, 540. HRMS (ESI): m/z of $C_{21}H_{26}BrO^+$ calcd.: 373.1162, found: 373.1176 $[M]^+$ (Figure S47).

(*E*)-2,6-di-*tert*-butyl-4-(3-fluorostyryl)pyrylium tetrafluoroborate (**3FSPyL**)

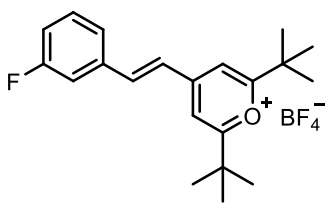

2,6-Di-*tert*-butyl-4-methylpyrylium tetrafluoroborate (588 mg, 2.0 mmol) and 3-fluorobenzaldehyde (298 mg, 2.4 mmol) were condensed to synthesize **3FSPyL**, which was obtained as needle-like yellow crystals (764 mg, 95%). m.p.:

213.2−214.5 °C. ^{1}H NMR (400 MHz, $CDCl_3$) δ (ppm) 8.25 (d, *J* = 16.1 Hz, 1H), 8.00 (s, 2H), 7.63 (d, *J* = 7.9 Hz, 1H), 7.51 (d, *J* = 9.5 Hz, 1H), 7.42 (d, *J* = 16.1 Hz, 1H), 7.33 – 7.29 (m, 1H), 7.01 (td, *J* = 8.3, 2.0 Hz, 1H), 1.50 (s, 18H) (Figure S48). ^{13}C NMR (100 MHz, $CDCl_3$) δ (ppm) 184.94, 165.45, 162.67 (d, *J* = 247.3 Hz), 149.58, 136.62, 130.86 (d, *J* = 7.3 Hz), 126.62, 124.44, 119.12 (d, *J* = 21.2 Hz), 116.24 (d, *J* = 22.0 Hz), 114.65, 38.87, 28.13 (Figure S49). FT-IR (KBr, cm^{-1}) 1611, 1606, 1580, 1523, 1484, 1448, 1371, 1328, 1285, 1267, 1241, 1213, 1156, 1114, 1055, 999, 972, 949, 917, 881, 793, 683, 533, 519. HRMS (ESI): m/z of $C_{21}H_{26}FO^+$ calcd.: 313.1968, found: 313.1935 $[M]^+$ (Figure S50).

(*E*)-2,6-di-*tert*-butyl-4-(3-chlorostyryl)pyrylium tetrafluoroborate (**3ClSPyL**)

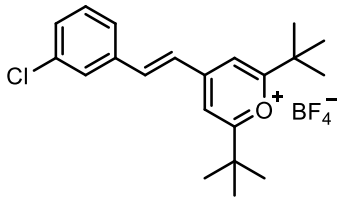

2,6-Di-*tert*-butyl-4-methylpyrylium tetrafluoroborate (588 mg, 2.0 mmol) and 3-chlorobenzaldehyde (338 mg, 2.4 mmol) were condensed to synthesize **3ClSPyL**, which was obtained as needle-like yellow crystals (743 mg, 89%). m.p.: 206.2−207.6 °C. ^{1}H NMR (400 MHz, $CDCl_3$) δ (ppm) 8.19 (d, *J* = 16.2 Hz, 1H), 7.97 (s, 2H), 7.76 – 7.71 (m, 2H), 7.37 – 7.32 (m, 3H), 1.53 (s, 18H) (Figure S51). ^{13}C NMR (100 MHz, $CDCl_3$) δ (ppm) 184.97, 165.30, 149.13, 136.24, 134.71, 132.10, 130.68, 129.84, 128.48, 124.29, 114.72, 38.89, 28.16 (Figure S52). FT-IR (KBr, cm^{-1}) 1639, 1604, 1562, 1524, 1474, 1460 ,1430 ,1369, 1331, 1240, 1203, 1117, 1057, 1035, 991 ,984, 948, 904, 890, 799, 686, 532. HRMS (ESI): m/z of $C_{21}H_{26}ClO^+$ calcd.: 329.1672, found: 329.1657 $[M]^+$ (Figure S53).

(*E*)-2,6-di-*tert*-butyl-4-(3-bromostyryl)pyrylium tetrafluoroborate (**3BrSPyL**)

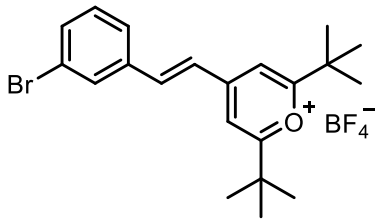

2,6-Di-*tert*-butyl-4-methylpyrylium tetrafluoroborate (588 mg, 2.0 mmol) and 3-bromobenzaldehyde (444 mg, 2.4 mmol) were condensed to synthesize **3BrSPyL**, which was obtained as sheet-like green crystals (831 mg, 90%). m.p.: 190.1−192.2 °C. ^{1}H NMR (400 MHz, $CDCl_3$) δ (ppm) 8.17 (d, *J* = 16.1 Hz, 1H), 8.00 (s, 2H), 7.85 (s, 1H), 7.75 (t, *J* = 6.8 Hz, 1H), 7.45 (t, *J* = 6.1 Hz, 1H), 7.33 (d, *J* = 16.1 Hz, 1H), 7.24 (q, *J* = 7.8 Hz, 1H), 1.52 (d, *J* = 4.0 Hz, 18H) (Figure S54). ^{13}C NMR (100 MHz, $CDCl_3$) δ (ppm) 184.96, 165.27, 148.92, 136.55, 134.96,

132.81, 130.90, 128.77, 124.29, 122.83, 114.78 (d, J = 2.3 Hz), 38.88, 28.17 (Figure S55). FT-IR (KBr, cm^{-1}) 1638, 1589, 1562, 1522, 1463, 1430, 1368, 1335, 1301, 1244, 1216, 1201, 1112, 1046, 992, 976, 948, 908, 887, 797, 687, 532. HRMS (ESI): m/z of $C_{21}H_{26}BrO^+$ calcd.: 373.1167, found: 373.1173 $[M]^+$ (Figure S56).

(*E*)-2,6-Di-*tert*-butyl-4-(4-fluorostyryl)pyrylium tetrafluoroborate (**4FSPyL**)

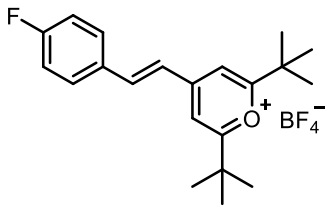

2,6-Di-*tert*-butyl-4-methylpyrylium tetrafluoroborate (588 mg, 2.0 mmol) and 4-fluorobenzaldehyde (298 mg, 2.4 mmol) were condensed to synthesize **4FSPyL**, which was obtained as sheet-like yellow crystals (799 mg, ~100 %). m.p.: 247.3−248.5 °C. ^{1}H NMR (400 MHz, $CDCl_3$) δ (ppm) 8.30 (d, J = 16.1 Hz, 1H), 7.95 – 7.90 (m, 4H), 7.38 (d, J = 16.1 Hz, 1H), 6.98 (t, J = 8.5 Hz, 2H), 1.50 (s, 18H) (Figure S57). ^{13}C NMR (100 MHz, $CDCl_3$) δ (ppm) 184.22, 165.53, 150.41, 133.25 (d, J = 9.1 Hz), 131.03 (d, J = 3.1 Hz), 122.97, 116.53, 116.31, 114.03, 38.73, 28.11 (Figure S58). FT-IR (KBr, cm^{-1}) 1638, 1607, 1582, 1522, 1510, 1457, 1424, 1371, 1345, 1333, 1308, 1239, 1217, 1201, 1163, 1109, 1095, 1057, 997, 947, 905, 876, 837, 515, 493. HRMS (ESI): m/z of $C_{21}H_{26}FO^+$ calcd.: 313.1968, found: 313.1953 $[M]^+$ (Figure S59).

(*E*)-2,6-di-*tert*-butyl-4-(4-chlorostyryl)pyrylium tetrafluoroborate (**4ClSPyL**)

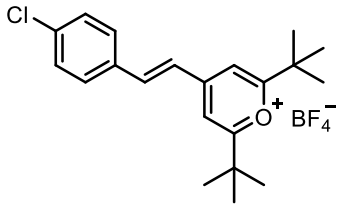

2,6-Di-*tert*-butyl-4-methylpyrylium tetrafluoroborate (588 mg, 2.0 mmol) and 4-chlorobenzaldehyde (338 mg, 2.4 mmol) were condensed to synthesize **4ClSPyL**, which was obtained as needle-like yellow-green crystals (792 mg, 91%). m.p.: 212.8−214.5 °C. ^{1}H NMR (400 MHz, $CDCl_3$) δ (ppm) 8.23 (d, J = 16.0 Hz, 1H), 7.90 (s, 2H), 7.84 (d, J = 8.3 Hz, 2H), 7.39 (d, J = 16.0 Hz, 1H), 7.27 (d, J = 8.4 Hz, 2H), 1.51 (s, 18H) (Figure S60). ^{13}C NMR (100 MHz, $CDCl_3$) δ (ppm) 184.50, 165.37, 150.05, 138.57, 133.06, 132.00, 129.48, 123.65, 114.23, 38.80, 28.18 (Figure S61). FT-IR (KBr, cm^{-1}) 1638, 1605, 1585, 1563, 1524, 1491, 1462, 1419, 1404, 1368, 1341, 1308, 1242, 1203, 1119, 1086, 1058, 1037, 983, 948, 908, 868, 820, 498. HRMS (ESI): m/z of $C_{21}H_{26}ClO^+$ calcd.: 329.1672, found: 329.1662 $[M]^+$ (Figure S62).

(*E*)-2,6-di-*tert*-butyl-4-(4-bromostyryl)pyrylium tetrafluoroborate (**4BrSPyL**)

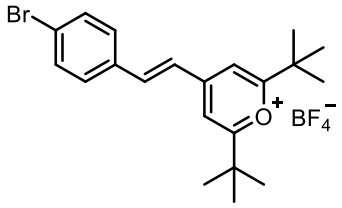

2,6-Di-*tert*-butyl-4-methylpyrylium tetrafluoroborate (588 mg, 2.0 mmol) and 4-bromobenzaldehyde (444 mg, 2.4 mmol) were condensed to synthesize **4BrSPyL**, which was obtained as sheet-like yellow crystals (763 mg, 82%). m.p.: 209.1−210.3 ℃. ^{1}H NMR (400 MHz, $CDCl_3$) δ (ppm) 8.25 (d, *J* = 16.0 Hz, 1H), 7.93 (s, 2H), 7.76 (d, *J* = 8.2 Hz, 2H), 7.45 – 7.40 (m, 3H), 1.51 (s, 18H) (Figure S63). ^{13}C NMR (100 MHz, $CDCl_3$) δ (ppm) 184.59, 165.36, 150.05, 133.43, 132.47, 132.02, 127.40, 123.73, 114.30, 38.82, 28.19 (Figure S64). FT-IR (KBr, cm^{-1}) 3068, 2973, 1639, 1606, 1580, 1561, 1523, 1486, 1461, 1338, 1119, 1070, 1054, 1034, 1007, 984, 948, 516, 494. HRMS (ESI): m/z of $C_{21}H_{26}BrO^+$ calcd.: 373.1167, found: 373.1162 $[M]^+$ (Figure S65).

(*E*)-2,6-di-tert-butyl-4-(2,4-difluorostyryl)pyrylium tetrafluoroborate (**24FSPyL**)

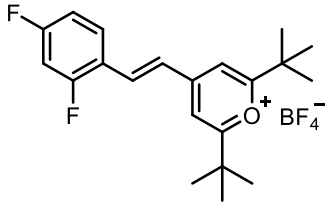

2,6-Di-*tert*-butyl-4-methylpyrylium tetrafluoroborate (588 mg, 2.0 mmol) and 2,4-difluoro benzaldehyde (341 mg, 2.4 mmol) were condensed to synthesize **24FSPyL**, which was obtained as sheet-like yellow crystals (802 mg, 96%). m.p.: 190.2−192.4 ℃. ^{1}H NMR (400 MHz, $CDCl_3$) δ (ppm) 8.22 (dd, *J* = 16.3, 2.9 Hz, 1H), 8.10 (dtd, *J* = 14.8, 8.6, 6.3 Hz, 1H), 7.95 (d, *J* = 3.4 Hz, 2H), 7.58 (dd, *J* = 16.2, 8.5 Hz, 1H), 7.02 – 6.94 (m, 1H), 6.84 (ddt, *J* = 10.6, 8.5, 2.2 Hz, 1H), 1.52 (d, *J* = 4.8 Hz, 18H) (Figure S66). ^{13}C NMR (100 MHz, $CDCl_3$) δ (ppm)185.09, 165.59, 161.31, 141.78 (d, *J* = 6.7 Hz), 133.53 (d, *J* = 9.9 Hz), 125.13 (d, *J* = 5.5 Hz), 119.23 (d, *J* = 11.0 Hz), 114.50, 113.19 (d, *J* = 18.6 Hz), 104.58 (t, *J* = 25.7 Hz), 38.89, 28.13 (d, *J* = 3.1 Hz) (Figure S67). FT-IR (KBr, cm^{-1}) 1635, 1598, 1522, 1501, 1461, 1433, 1371, 1344, 1327, 1293, 1276, 1257, 1242, 1220, 1140, 1114, 1077, 1048, 4034, 982, 970, 945, 856, 518, 488. HRMS (ESI): m/z of $C_{21}H_{25}F_2O^+$ calcd.: 331.1873, found: 331.1865 $[M]^+$ (Figure S68).

(*E*)-2,6-di-tert-butyl-4-(2,4-dichlorostyryl)pyrylium tetrafluoroborate (**24ClSPyL**)

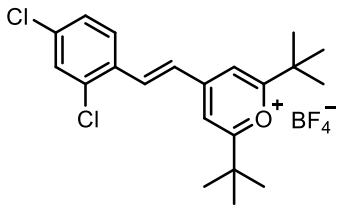

2,6-Di-*tert*-butyl-4-methylpyrylium tetrafluoroborate (588 mg, 2.0 mmol) and 2,4-dichloro benzaldehyde (420 mg, 2.4 mmol) were condensed to synthesize **24ClSPyL**, which was obtained as cluster-like yellow crystals (703 mg, 78%). m.p.: 213.3−215.7 °C. ^{1}H NMR (400 MHz, $CDCl_3$) δ (ppm) 8.24 (d, *J* = 16.2 Hz, 1H), 8.11 (d, *J* = 8.6 Hz, 1H), 7.99 (s, 2H), 7.74 (d, *J* = 16.1 Hz, 1H), 7.42 (d, *J* = 2.1 Hz, 1H), 7.37 (dd, *J* = 8.6, 2.1 Hz, 1H), 1.54 (s, 18H) (Figure S69). ^{13}C NMR (100 MHz, $CDCl_3$) δ (ppm) 185.43, 165.24, 142.59, 138.96, 136.59, 130.78, 130.62, 129.99, 128.62, 126.47, 114.91, 38.96, 28.17 (Figure S70). FT-IR (KBr, cm^{-1}) 1636, 1612, 1581, 1528, 1470, 1386, 1369, 1339, 1324, 1239, 1200, 1138, 1100, 1051, 1036, 970, 950, 907, 861, 852, 821, 766, 627, 520. HRMS (ESI): m/z of $C_{21}H_{25}Cl_2O^+$ calcd.: 363.1282, found: 363.1290 $[M]^+$ (Figure S71).

(*E*)-2,6-di-tert-butyl-4-(2,4-dibromostyryl)pyrylium tetrafluoroborate (**24BrSPyL**)

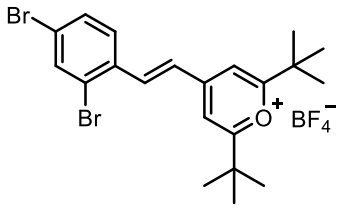

2,6-Di-*tert*-butyl-4-methylpyrylium tetrafluoroborate (588 mg, 2.0 mmol) and 2,4-dibromo benzaldehyde (633 mg, 2.4 mmol) were condensed to synthesize **24BrSPyL**, which was obtained as cluster-like tan crystals (0.78 g, 72 %). m.p.: 222.5−223.7 °C. ^{1}H NMR (400 MHz, $CDCl_3$) δ (ppm) 8.18 (d, *J* = 16.1 Hz, 1H), 8.03 (d, *J* = 8.5 Hz, 1H), 8.00 (s, 2H), 7.78 (d, *J* = 2.0 Hz, 1H), 7.74 (d, *J* = 16.1 Hz, 1H), 7.58 (dd, *J* = 8.5, 2.0 Hz, 1H), 1.55 (s, 18H) (Figure S72). ^{13}C NMR (100 MHz, $CDCl_3$) δ (ppm) 185.48, 165.13, 145.12, 135.84, 132.61, 132.01, 130.85, 127.25, 127.08, 126.73, 114.97, 38.95, 28.15 (Figure S73). FT-IR (KBr, cm^{-1}) 1637, 1612, 1572, 1528, 1482, 1464, 1370, 1338, 1324, 1200, 1054, 1035, 970, 951, 863, 852, 820, 725, 520. HRMS (ESI): m/z of $C_{21}H_{25}Br_2O^+$ calcd.: 453.0247 (100.0%), 451.0267 (51.4%), 455.0226 (48.6%), found: 453.0252, 451.0277, 455.0245 $[M]^+$ (Figure S74).

(*E*)-2,6-di-*tert*-butyl-4-(3,5-difluorostyryl)pyrylium tetrafluoroborate (**35FSPyL**).

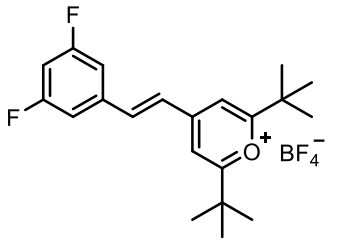

2,6-Di-*tert*-butyl-4-methylpyrylium tetrafluoroborate (1.47 g, 5.0 mmol) and 3,5-difluoro benzaldehyde (852 mg, 6.0 mmol) were condensed to synthesize **35FSPyL**, which was obtained as needle-like yellow crystals (1750 mg, 84%). m.p.: 190.2−192.4 ℃. ^{1}H NMR (400 MHz, DMSO-d_6) δ (ppm) 8.50 (d, J = 16.2 Hz, 1H), 8.23 (s, 2H), 7.79 (d, J = 16.2 Hz, 1H), 7.58 – 7.48 (m, 3H), 1.50 (s, 18H) (Figure S75). ^{13}C NMR (100 MHz, DMSO-d_6) δ (ppm) 185.66, 164.15, 163.24 (dd, J = 247.4, 13.6 Hz), 145.79, 138.65 (d, J = 9.9 Hz), 126.85, 115.59, 112.35 (dd, J = 18.9, 7.2 Hz), 107.72 (d, J = 26.0 Hz), 39.05, 28.15 (Figure S76). FT-IR (KBr, cm^{-1}) 1613, 1589, 1523, 1456, 1446, 1371, 1313, 1290, 1240, 1213, 1203, 1119, 1058, 997, 984, 948, 875, 677, 549, 521. HRMS (ESI): m/z of $C_{21}H_{25}F_2O^+$ calcd.: 331.1873, found: 331.1843 $[M]^+$ (Figure S77).

(*E*)-2,6-di-tert-butyl-4-(3,5-dichlorostyryl)pyrylium tetrafluoroborate (**35ClSPyL**)

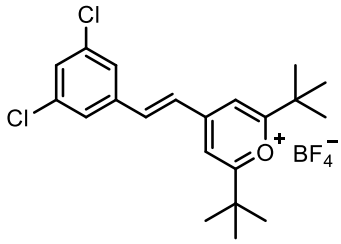

2,6-Di-*tert*-butyl-4-methylpyrylium tetrafluoroborate (588 mg, 2.0 mmol) and 3,5-dichloro benzaldehyde (420 mg, 2.4 mmol) were condensed to synthesize **35ClSPyL**, which was obtained as needle-like colorless crystals (723 mg, 80%). m.p.: 230.3−232.4 ℃. ^{1}H NMR (400 MHz, $CDCl_3$) δ (ppm) 8.13 (d, J = 16.1 Hz, 1H), 8.03 (s, 2H), 7.65 (s, 2H), 7.37 (d, J = 16.1 Hz, 1H), 7.32 (s, 1H), 1.52 (s, 18H) (Figure S78). ^{13}C NMR (100 MHz, $CDCl_3$) δ (ppm) 185.57, 165.03, 147.03, 137.30, 135.66, 131.37, 127.89, 125.48, 115.19, 38.99, 28.15 (Figure S79). FT-IR (KBr, cm^{-1}) 1636, 1619, 1613, 1560, 1524, 1481, 1462, 1428, 1405, 1369, 1331, 1243, 1207, 1120, 1054, 978, 950, 898, 882, 858, 799, 679, 536, 519. HRMS (ESI): m/z of $C_{21}H_{25}Cl_2O^+$ calcd.: 363.1277, found: 363.1274 $[M]^+$ (Figure S80).

(*E*)-2,6-di-tert-butyl-4-(3,5-dibromostyryl)pyrylium tetrafluoroborate (**35BrSPyL**)

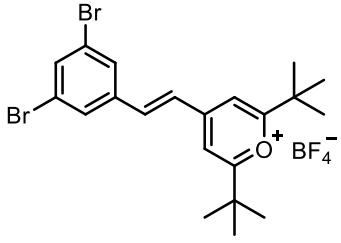

2,6-Di-*tert*-butyl-4-methylpyrylium tetrafluoroborate (588 mg, 2.0 mmol) and 3,5-dibromo benzaldehyde (633 mg, 2.4 mmol) were condensed to synthesize **35BrSPyL**, which was obtained as needle-like colorless crystals (830 mg, 77%). m.p.: 250.2−251.8 ℃. ^{1}H NMR (400 MHz,

$CDCl_3$) δ (ppm) 8.09 (d, *J* = 16.1 Hz, 1H), 8.02 (s, 2H), 7.82 (d, *J* = 1.8 Hz, 2H), 7.64 (t, *J* = 1.6 Hz, 1H), 7.33 (d, *J* = 16.1 Hz, 1H), 1.52 (s, 18H) (Figure S81).^{13}C NMR (100 MHz, $CDCl_3$) δ (ppm) 185.56, 164.90, 146.68, 137.79, 136.84, 131.11, 125.46, 123.56, 115.21, 38.99, 28.17 (Figure S82). FT-IR (KBr, cm^{-1}) 3073, 2972, 2934, 2910, 1640,1618, 1545, 1523, 1462, 1424, 1368, 1331, 1243, 1202, 1053, 1038, 950, 741, 679, 536, 521. HRMS (ESI): m/z of $C_{21}H_{25}Br_2O^+$ calcd.: 453.0247 (100.0%), 451.0267 (51.4%), 455.0226 (48.6%), found: 453.0249, 451.0256, 455.0219 $[M]^+$ (Figure S83).

(*E*)-2,6-di-*tert*-butyl-4-(3,4,5-trifluorostyryl)pyrylium tetrafluoroborate (**345FSPyL**).

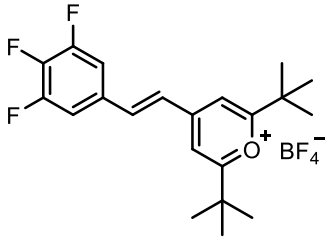

2,6-Di-*tert*-butyl-4-methylpyrylium tetrafluoroborate (294 mg, 1.0 mmol) and 3,4,5-trifluoro benzaldehyde (192 mg, 1.2 mmol) were condensed to synthesize **345FSPyL**, which was obtained as needle-like colorless crystals (380 mg, 88%). m.p.: 250.0−252.1 ℃. ^{1}H NMR (400 MHz, $CDCl_3$) δ (ppm) 8.20 (d, *J* = 16.1 Hz, 1H), 8.08 (s, 2H), 7.59 – 7.55 (m, 2H), 7.40 (d, *J* = 16.1 Hz, 1H), 1.53 (s, 18H) (Figure S84).^{13}C NMR (100 MHz, $CDCl_3$) δ (ppm) 185.51, 165.29, 152.35 (d, *J* = 9.2 Hz), 147.29, 145.05 (dd, *J* = 156.7, 10.8 Hz), 131.04, 125.19, 115.00, 114.35 (dd, *J* = 16.0, 6.0 Hz), 38.97, 28.06 (Figure S85). FT-IR (KBr, cm^{-1}) 1635, 1598, 1522, 1501, 1461, 1433, 1371, 1344, 1327, 1293, 1276, 1257, 1242, 1220, 1140, 1114, 1077, 1048, 4034, 982, 970, 945, 856, 518, 488. HRMS (ESI): m/z of $C_{21}H_{24}F_3O^+$ calcd.: 349.1774, found: 349.1766 $[M]^+$ (Figure S86).

Table S1. Single crystal data and structure refinement for **35FSPyL**, **3FSPyL**, **2FSPyL**, **4ClSPyL**, and **2ClSPyL**.

Compound	**35FSPyL**	**3FSPyL**	**2FSPyL**	**4ClSPyL**	**2ClSPyL**
Temperature/K	100.0	100.0	100.0	100.0	100.0
Formula	$C_{21}H_{25}BF_6O$	$C_{21}H_{26}BF_5O$	$C_{21}H_{26}BF_5O$	$C_{21}H_{26}BClF_4O$	$C_{21}H_{26}BClF_4O$
Formula weight	418.22	400.23	400.23	416.68	416.68
Crystal system	monoclinic	monoclinic	monoclinic	monoclinic	monoclinic
Space Group	$P2_1/n$	$P2_1/n$	$P2_1/n$	$C2/c$	$P2_1/c$
a/Å	7.4697(7)	7.4074(4)	10.0804(6)	31.7392(18)	24.306(11)
b/Å	16.1911(16)	16.1757(8)	13.3301(6)	7.4931(4)	13.401(6)
c/Å	17.1680(17)	17.1380(7)	15.6017(9)	24.0683(13)	21.057(10)
α/deg	90	90	90	90	90
β/deg	90.376(4)	91.048(2)	101.264(2)	126.419(2)	102.610(13)
γ/deg	90	90	90	90	90
Volume/Å^3	2076.3(3)	2053.13(17)	2056.06(19)	4606.1(4)	6693(5)
Z	4	4	4	8	12
ρ_{cal}, g/cm^3	1.338	1.295	1.293	1.323	1.240
μ/mm^{-1}	0.117	0.108	0.108	0.216	0.212
Final R indexes [I>=2σ(I)]	R_1 = 0.0708, wR_2 = 0.1712	R_1 = 0.0860, wR_2 = 0.1855	R_1 = 0.0507, wR_2 = 0.1229	R_1 = 0.0646, wR_2 = 0.1671	R_1 = 0.1146, wR_2 = 0.2634
Final R indexes [all data]	R_1 = 0.1645, wR_2 = 0.2332	R_1 = 0.1408, wR_2 = 0.2222	R_1 = 0.0664, wR_2 = 0.1353	R_1 = 0.0967, wR_2 = 0.1951	R_1 = 0.2399, wR_2 = 0.3238
GOF	1.010	1.058	1.020	1.049	1.209
CCDC	2290906	2295681	2290904	2402297	2401312

Table S2. Single crystal data and structure refinement for **35ClSPyL**, **35BrSPyL** and **2BrSPyL**.

Compound	**35ClSPyL**	**35BrSPyL**	**2BrSPyL**
Temperature/K	100.0	100.0	100.0
Formula	$C_{21}H_{25}BCl_2F_4O$	$C_{21}H_{25}BBr_2F_4O$	$C_{21}H_{26}BBrF_4O$
Formula weight	451.12	540.04	461.14
Crystal system	monoclinic	monoclinic	monoclinic
Space Group	$P2_1/c$	$P2_1/c$	$P2_1/c$
a/Å	15.0310(9)	15.3582(10)	19.8733(16)
b/Å	9.8440(5)	9.8242(6)	7.7437(5)
c/Å	16.3516(10)	16.3820(12)	14.9358(11)
α/deg	90	90	90
β/deg	113.798(2)	114.786(2)	103.698(3)
γ/deg	90	90	90
Volume/Å^3	2213.7(2)	2244.1(3)	2233.1(3)
Z	4	4	4
ρ_{cal}, g/cm^3	1.354	1.598	1.372
μ/mm^{-1}	0.336	3.654	1.881
Final R indexes [I>=2σ(I)]	R_1 = 0.0369, wR_2 = 0.0846	R_1 = 0.0443, wR_2 = 0.0612	R_1 = 0.0710, wR_2 = 0.1933
Final R indexes [all data]	R_1 = 0.0511, wR_2 = 0.0960	R_1 = 0.0921, wR_2 = 0.0721	R_1 = 0.1311, wR_2 = 0.2528
GOF	1.056	1.038	1.019
CCDC	2324900	2290907	2302956

Table S3. Single crystal data and structure refinement for **345FSPyL**, **SPyL**, **4FSPyL** and **24FSPyL**.

Compound	**345FPyL**	**SPyL**	**4FSPyL**	**24FSPyL**
Temperature/K	293.0	100.0	100.0	100.0
Formula	$C_{21}H_{24}BF_7O$	$C_{21}H_{27}BF_4O$	$C_{21}H_{26}BF_5O$	$C_{21}H_{25}BF_6O$
Formula weight	436.21	382.23	400.23	443.70
Crystal system	monoclinic	orthorhombic	orthorhombic	monoclinic
Space Group	$P2_1/c$	$Pca2_1$	$Pbcn$	$P2_1$
a/Å	10.9496(11)	16.5173(7)	17.8236(11)	10.4265(13)
b/Å	18.4711(16)	6.9163(3)	13.6056(10)	8.1911(10)
c/Å	12.0927(12)	17.8513(7)	16.7327(13)	14.0917(17)
α/deg	90	90	90	90
β/deg	112.412(4)	90	90	105.729(5)
γ/deg	90	90	90	90
Volume/Å^3	2261.0(4)	2039.31(15)	4057.7(5)	1158.4(2)
Z	4	4	8	2
ρ_{cal}, g/cm^3	1.281	1.245	1.310	1.272
μ/mm^{-1}	0.116	0.099	0.109	0.175
Final R indexes	R_1 = 0.0687	R_1 = 0.0978	R_1 = 0.0479	R_1 = 0.0857
[I>=2σ(I)]	wR_2 = 0.1981	wR_2 = 0.2396	wR_2 = 0.1153	wR_2 = 0.2451
Final R indexes	R_1 = 0.1163	R_1 = 0.1259	R_1 = 0.0649	R_1 = 0.1059
[all data]	wR_2 = 0.2510	R_2 = 0.2666	wR_2 = 0.1330	wR_2 = 0.2648
GOF	1.030	1.130	1.076	1.078
CCDC	2297922	2402170	2306168	2424335

Table S4. Single crystal data and structure refinement for **4BrSPyL**, **3BrSPyL** and **3ClSPyL**.

Compound	**4BrSPyL**	**3BrSPyL**	**3ClSPyL**
Temperature/K	100.0	100.0	100.0
Formula	$C_{21}H_{26}BBrF_4O$	$C_{21}H_{26}BBrF_4O$	$C_{21}H_{26}BClF_4O$
Formula weight	546.06	461.14	416.68
Crystal system	orthorhombic	monoclinic	monoclinic
Space Group	*Pna*2$_1$	*C*2/*c*	*P*2$_1$/*c*
a/Å	30.226(3)	15.1741(8)	11.5695(15)
b/Å	8.3975(10)	11.2448(8)	18.589(2)
c/Å	9.9918(12)	25.3113(16)	9.9750(13)
α/deg	90	90	90
β/deg	90	101.307(3)	90.750(5)
γ/deg	90	90	90
Volume/Å^3	2536.1(5)	4235.0(5)	2145.1(5)
Z	4	8	4
ρ_{cal}, g/cm^3	1.430	1.446	1.290
μ/mm^{-1}	1.872	1.984	0.220
Final R indexes	R_1 = 0.1403	R_1 = 0.0305	R_1 = 0.0933
[I>=2σ(I)]	wR_2 = 0.2660	wR_2 = 0.0746	wR_2 = 0.2653
Final R indexes	R_1 = 0.1997	R_1 = 0.0373	R_1 = 0.1443
[all data]	wR_2 = 0.2871	wR_2 = 0.0786	wR_2 = 0.3368
GOF	1.294	1.027	1.239
CCDC	2424342	2424341	2306167

Table S5. Geometric parameters for topological [2+2] cycloaddition in the crystals of **35FSPyL**, **35ClSPyL**, **35BrSPyL**, **2FSPyL**, **3FSPyL**, **2ClSPyL**, **345FSPyL**, **2BrSPyL 4FSPyL** and **3ClSPyL**.

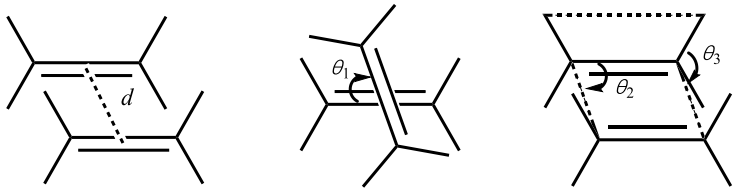

	d (Å)[a]	θ_1 (°)[b]	θ_2 (°)[c]	θ_3 (°)[d]
Ideal	< 4.2	0	90	90
35ClSPyL	5.224	0	96.76	56.63
35BrSPyL	5.328	0	97.65	55.52
35FSPyL	3.528	0	97.21	73.02
3FSPyL	3.513	0	96.36	71.02
2FSPyL	4.029	0	126.53	87.34
4ClSPyL	3.569	0	96.20	75.03
2ClSPyL	4.067	2.36	128.00, 119.23	88.56, 87.69 83.53, 82.79
2BrSPyL	5.200	0	139.04	67.87
345FSPyL[e]	7.077	0	155.94	82.77
4FSPyL[e]	6.816	45.86	—	—
4BrSPyL[e]	8.397	—	—	—
24FSPyL[e]	8.191	—	—	—
SPyL[e]	6.916	—	—	—
3ClSPyL[f]	—	—	—	—
3BrSPyL[f]	—	—	—	—

[a] The distance between the two parallel and reactive double bonds. [b] θ_1 corresponds to the rotational angle of one carbon-carbon double bond with respect to the other. [c] θ_2 corresponds to the obtuse angle of the parallelogram consisting four carbons in "olefin pair". [d] θ_3 corresponds to the dihedral angle between the parallelogram consisting four carbons in "olefin pair" and the plane consisting two carbon-carbon single bonds formed from the two substituted groups linked to one carbon on double bond. [e] The molecules in the crystal are "head-to-head" type in one-dimensional packing, where the distance between two parallel double bonds is far apart. [f] The molecules in the crystal are stacked in the spirally ascending and staggered one-dimensional columns, without parallel molecular pairs.

Table S6. Absorption bands of the synthesized styrylpyryliums in microcrystals.

Compound	λ_{Abs} (nm)			
SPyL	201	248	314	393
2FSPyL	203	—	319	385
2ClSPyL	202	—	318	395
2BrSPyL	208	—	319	390
3FSPyL	—	241	315	384
3ClSPyL	—	255	316	389
3BrSPyL	210	257	317	389
4FSPyL	—	251	313	393
4ClSPyL	—	246	315	396
4BrSPyL	—	250	315	396
24FSPyL	203	251	317	383
24ClSPyL	204	261	321	388
24BrSPyL	209	268	322	392
35FSPyL	202	238	318	377
35ClSPyL	217	258	319	384
35BrSPyL	219	264	318	383
345FSPyL	—	240	319	373

Table S7. Single crystal data and structure refinement for **35ClSPyL**-1 and **2ClSPyL**-10.

Compound	**35ClSPyL**-1	**2ClSPyL**-10
Temperature/K	100.0	100.0
Formula	$C_{21}H_{25}BCl_2F_4O$	$C_{21}H_{26}BClF_4O$
Formula weight	451.12	416.68
Crystal system	monoclinic	monoclinic
Space Group	$P2_1/c$	$P2_1/c$
a/Å	15.0364(13)	23.8119(16)
b/Å	9.8485(7)	13.2996(7)
c/Å	16.3609(14)	20.7673(14)
α/deg	90	90
β/deg	113.743(3)	103.488(2)
γ/deg	90	90
Volume/Å^3	2217.8(3)	6395.4(7)
Z	4	12
ρ_{cal}, g/cm^3	1.351	1.298
μ/mm^{-1}	0.335	0.222
Final R indexes [I>=2σ(I)]	R_1 = 0.0524,	R_1 = 0.1102,
	wR_2 = 0.1357	wR_2 = 0.2549
Final R indexes [all data]	R_1 = 0.0616,	R_1 = 0.1427,
	wR_2 = 0.1437	wR_2 = 0.2854
Goodness-of-fit on F^2	1.123	1.097
CCDC	2324901	2310518

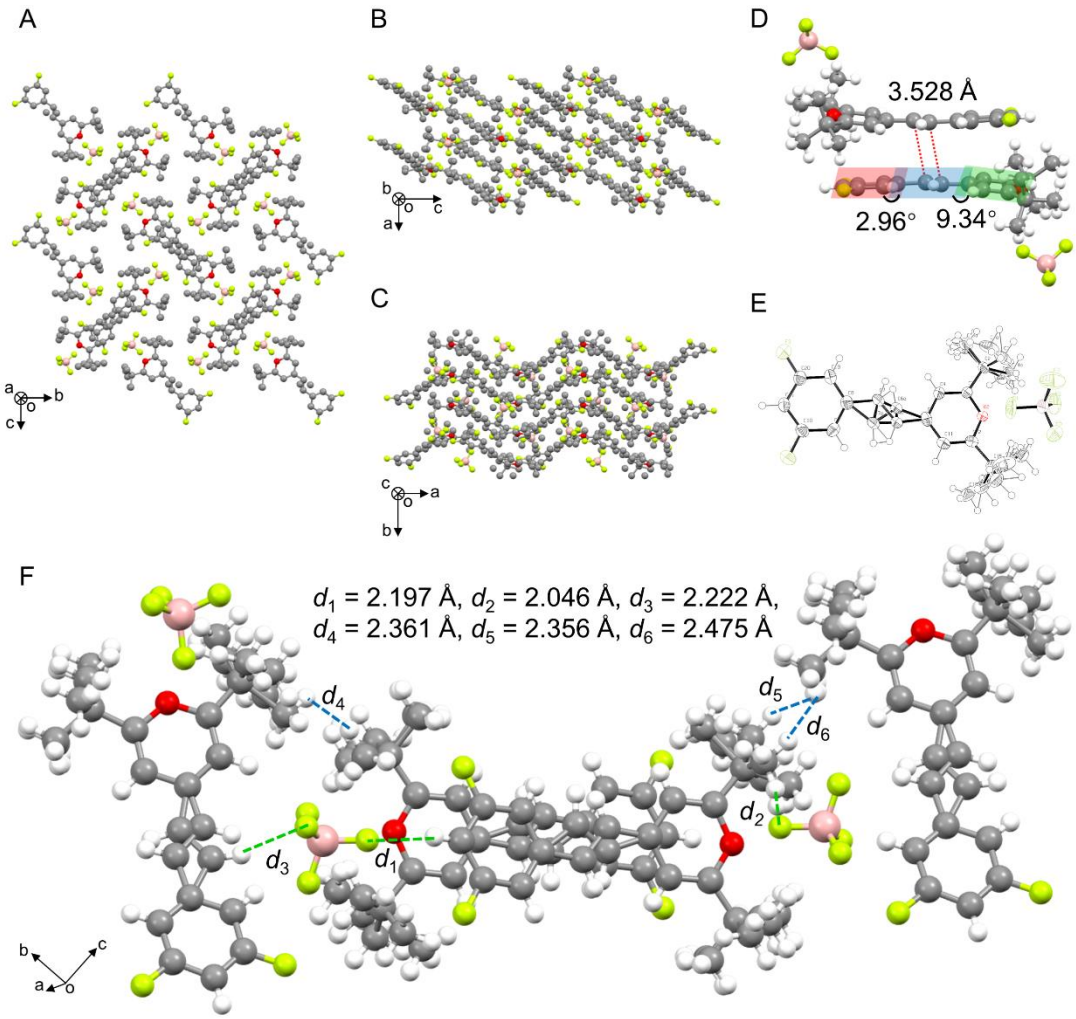

Figure S1. Molecular packing of **35FSPyL** in crystal viewed along the a-axis (A), the b-axis (B) and the c-axis (C) (hydrogen atoms are omitted for clarity); (D) The dihedral angle between phenyl and vinyl as well as that between pyrylium and vinyl, and the distance between the two double bonds in π-dimer; (E) Oak Ridge Thermal Ellipse Plots (ORTEP) of **35FSPyL** showing disorder around the vinyl group and *tert*-butyl groups; (F) Atomic distances representing the intermolecular C−H···F (d_1, d_2 and d_3) and C−H···H (d_4, d_5 and d_6) interactions.

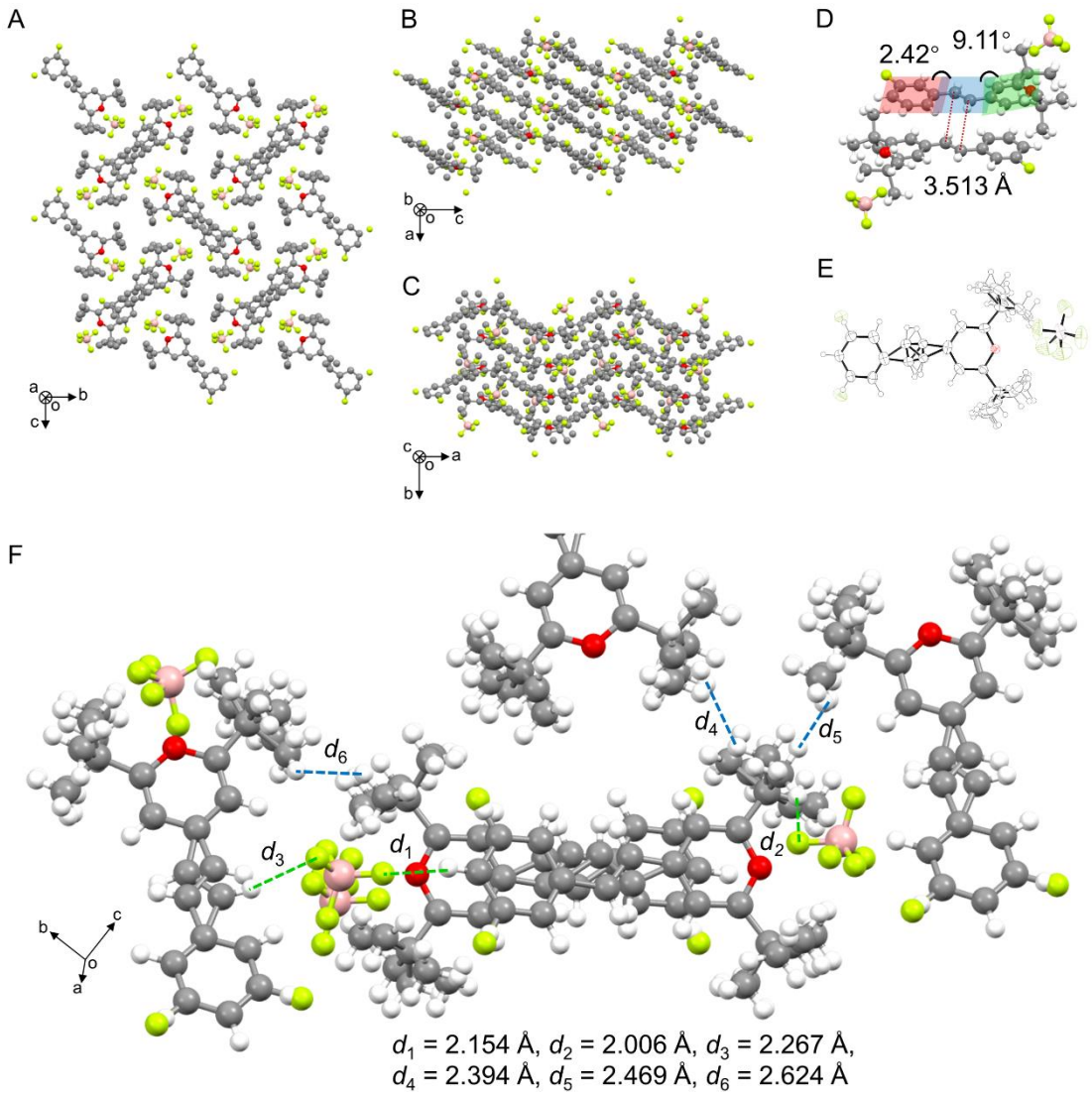

Figure S2. Molecular packing of **3FSPyL** in crystal viewed along the a-axis (A), the b-axis (B) and the c-axis (C) (the hydrogen atoms are omitted for clarity); (D) The dihedral angle between phenyl and vinyl as well as that between pyrylium and vinyl, and the distance between the two double bonds in π-dimer; (E) ORTEP of **3FSPyL** in crystal showing disorder around the vinyl group, 3-position fluorine atom on phenyl, *tert*-butyl groups and the tetrafluoroborate anion; (F) Atomic distances representing the intermolecular C−H···F (d_1, d_2 and d_3) and C−H···H (d_4, d_5 and d_6) interactions.

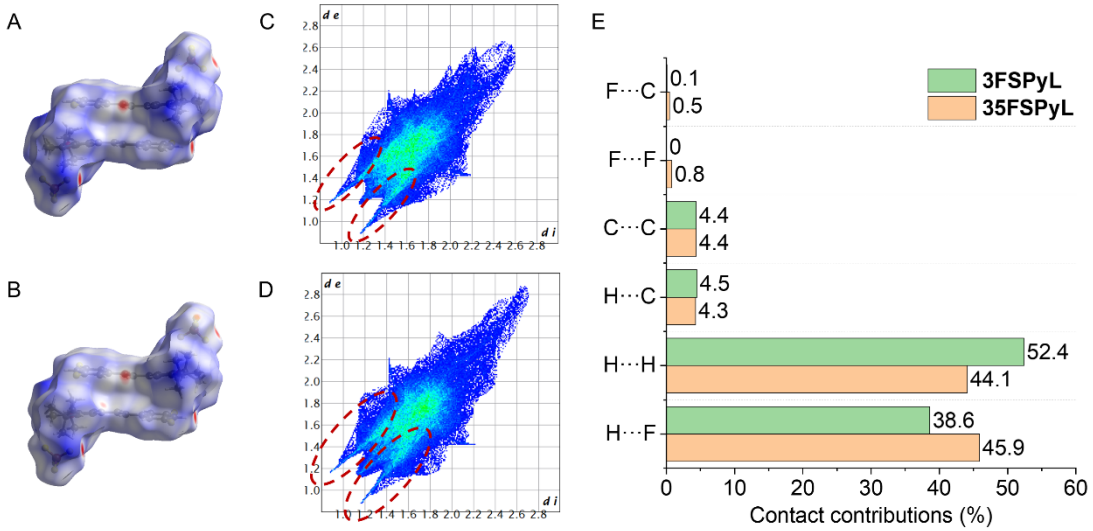

Figure S3. Hirshfeld surfaces of the crystals of **3FSPyL** (A) and **35FSPyL** (B) mapped with d_{norm}; 2D fingerprint plots of the crystals of **3FSPyL** (C) and **35FSPyL** (D, the red circles highlight the H···F contacts); (E) Diagram of the contributions of the atomic contacts to the Hirshfeld surface of the crystals of **3FSPyL** and **35FSPyL**.

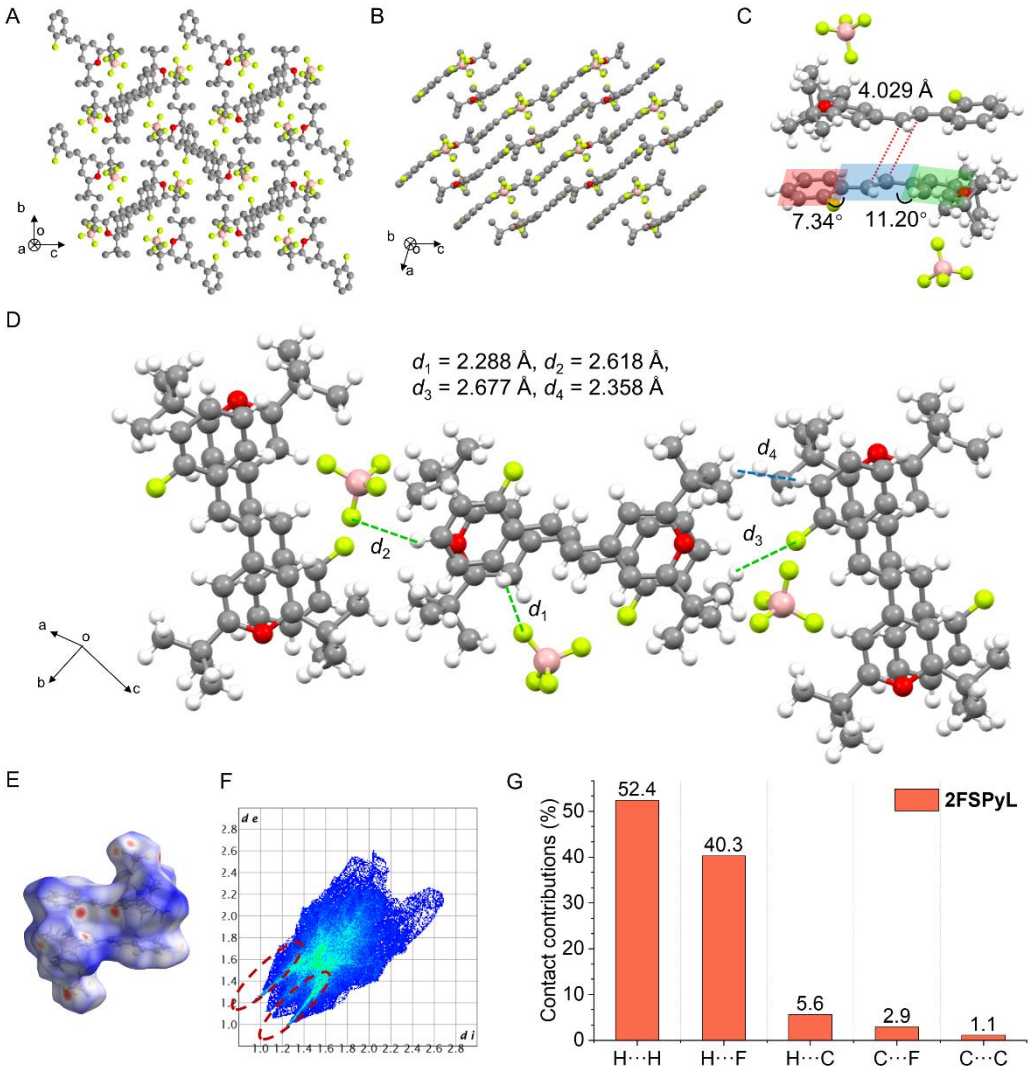

Figure S4. Molecular packing of **2FSPyL** in crystal viewed along the a-axis (A) and the b-axis (B) (the hydrogen atoms are omitted for clarity); (C) The dihedral angle between phenyl and vinyl as well as that between pyrylium and vinyl, and the distance between the two double bonds in π-dimer; (D) Atomic distances representing the intermolecular C−H···F (d_1, d_2 and d_3) and C−H···H (d_4) interactions; (E) Hirshfeld surface mapped with d_{norm} and (F) 2D fingerprint plots of the crystal of **2FSPyL** (the red circles highlight the H···F contacts); (G) Diagram of the contributions of the atomic contacts to the Hirshfeld surface.

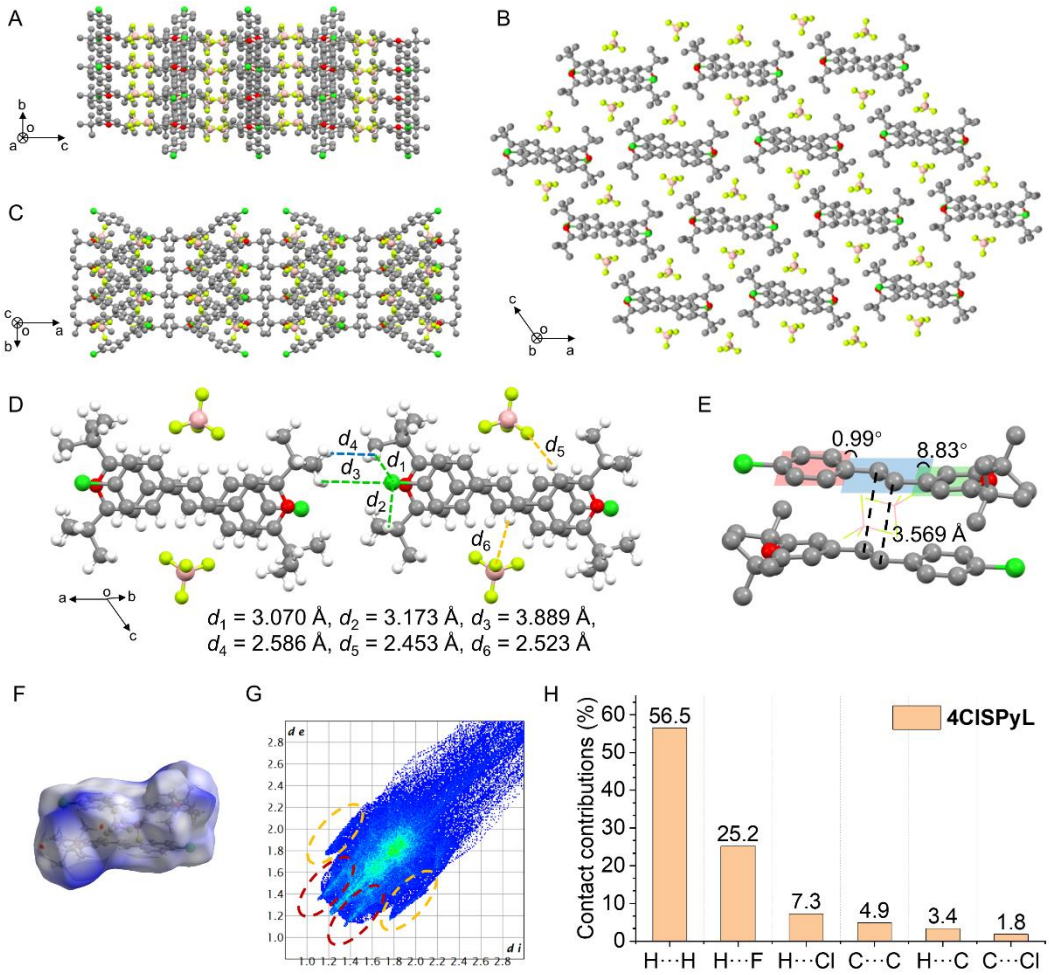

Figure S5. Molecular packing of **4ClSPyL** in crystal viewed along the a-axis (A), the b-axis (B) and the c-axis (C); (D) Atomic distances representing the intermolecular C–H···Cl (d_1, d_2 and d_3), C–H···H (d_4) and C–H···F (d_5 and d_6) interactions; (E) The dihedral angle between phenyl and vinyl as well as that between pyrylium and vinyl, and the distance between the carbon-carbon double bonds in adjacent molecules. The hydrogen atoms are omitted for clarity; Hirshfeld surface (F) mapped with d_{norm} and 2D fingerprint plots (G) of the crystal of **4ClSPyL** (the red and yellow circles highlight the H···F and the H···Cl contacts); (H) Diagram of the contributions of the atomic contacts to the Hirshfeld surface.

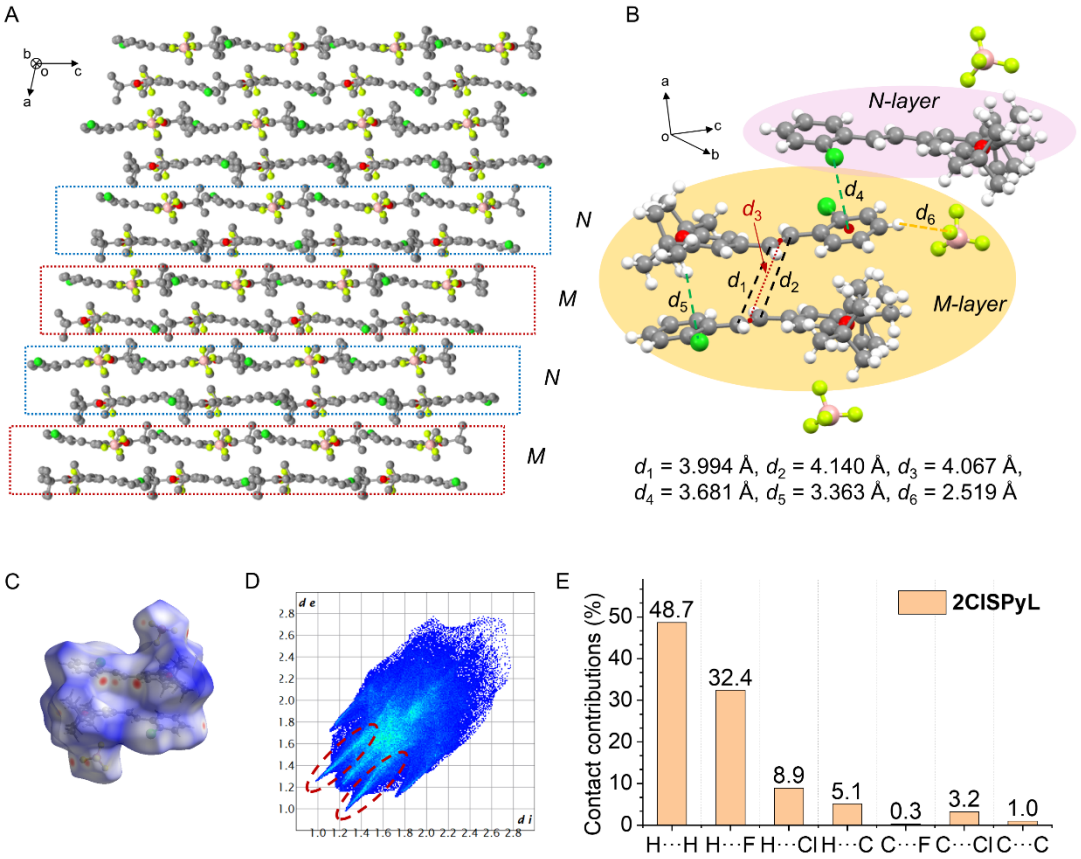

Figure S6. (A) Molecular packing of **2ClSPyL** in crystal viewed along the b-axis showing the alternating *M*-*N*-*M*-*N* layered structure (the hydrogen atoms are omitted for clarity); (B) The distance between the carbon-carbon atoms of double bonds in adjacent molecules (d_1, d_2 and d_3) in the *M*-layer and atomic distances representing intermolecular C···Cl (d_4), C–H···Cl (d_5) and C–H···F (d_6) interactions(the red dots indicated the centers of the double bonds and the phenyl); (C) Hirshfeld surface mapped with d_{norm} and (D) 2D fingerprint plot of the crystal of **2ClSPyL** (the red circles highlight the H···F contacts); (E) Diagram of the contributions of the atomic contacts to the Hirshfeld surface.

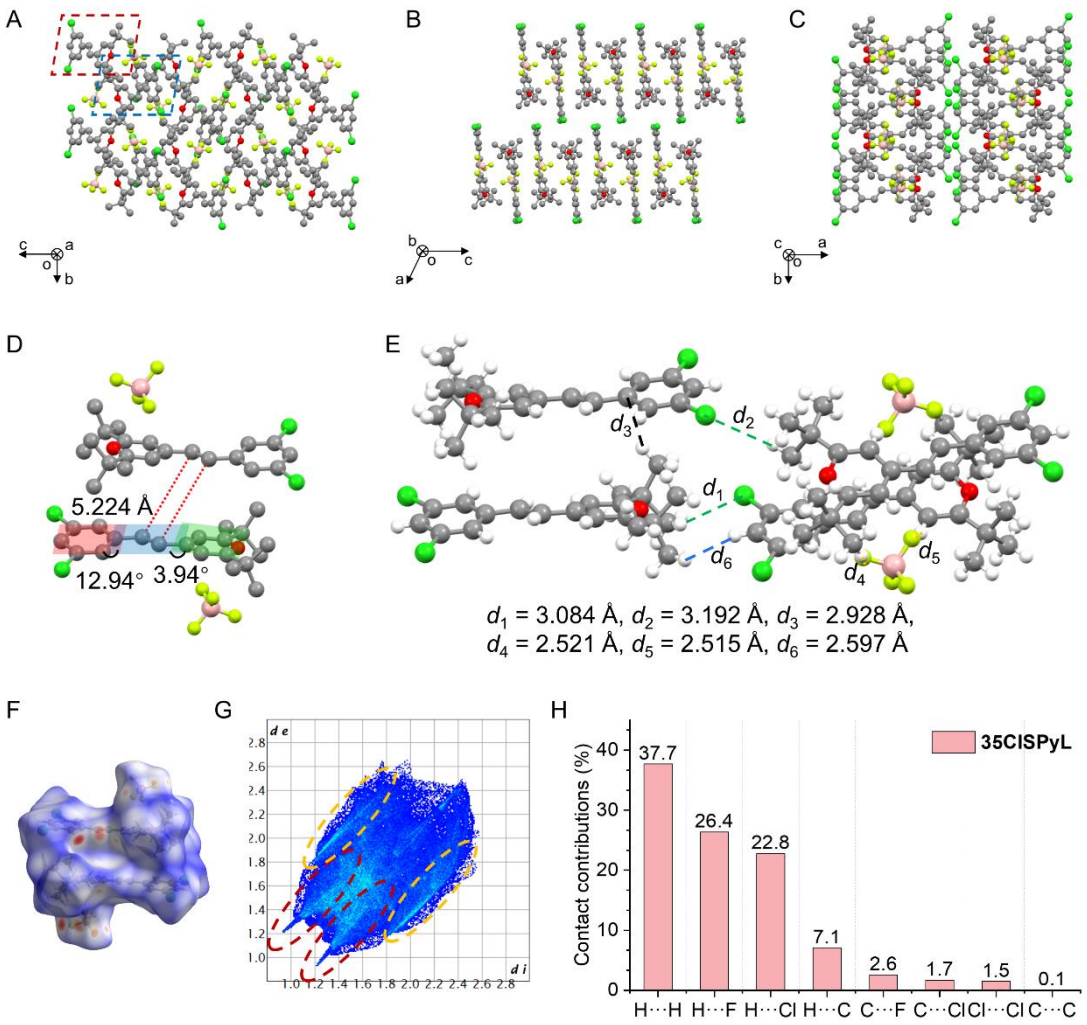

Figure S7. Molecular packing of **35ClSPyL** in crystal viewed along the a-axis (A), the b-axis (B) and the c-axis (C); (D) The dihedral angle between phenyl and vinyl as well as that between pyrylium and vinyl, and the distances between the carbon-carbon double bonds in adjacent molecules. The hydrogen atoms are omitted for clarity. (E) Atomic distances representing the intermolecular C−H···Cl (d_1 and d_2), C−H···C (d_3), C−H···F (d_4 and d_5) and C−H···H (d_6) interactions; Hirshfeld surface mapped with d_{norm} (F) and 2D fingerprint plots (G) of the crystal of **35ClSPyL** (the red and yellow circles highlight the H···F and the H···Cl contacts); (H) Diagram of the contributions of the atomic contacts to the Hirshfeld surface.

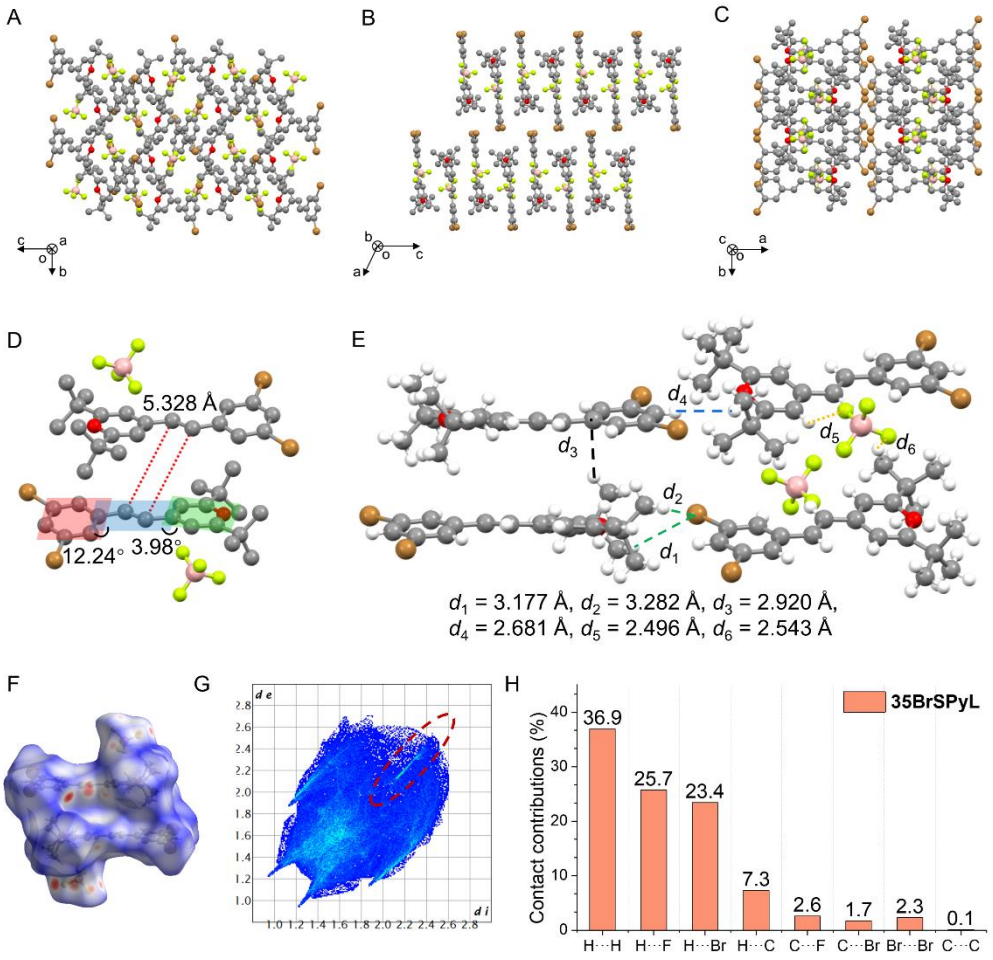

Figure S8. Molecular packing of **35BrSPyL** in crystal viewed along the a-axis (A), the b-axis (B) and the c-axis (C); (D) The dihedral angle between phenyl and vinyl as well as that between pyrylium and vinyl, and the distances between the carbon-carbon double bonds in adjacent molecules. The hydrogen atoms are omitted for clarity. (E) Atomic distances representing the intermolecular C−H···Br (d_1 and d_2), C−H···C (d_3), C−H···H (d_4) and C−H···F (d_5 and d_6) interactions; Hirshfeld surface mapped with d_{norm} (F) and 2D fingerprint plots (G) of the crystal of **35BrSPyL** (the red circle highlights the Br···Br contact); (H) Diagram of the contributions of the atomic contacts to the Hirshfeld surface.

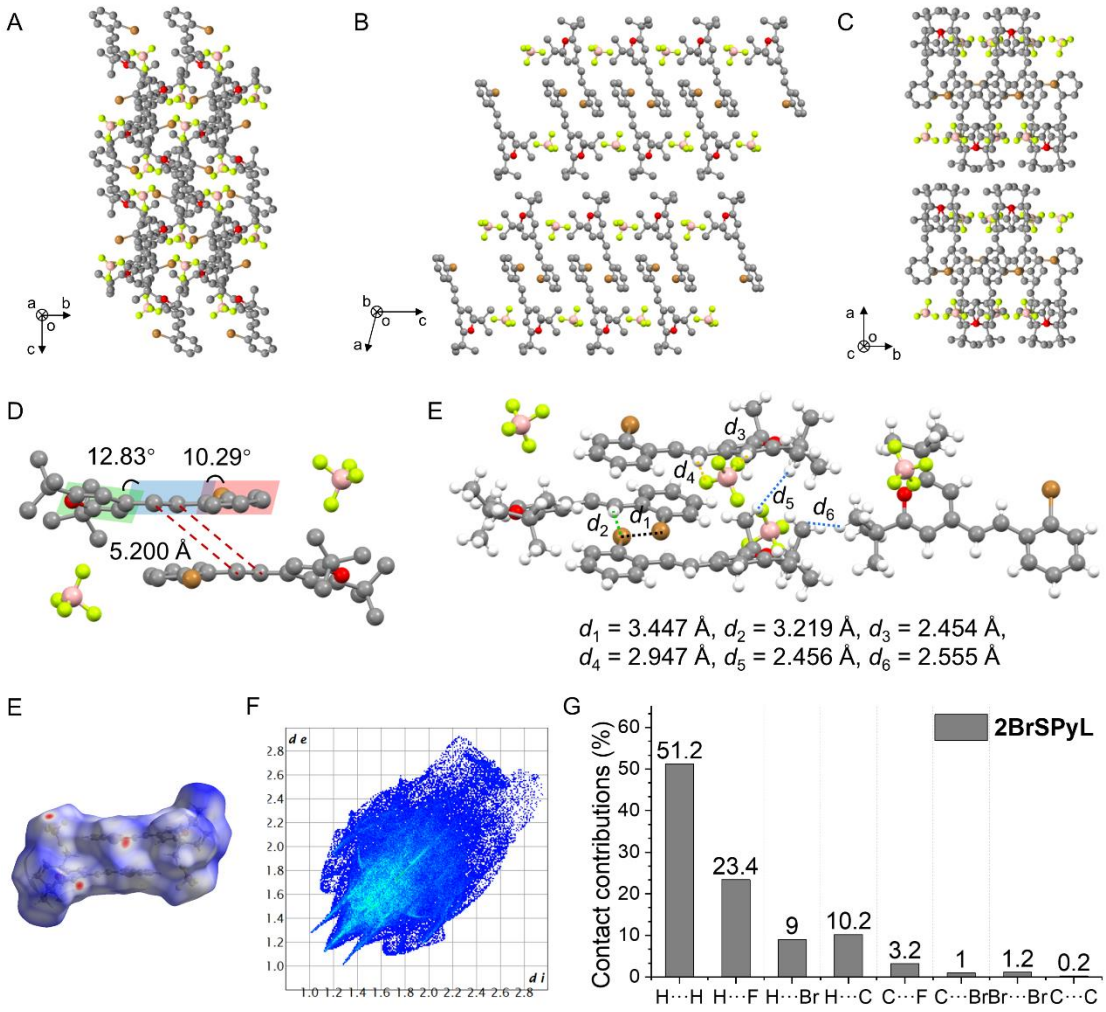

Figure S9. Molecular packing of **2BrSPyL** in crystal viewed along the a-axis (A), the b-axis (B) and the c-axis (C); (D) The dihedral angle between phenyl and vinyl as well as that between pyrylium and vinyl, and the distances between the carbon-carbon double bonds in adjacent molecules. The hydrogen atoms are omitted for clarity. (E) Atomic distances representing the intermolecular Br···Br (d_1), C–H···Br (d_2), C–H···F (d_3 and d_4) and C–H···H (d_5 and d_6) interactions; Hirshfeld surface mapped with d_{norm} (F) and 2D fingerprint plots (G) of the crystal of **2BrSPyL**; (H) Diagram of the contributions of the atomic contacts to the Hirshfeld surface.

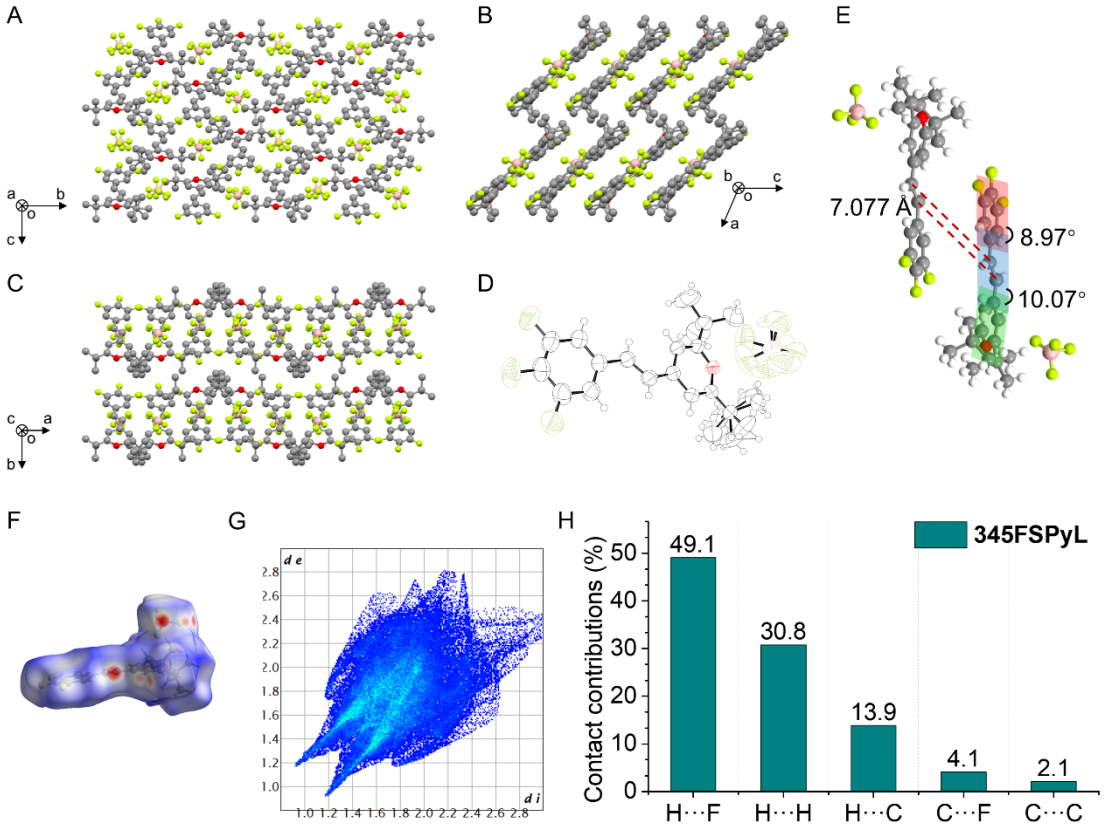

Figure S10. Molecular packing of **345FSPyL** in crystal viewed along the a-axis (A), the c-axis (B) and the b-axis (C); (D) ORTEP of **345FSPyL** in crystal showing partial disorder around the tetrafluoroborate anion and *tert*-butyl group; (E) The dihedral angles between phenyl and vinyl as well as that between pyrylium and vinyl, and the distances between the carbon-carbon double bonds in adjacent molecules; Hirshfeld surface (F) mapped with d_{norm} and 2D fingerprint plots (G) of the crystal of **345FSPyL**; (H) Diagram of the contributions of the atomic contacts to the Hirshfeld surface.

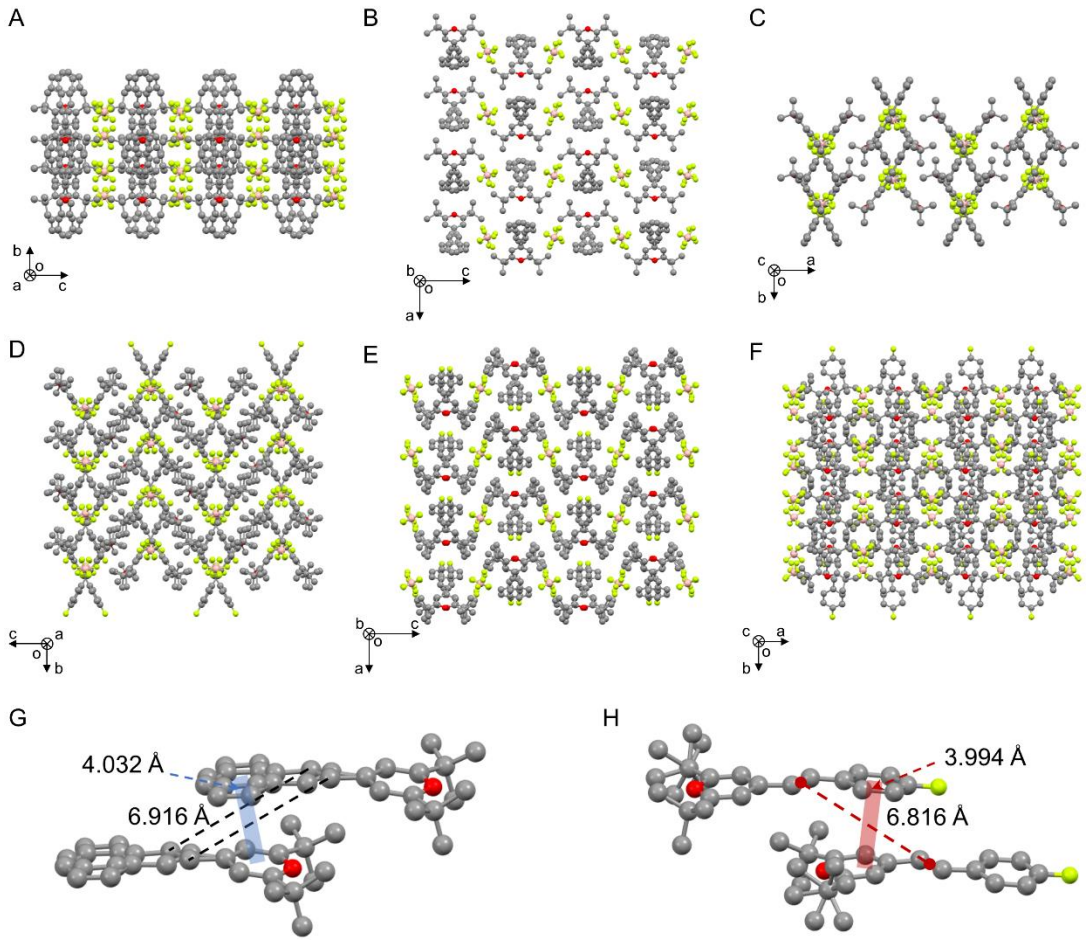

Figure S11. Molecular packing of **SPyL** in crystal viewed along the a-axis (A), the b-axis (B) and the c-axis (C); Molecular packing of **4FSPyL** in crystal viewed along the a-axis (D), the b-axis (E) and the c-axis (F); The distances between the carbon-carbon double bonds in adjacent molecules of **SPyL** (G) and distance of the centers of double bonds in adjacent molecules of **4FSPyL** (H). The distances representing cation-π interactions are labelled.

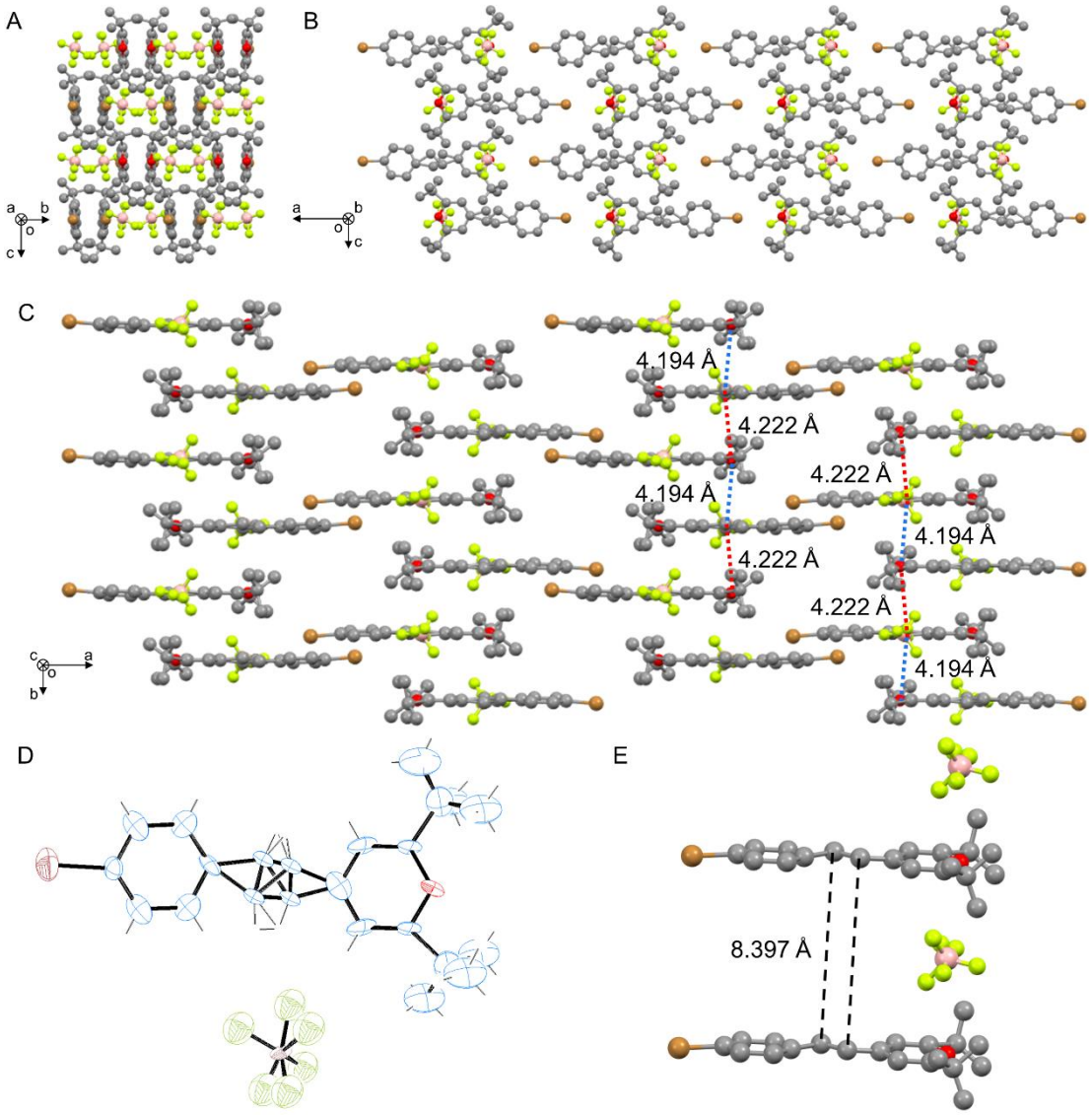

Figure S12. Molecular packing of **4BrSPyL** in crystal viewed along the a-axis (A), the b-axis (B) and the c-axis (C). Distances representing electrostatic interaction between cation oxygen atoms and anion boron atoms in the two distinct one-dimensional columns are labeled; (D) ORTEP of **4BrSPyL** in crystal showing partial disorder around the vinyl group; (E) Atomic distance of carbon-carbon double bonds in the head-to-head type dimer of **4BrSPyL**.

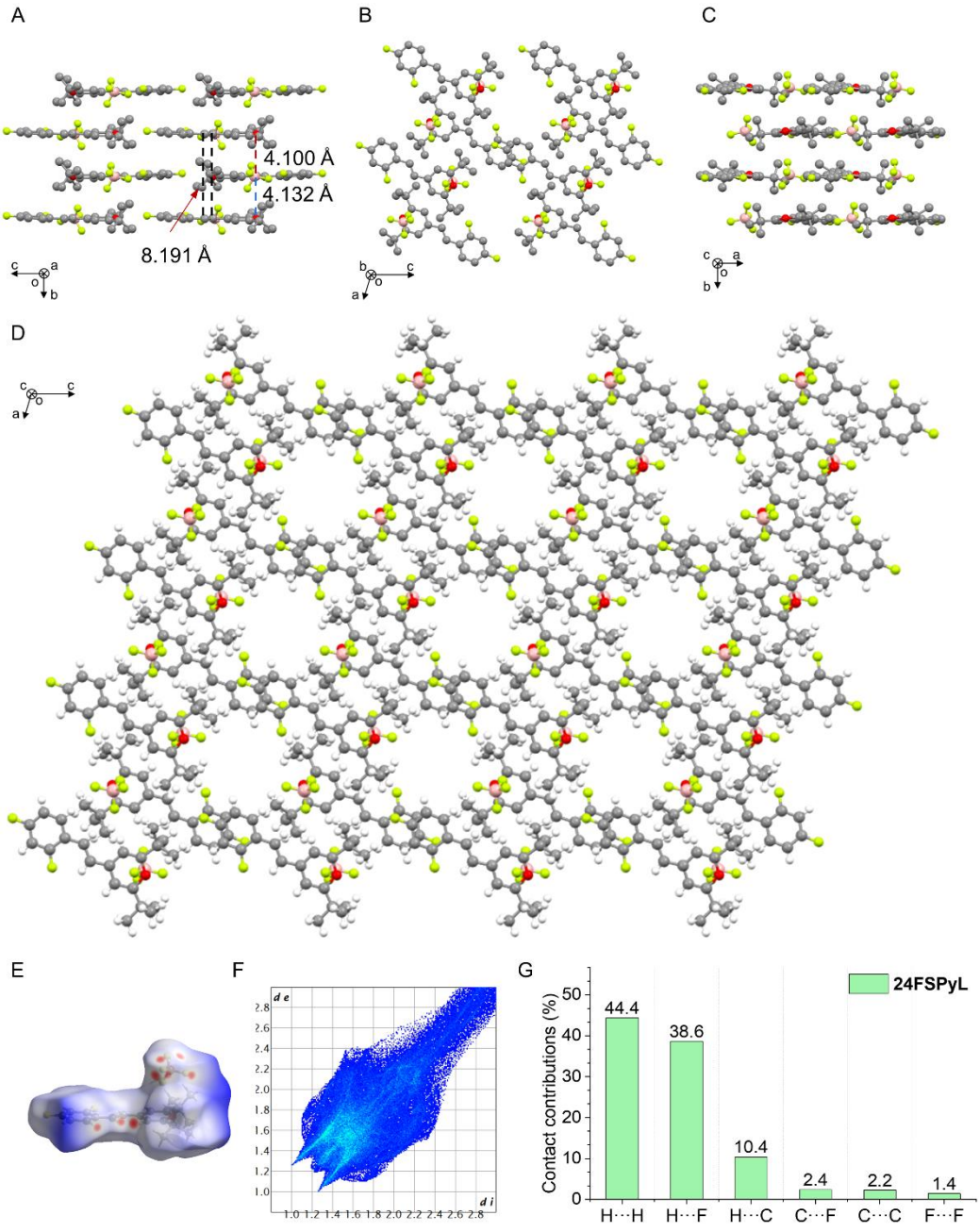

Figure S13. Molecular packing of **24FSPyL** in crystal viewed along the a-axis (A), the c-axis (B) and the b-axis (C); (D) A porous structure in the crystal of **24FSPyL** viewed along the b-axis of the crystal, contained solvent molecules of dichloromethane; Hirshfeld surface (E) mapped with d_{norm} and 2D fingerprint plots (F) of the crystal of **345FSPyL**; (G) Diagram of the contributions of the atomic contacts to the Hirshfeld surface.

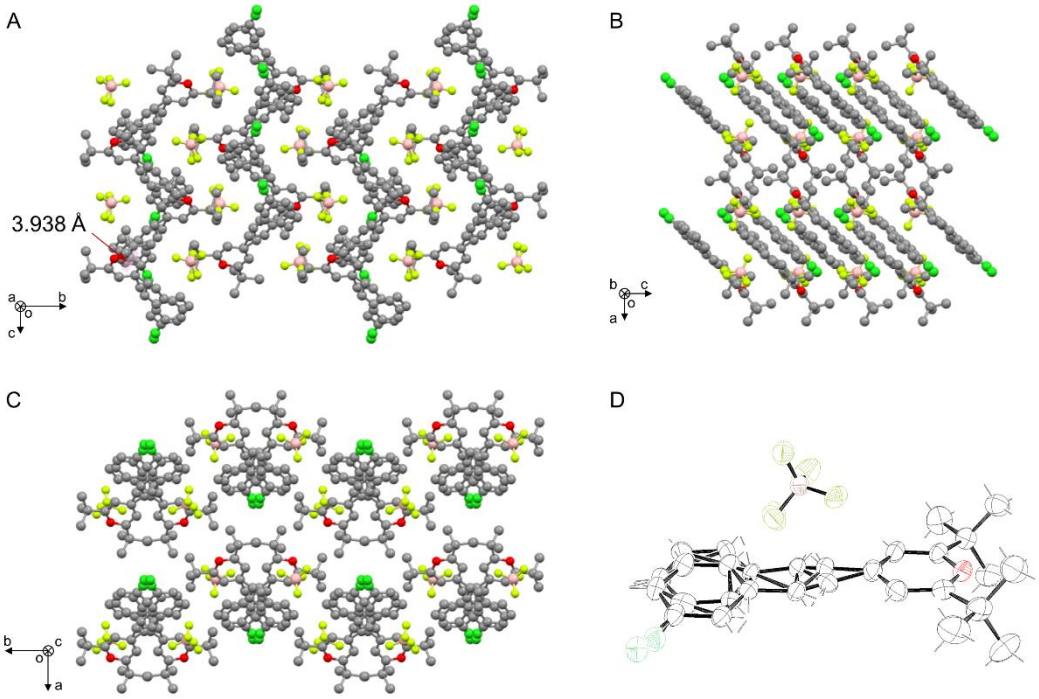

Figure S14. Molecular packing of **3ClSPyL** in crystal viewed along the a-axis (A), b-axis (B) and c-axis (C); (D) ORTEP of **3ClSPyL** in crystal showing partial disorder around the tetrafluoroborate anion and styryl group.

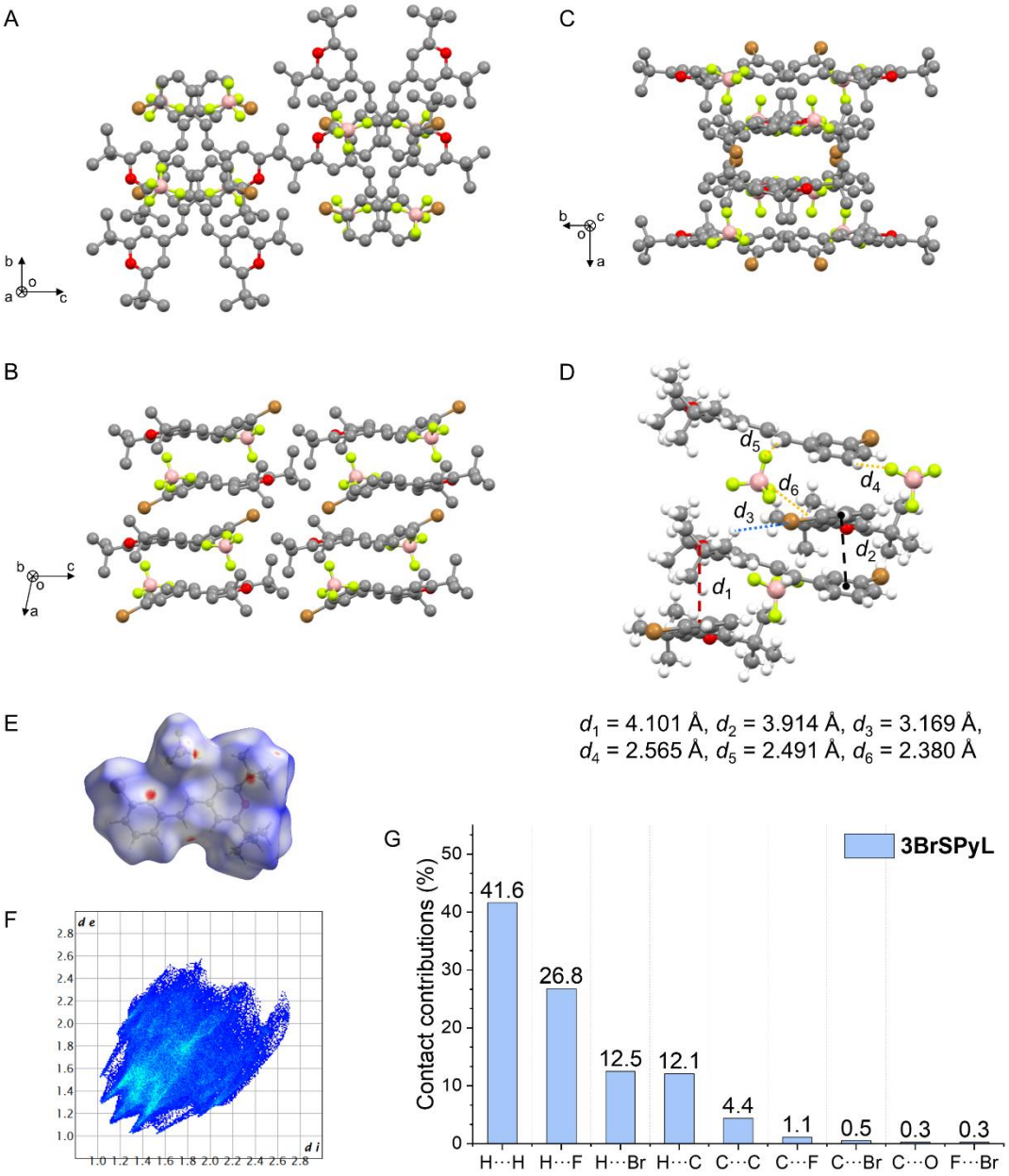

Figure S15. Molecular packing of **3BrSPyL** in crystal viewed along the a-axis (A), the b-axis (B) and the c-axis (C); (D) Atomic distances representing the intermolecular cation–π (d_1), π–π (d_2), C–H···Br (d_3), C–H···F (d_4, d_5 and d_6) interactions; Hirshfeld surface mapped with d_{norm} (E) and 2D fingerprint plots (F) of the crystal of **3BrSPyL**; (G) Diagram of the contributions of the atomic contacts to the Hirshfeld surface.

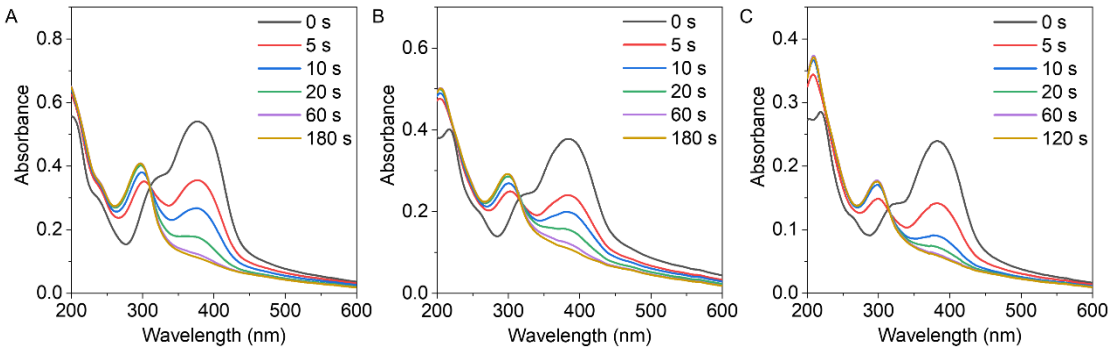

Figure S16. UV-vis absorption spectra of **35FSPyL** (A), **35ClSPyl** (B) and **35BrSPyL** (C) in powders before and after irradiation with 365 nm light (5 W) for different times.

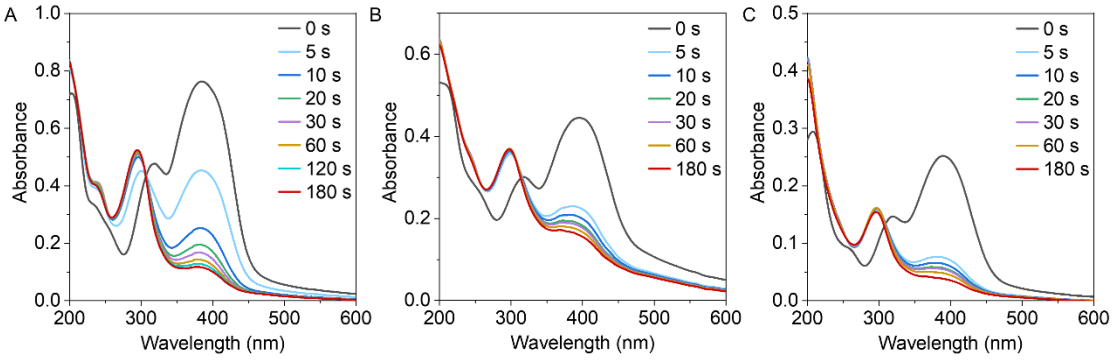

Figure S17. UV-vis absorption spectra of **2FSPyL** (A), **2ClSPyl** (B) and **2BrSPyL** (C) in powders before and after irradiation with 365 nm light (5 W) for different times.

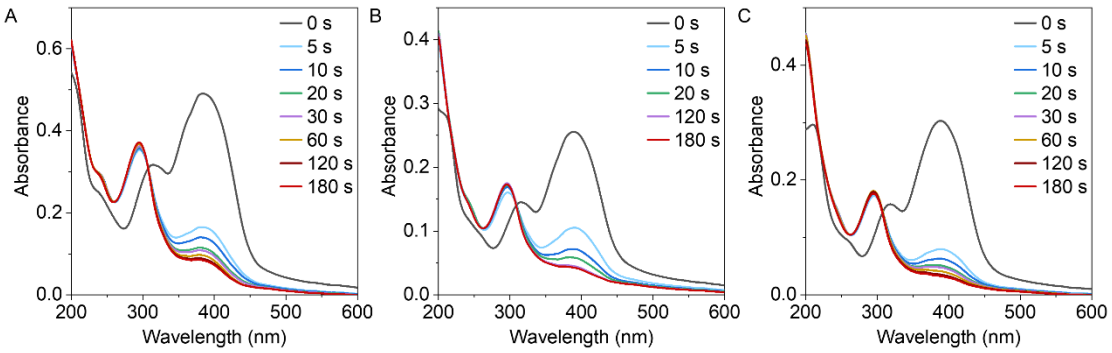

Figure S18. UV-vis absorption spectra of **3FSPyL** (A), **3ClSPyl** (B) and **3BrSPyL** (C) in powders before and after irradiation with 365 nm light (5 W) for different times.

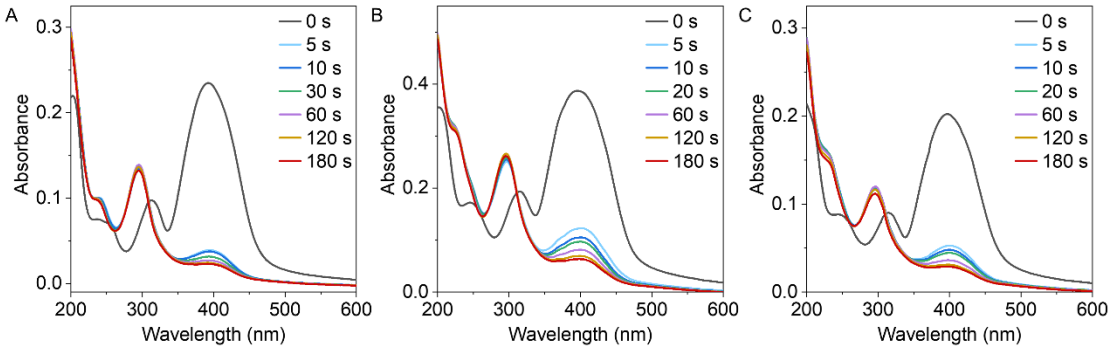

Figure S19. UV-vis absorption spectra of **4FSPyL** (A), **4ClSPyl** (B) and **4BrSPyL** (C) in powders before and after irradiation with 365 nm light (5 W) for different times.

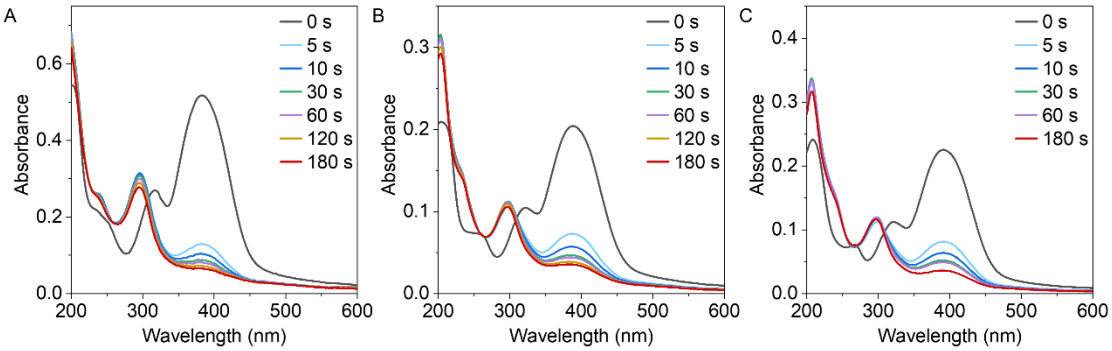

Figure S20. UV-vis absorption spectra of **24FSPyL** (A), **24ClSPyl** (B) and **24BrSPyL** (C) in powders before and after irradiation with 365 nm light (5 W) for different times.

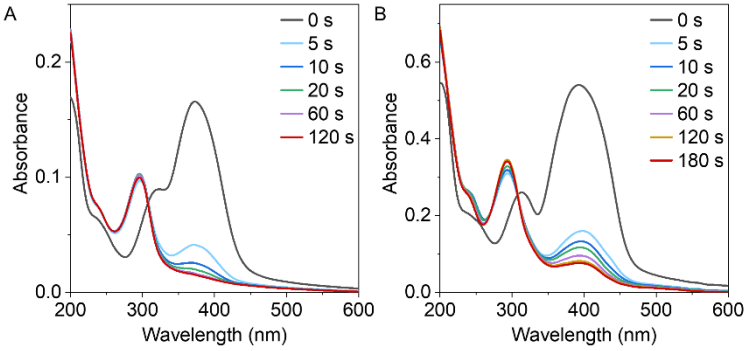

Figure S21. UV-vis absorption spectra of (a) **345FSPyL** and (b) **SPyL** in powders before and after irradiation with 365 nm light (5 W) for different times.

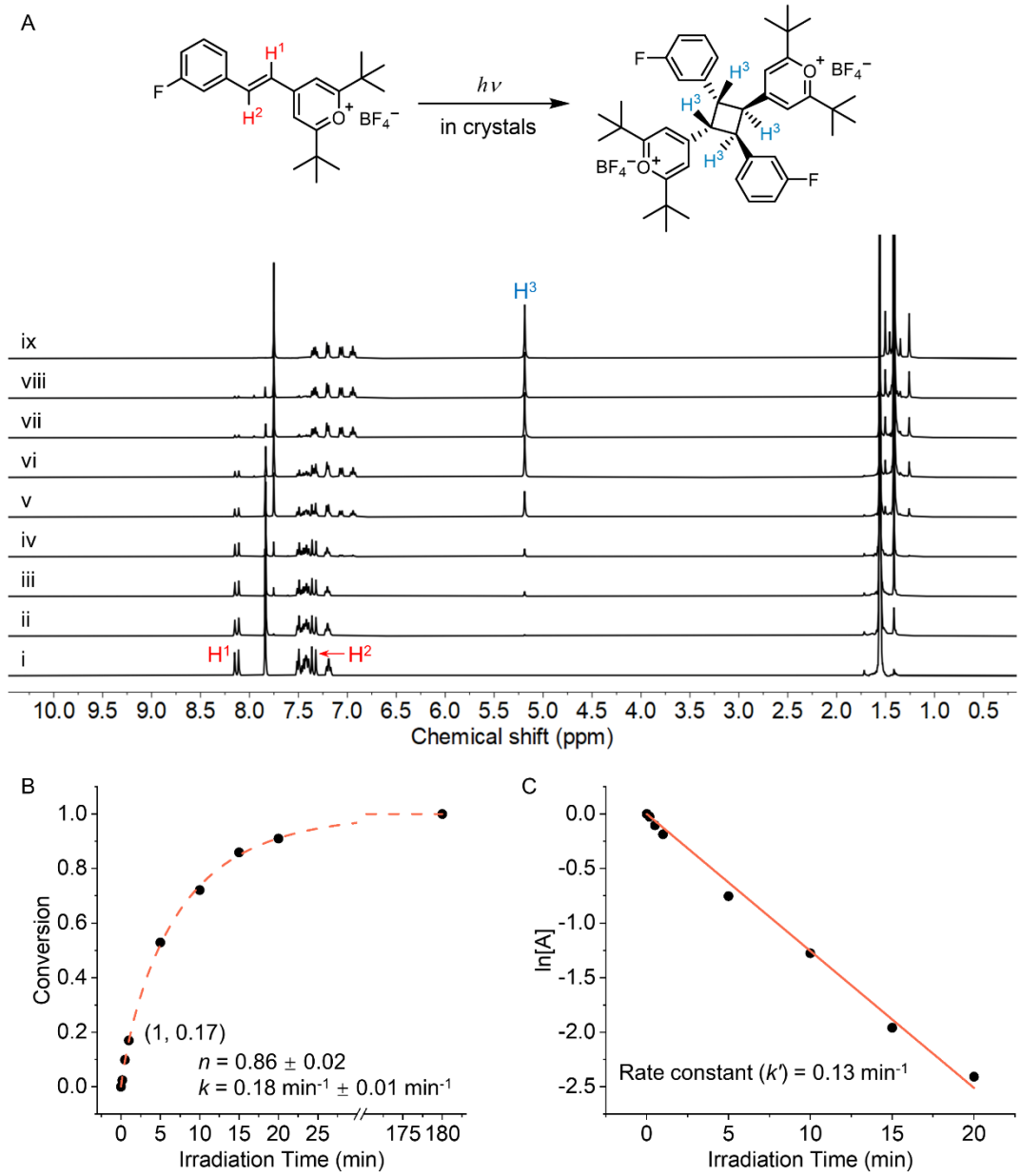

Figure S22. Photoinduced [2+2] cycloaddition of **3FSPyL** and ^{1}H NMR spectra of **3FSPyL** before (i) and after irradiation of the microcrystals with 365 nm light (5 W) for 10 s (ii), 30 s (iii), 1 min (iv), 5 min (v), 10 min (vi), 20 min (vii), 30 min (viii) and 3 h (ix), followed by dissolving in TFA-*d* (400 MHz); (B) Conversion ratios of the photodimerization of **3FSPyL** in microcrystals (fitting equation: $y = 1 - e \wedge (-0.1844 \times t \wedge 0.8595)$, $R^2 = 0.9995$); (C) First-order kinetics of the photodimerization of **3FSPyL** in microcrystals (ln[A]: logarithm of the relative concentration of reactants/photodimerization products, linearly fitting equation: $y = -0.1255 \times x$, $R^2 = 0.9964$).

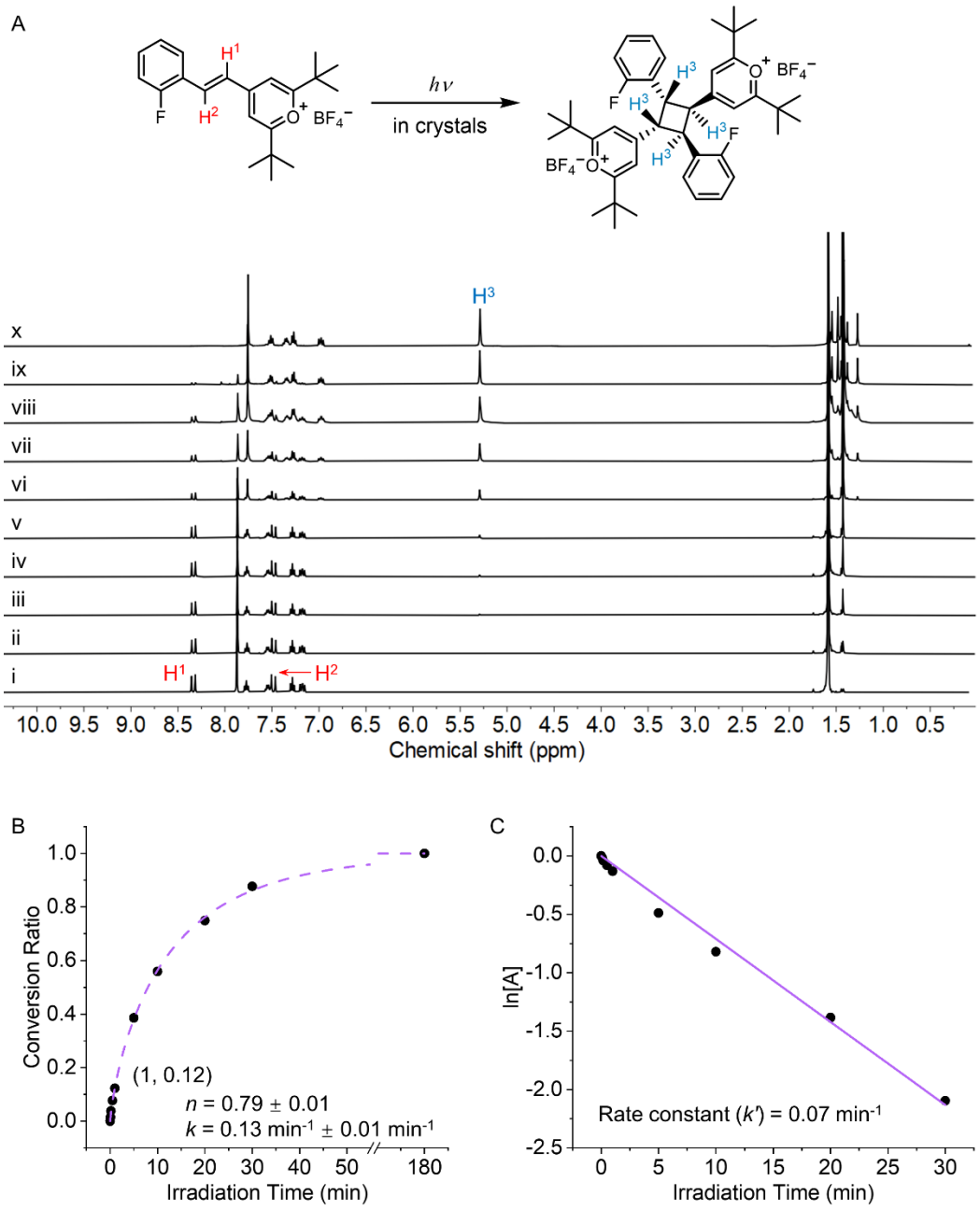

Figure S23. Photoinduced [2+2] cycloaddition of **2FSPyL** and ^{1}H NMR spectra of **2FSPyL** before (i) and after irradiation of the microcrystals with 365 nm light (5 W) for 5 s (ii), 10 s (iii), 30 s (iv), 1 min (v), 5 min (vi), 10 min (vii), 20 min (viii), 30 min (ix) and 3 h (x), followed by dissolving in TFA-*d* (400 MHz); (B) Conversion ratios of the photodimerization of **2FSPyL** in microcrystals (fitting equation: $y = 1 - e \wedge (-0.1342 \times t \wedge 0.7911)$, $R^2 = 0.9996$); (C) First-order kinetics of the photodimerization of **2FSPyL** in microcrystals (ln[A]: logarithm of the relative concentration of reactants/photodimerization products, linearly fitting equation: $y = -0.0711 \times x$, $R^2 = 0.9940$).

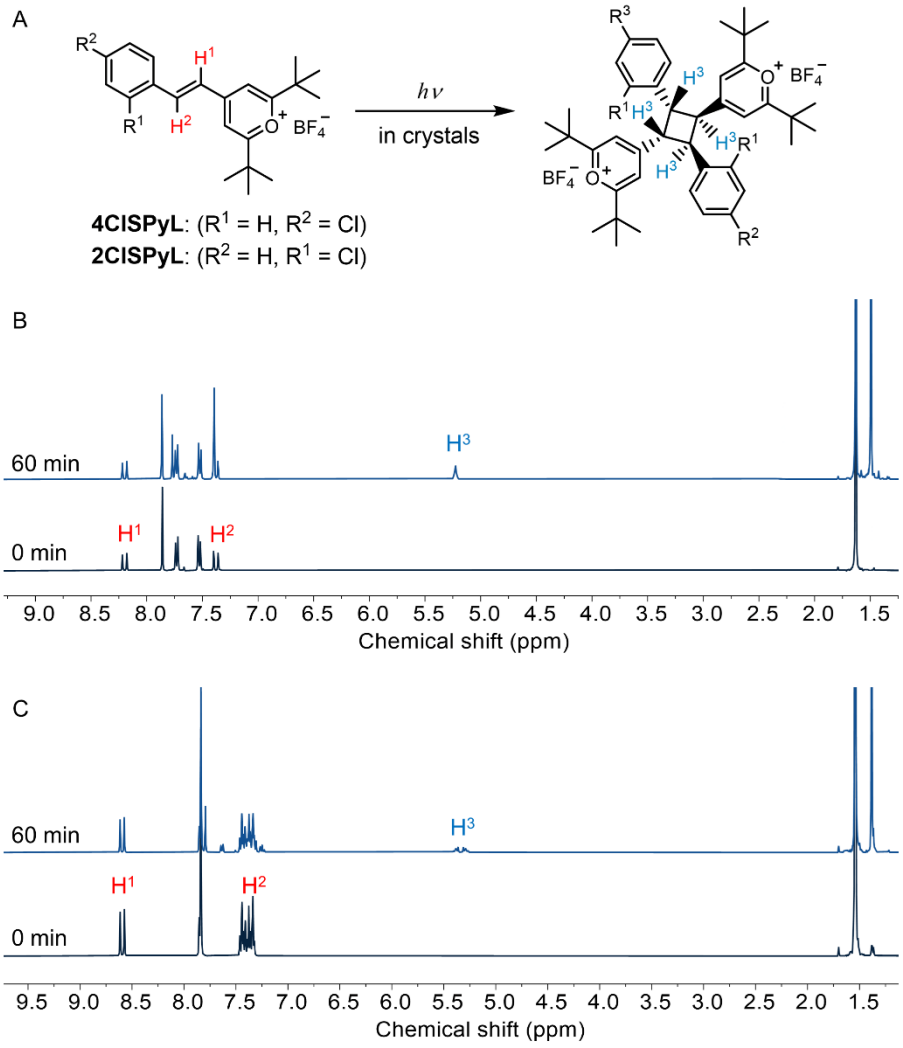

Figure S24. (A) Photoinduced [2+2] cycloaddition of **2ClSPyL** and **4ClSPyL**; ^{1}H NMR spectra of **2ClSPyL** (B) and **4ClSPyL** (C) in TFA-*d* (400 MHz) before and after exposing the microcrystals to 365 nm light (5 W) for 60 min.

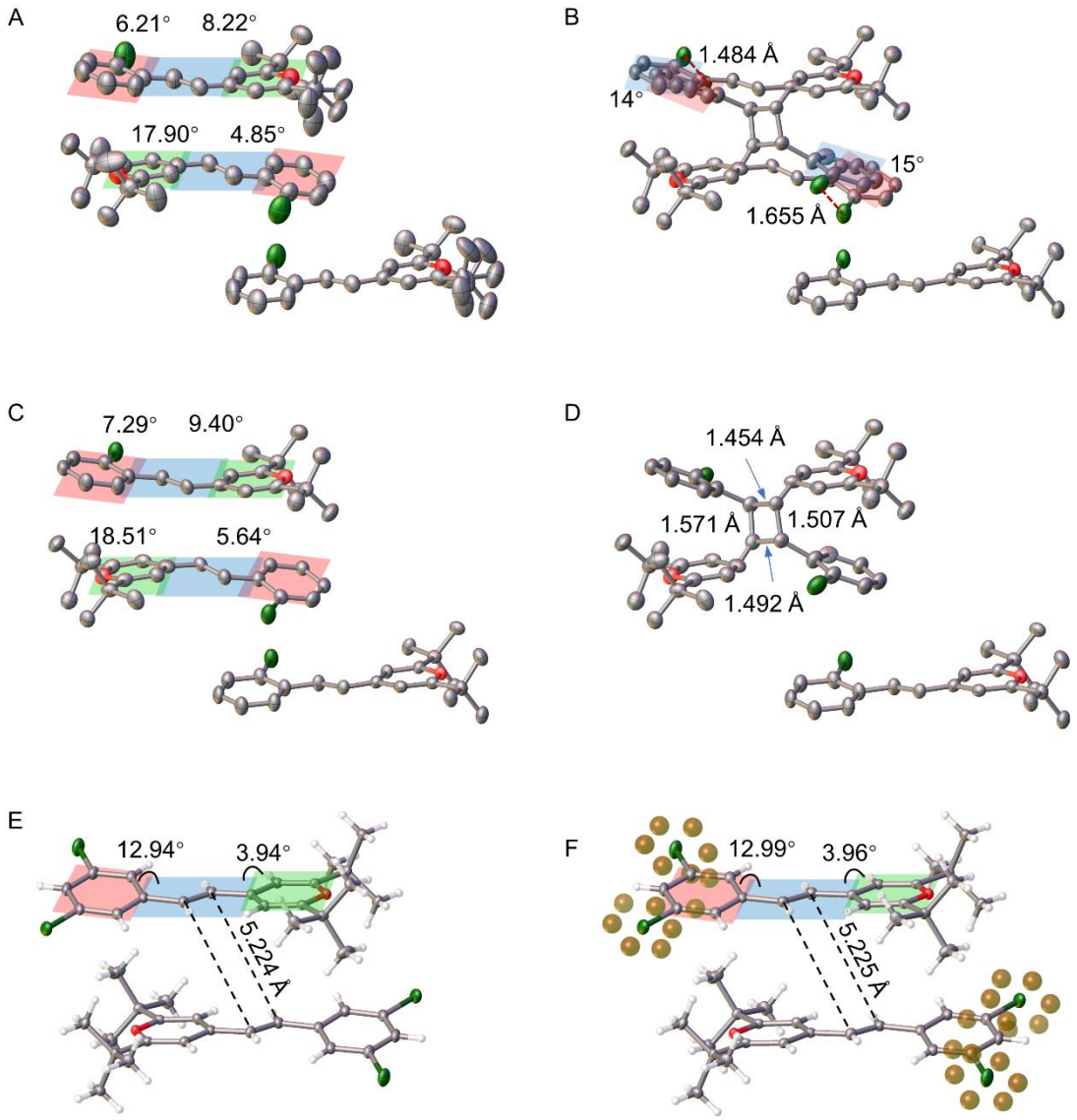

Figure S25. (A) ORTEPs of the crystals of **2ClSPyL** showing the dihedral angles between phenyl and vinyl as well as that between pyrylium and vinyl; ORTEPs of the crystals of **2ClSPyL-**10 showing the dihedral angles between the phenyls of the unreacted π-dimer and the newly formed σ-dimer and the distances between chlorine atoms (B), the dihedral angles between phenyl and vinyl as well as that between pyrylium and vinyl involved in the unreacted π-dimer (C), and the distances between carbon-carbon atoms of the newly formed cyclobutane in the σ-dimer; ORTEPs of the crystals of **35ClSPyL** (E) and **35ClSPyL-**1 (F) showing the distances between the carbon-carbon double bonds and the dihedral angle between phenyl and vinyl as well as that between pyrylium and vinyl.

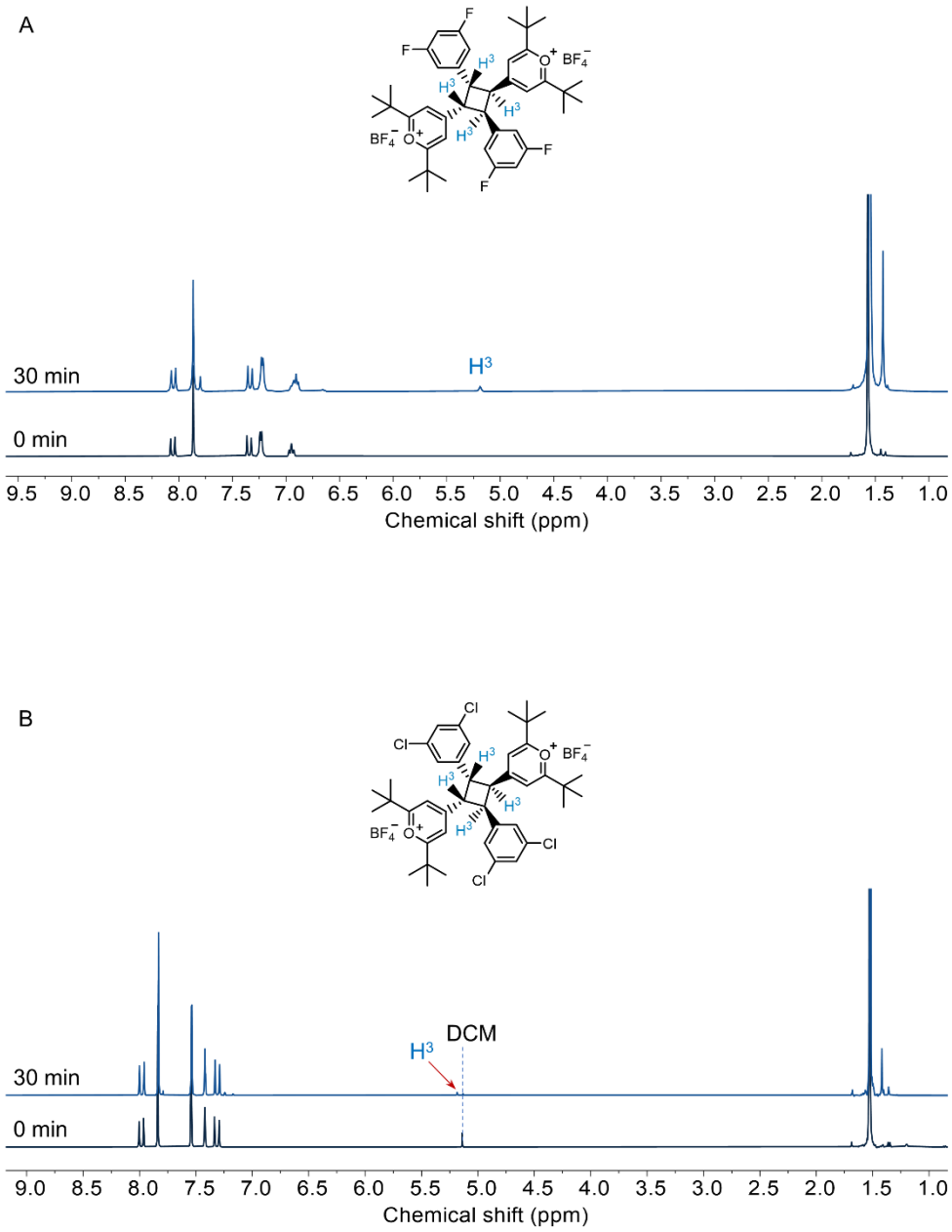

Figure S26. ^{1}H NMR spectra of **35FSPyL** (A) and **35ClSPyL** (B) in TFA-*d* (400 MHz) before and after irradiation of the microcrystals with 365 nm (5 W) for 30 min at −70 °C.

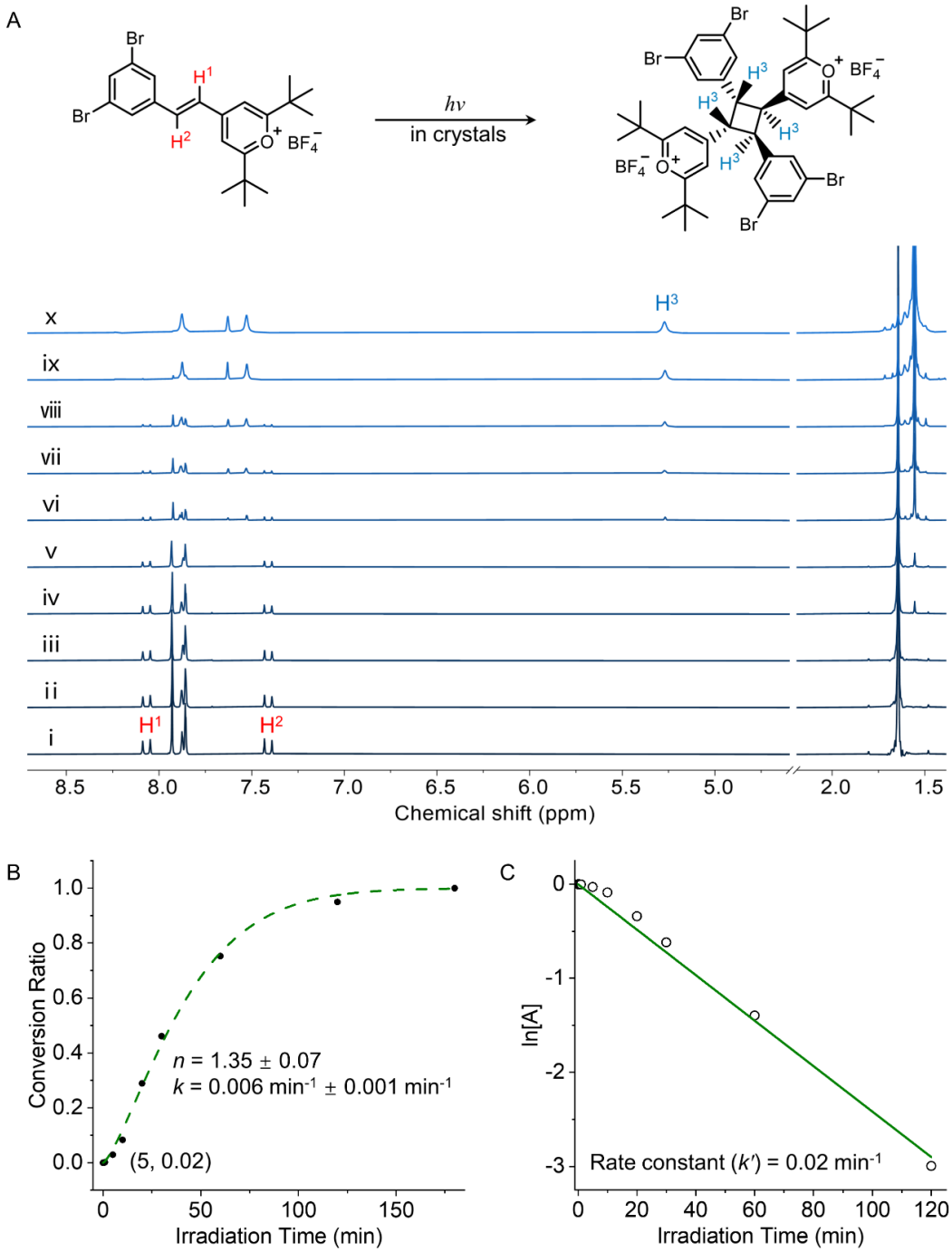

Figure S27. Photoinduced [2+2] cycloaddition of **35BrSPyL** and ^{1}H NMR spectra of **35BrSPyL** before (i) and after irradiation of the microcrystals with 365 nm light (5 W) for 30 s (ii), 1 min (iii), 5 min (iv), 10 min (v), 20 min (vi), 30 min (vii), 1 h (viii), 2 h (ix) and 3 h (x), followed by dissolving in TFA-*d* (400 MHz); (B) Conversion ratios of the photodimerization of **35BrSPyL** in microcrystals (fitting equation: $y = 1 - e \wedge (-0.0057 \times t \wedge 1.3508)$, $R^2 = 0.9977$); (C) First-order kinetics of the photodimerization of **35BrSPyL** in microcrystals (ln[A]: logarithm of the relative concentration of reactants/photodimerization products, linearly fitting equation: $y = -0.0242 \times x$, $R^2 = 0.9933$).

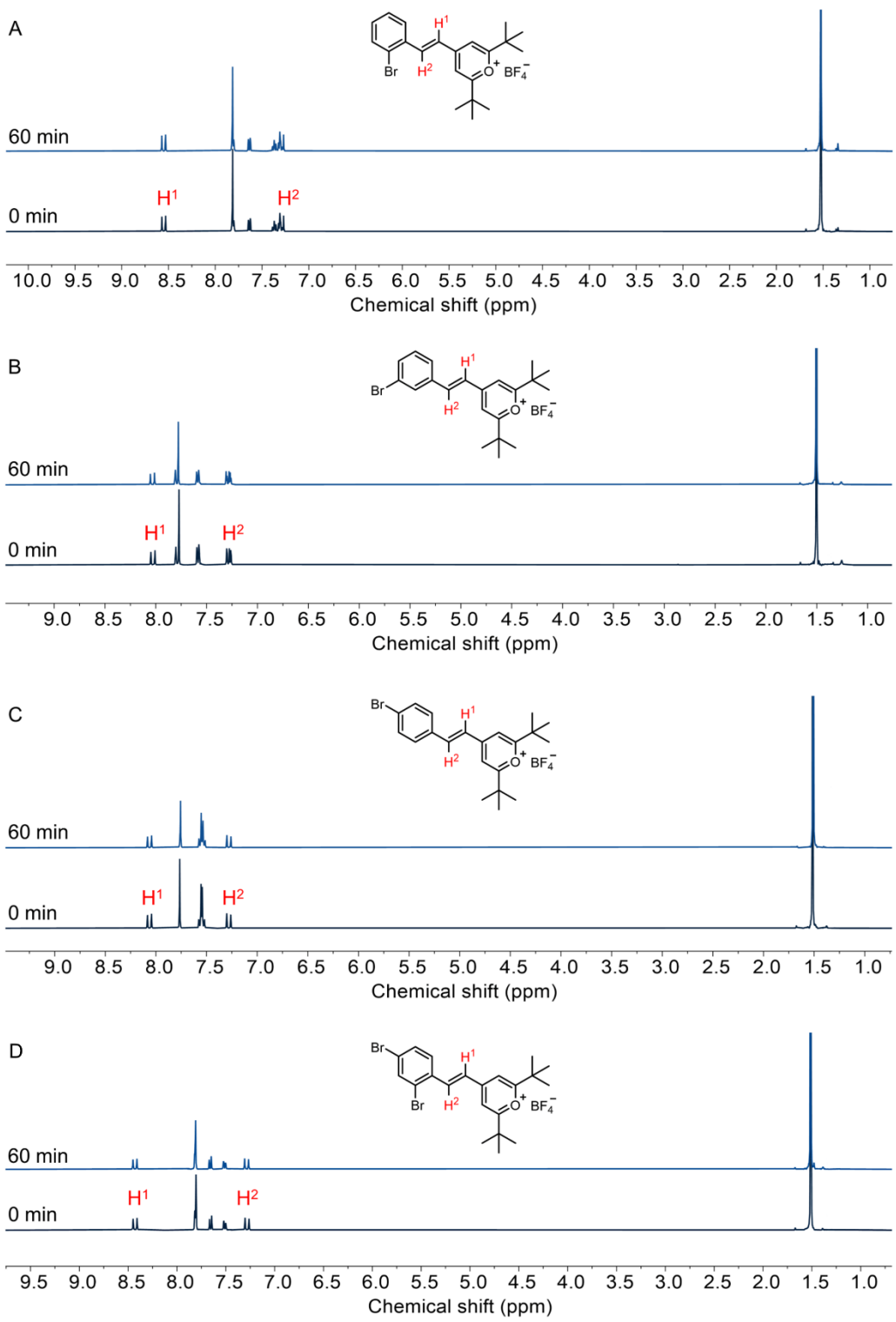

Figure S28. ^{1}H NMR spectra of **2BrSPyL** (A), **3BrSPyL** (B), **4BrSPyL** (C) and **24BrSPyL** (D) in TFA-*d* (400 MHz) before and after irradiation of the microcrystals with 365 nm light (5 W) for 60 min.

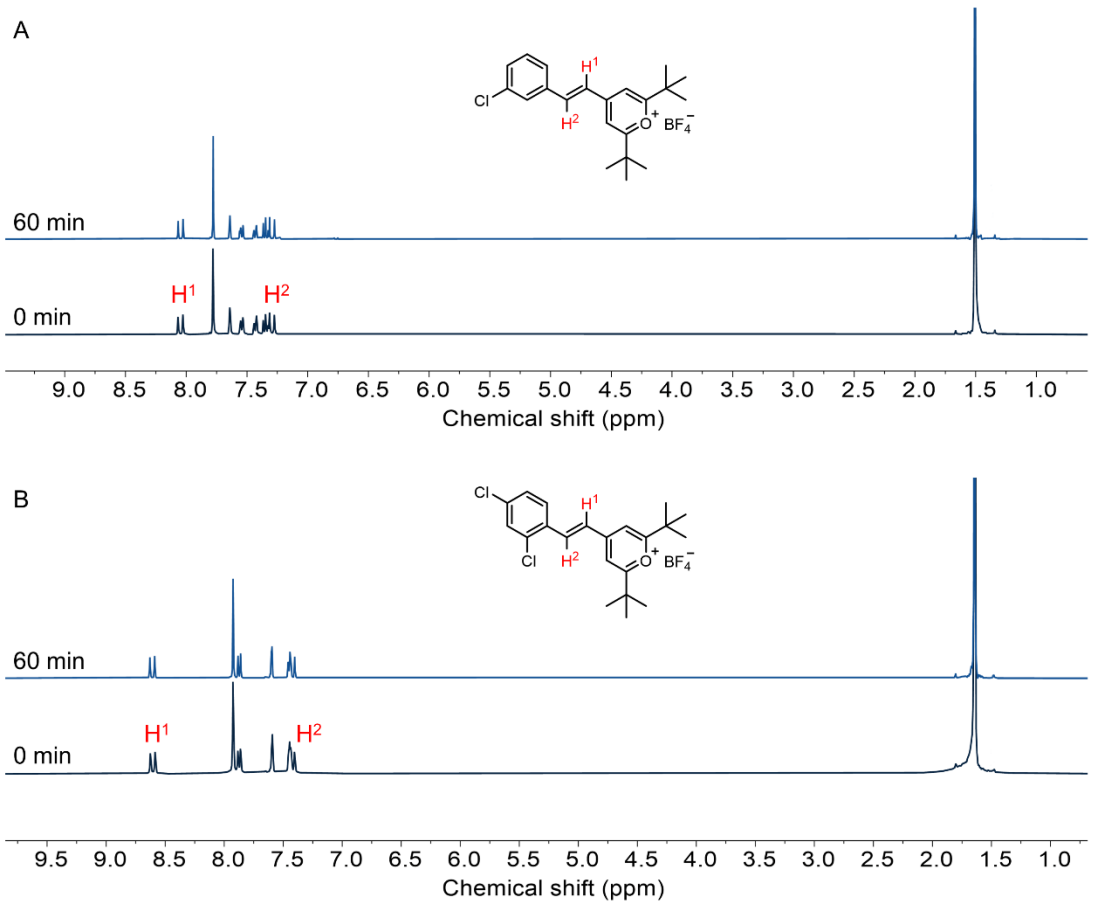

Figure S29. ^{1}H NMR spectra of **3ClSPyL** (A) and **24ClSPyL** (B) in TFA-*d* (400 MHz) before and after irradiation of the microcrystals with 365 nm light (5 W) for 60 min.

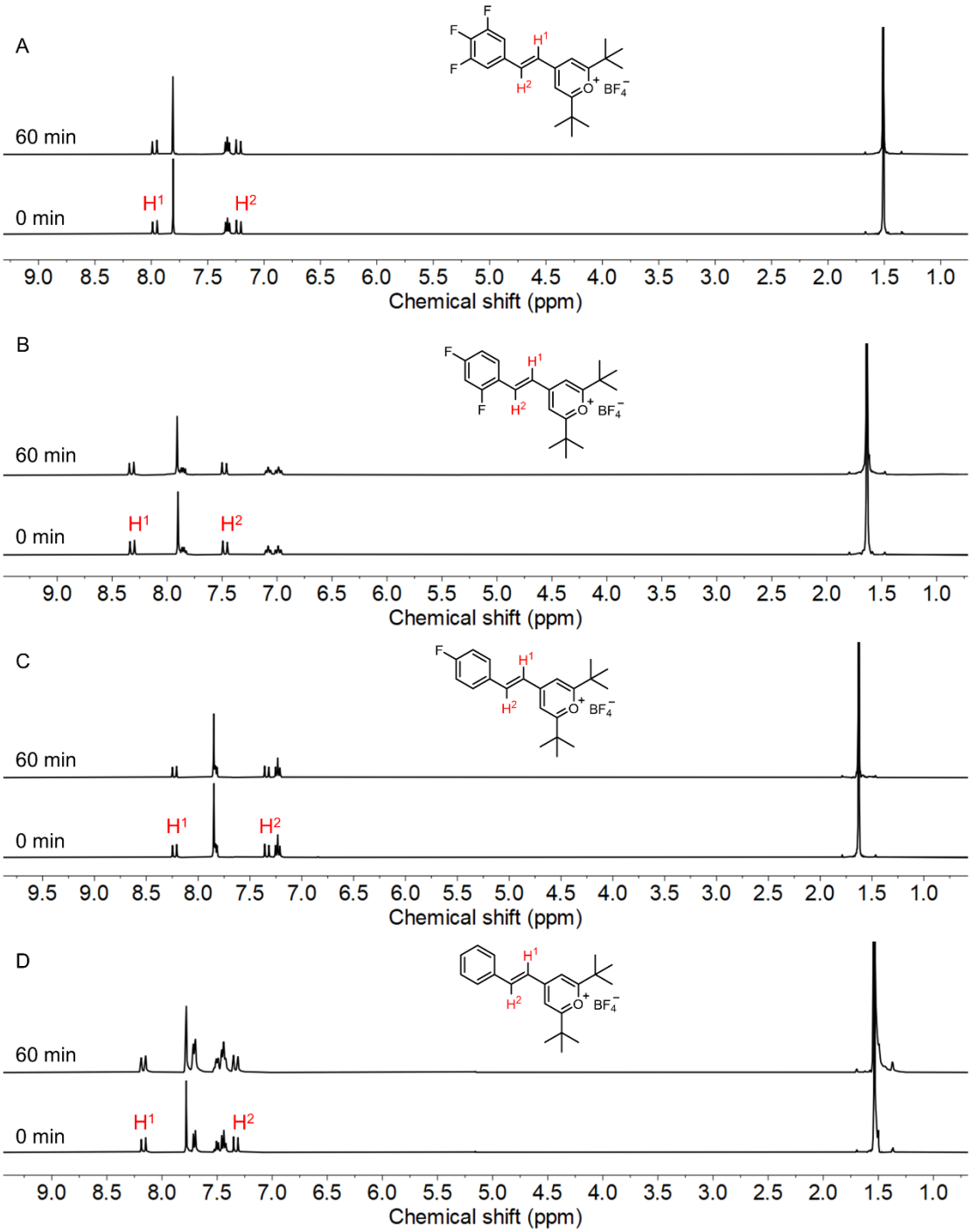

Figure S30. ^{1}H NMR spectra of **345FSPyL** (A), **24FSPyL** (B), **4FSPyL** (C) and **SPyL** (D) in TFA-*d* (400 MHz) before and after irradiation of the microcrystals with 365 nm light (5 W) for 60 min.

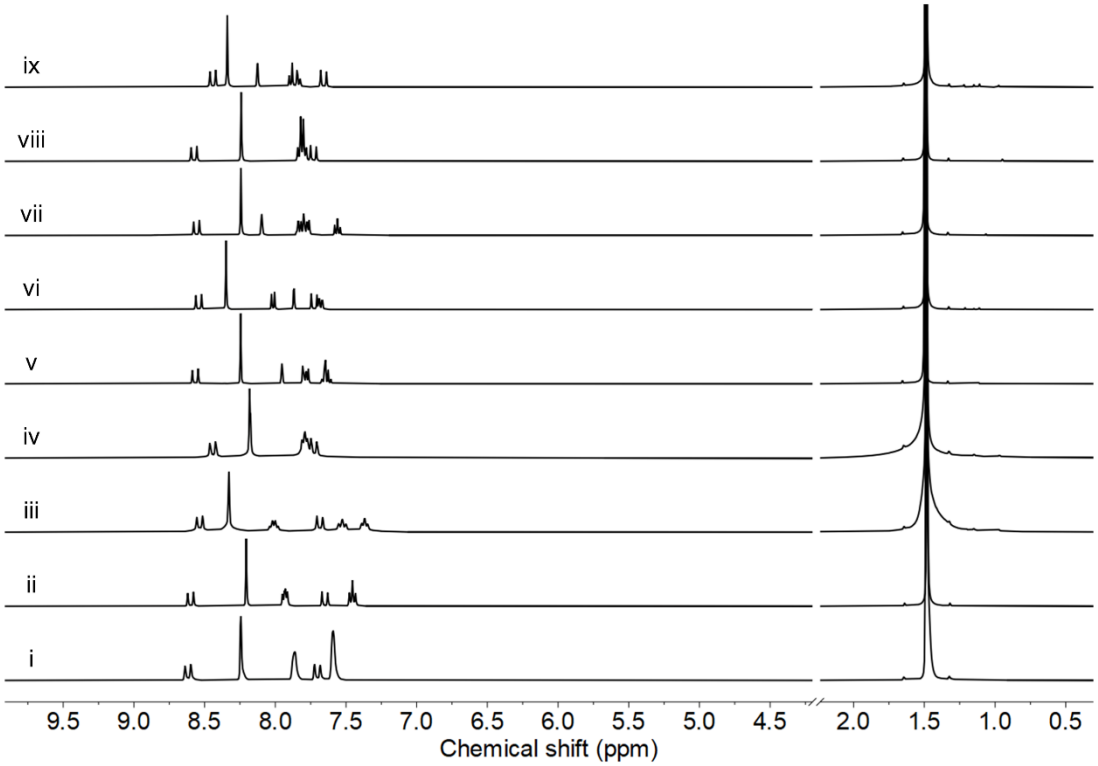

Figure S31. ^{1}H NMR spectra of **SPyL** (i), **4FSPyL** (ii), **24FSPyL** (iii), **345FSPyL** (iv), **3ClSPyL** (v), **24ClSPyL** (vi), **3BrSPyL** (vii), **4BrSPyL** (viii) and **24BrSPyL** (ix) after irradiation of the microcrystals with medium mercury lamp (100 W) for 60 min, followed by dissolving in TFA-*d* (400 MHz).

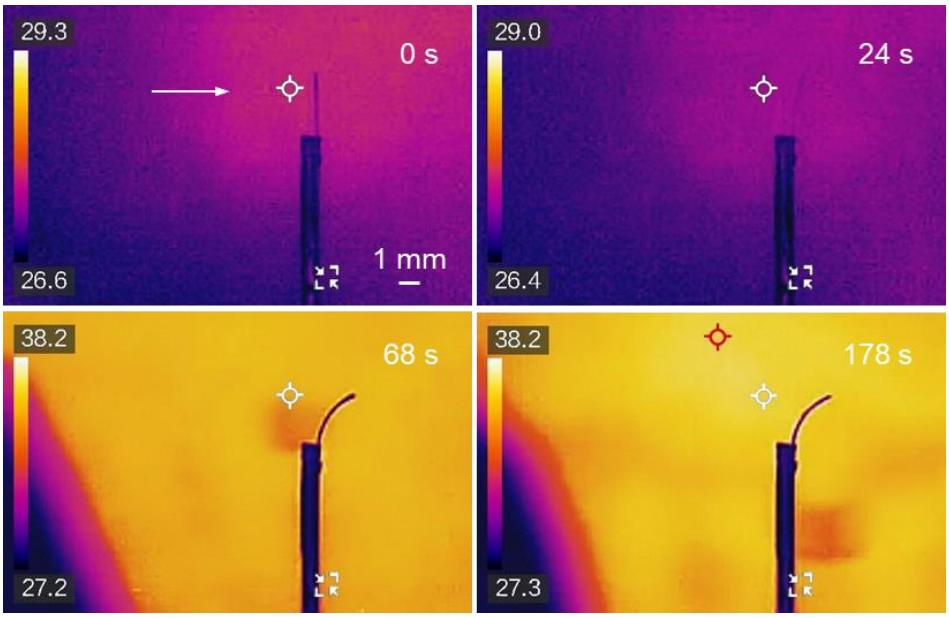

Figure S32. Thermal imaging showing the photoinduced bending of the needle-like crystal of **35ClSPyL** upon irradiation with 365 nm light (5 W) from the left side. The images recorded at 68 s and 178 s were shot by using hand as background for clarity.

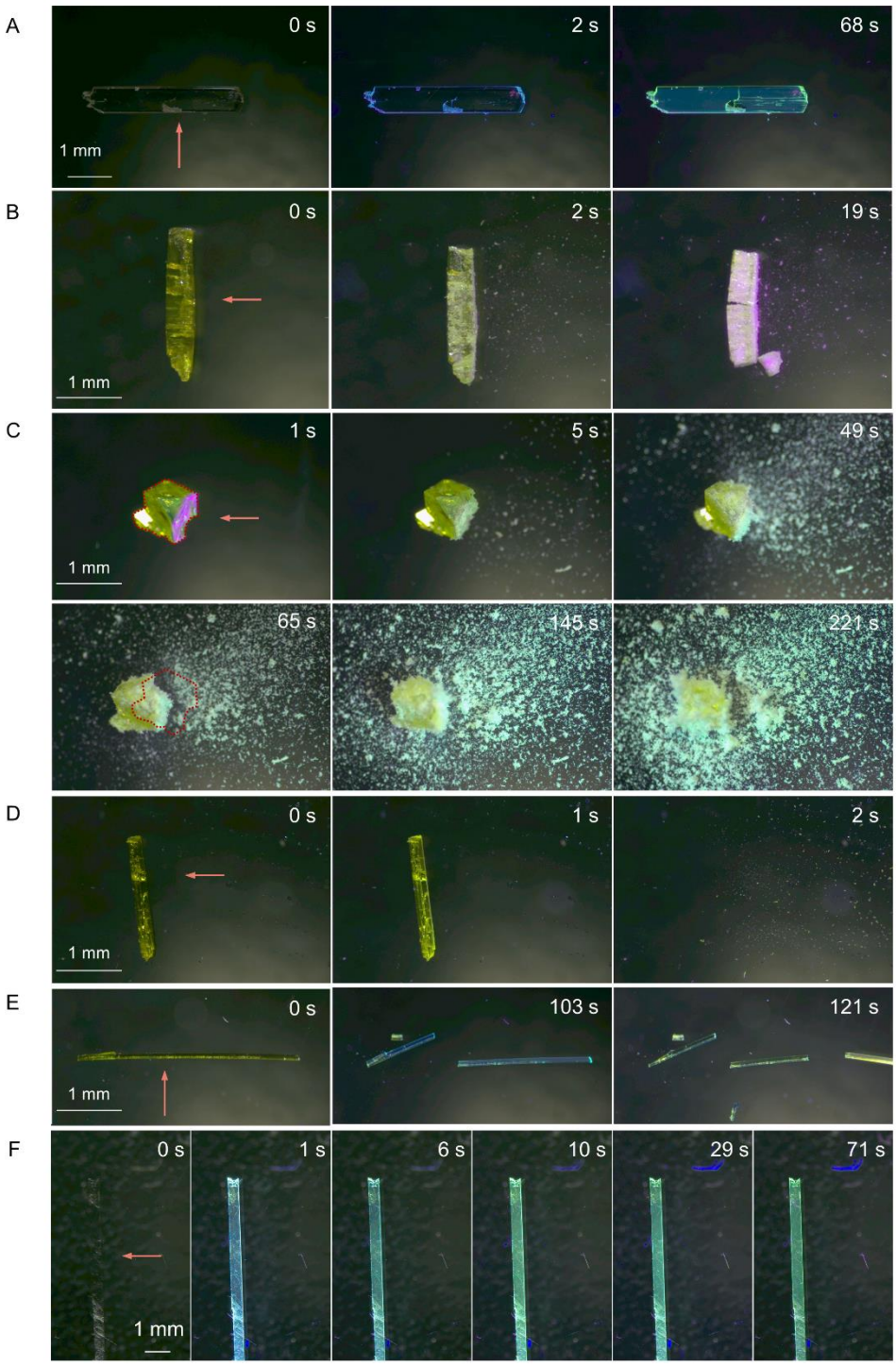

Figure S33. Optical microscopic photographs of the ribbon-like crystal of **35BrSPyL** (A, photoinduced cracking), the bulk crystal of **35FSPyL** (B, photoinduced cracking and photosalient effect) , the block crystal of **2FSPyL** (C, photosalient effect), the rod-like crystal of **3FSPyL** (D, photoinduced jumping), the rod-like crystal of **2ClSPyL** (E, photoinduced breaking) and sheet-like crystal of **4ClSPyL** (F, motionless) exposed to upon irradiation by 365 nm light (5 W) for different times. The arrows indicate the irradiation directions.

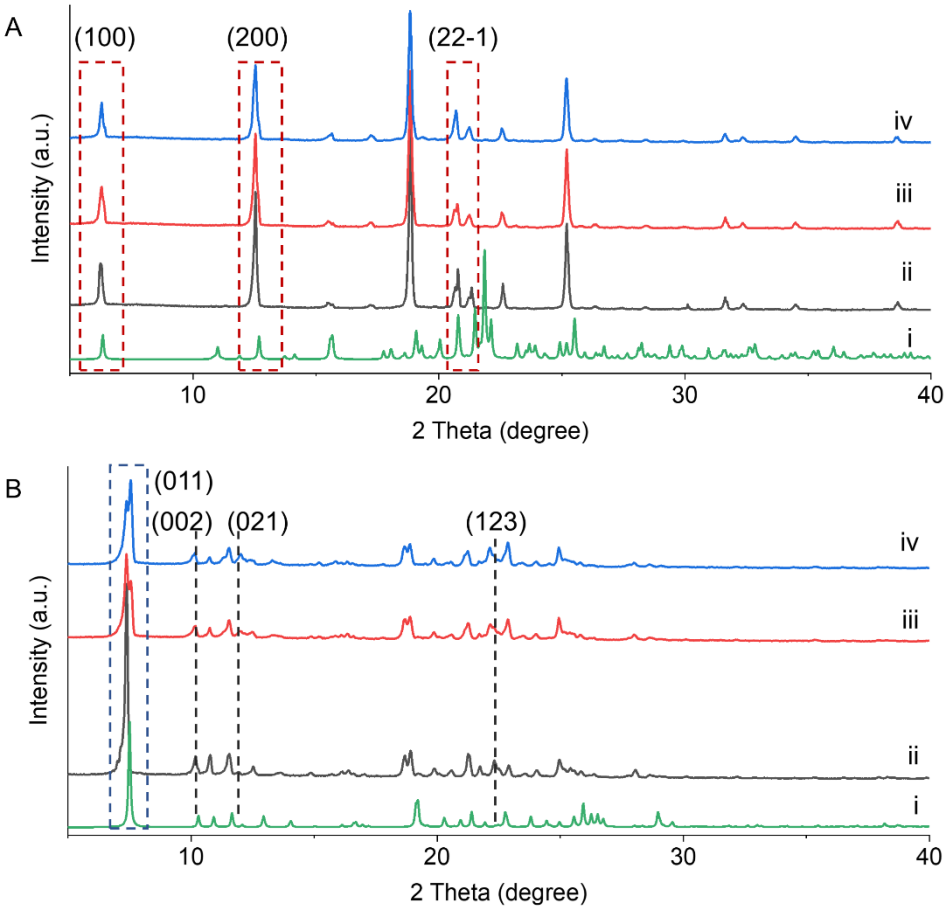

Figure S34. (A) PXRD pattern simulated from the single crystal data of **35BrSPyL** (i) and PXRD patterns of the microcrystals of **35BrSPyL** before (ii) and after in-situ irradiation by 365 nm light for 1 min (iii) and for 5 min (iv); (B) PXRD pattern simulated from the single crystal data of **35FSPyL** (i); PXRD patterns of the microcrystals of **35FSPyL** before (ii) and after in-situ irradiation by 365 nm light for 1 min (iii) and for 5 min (iv).

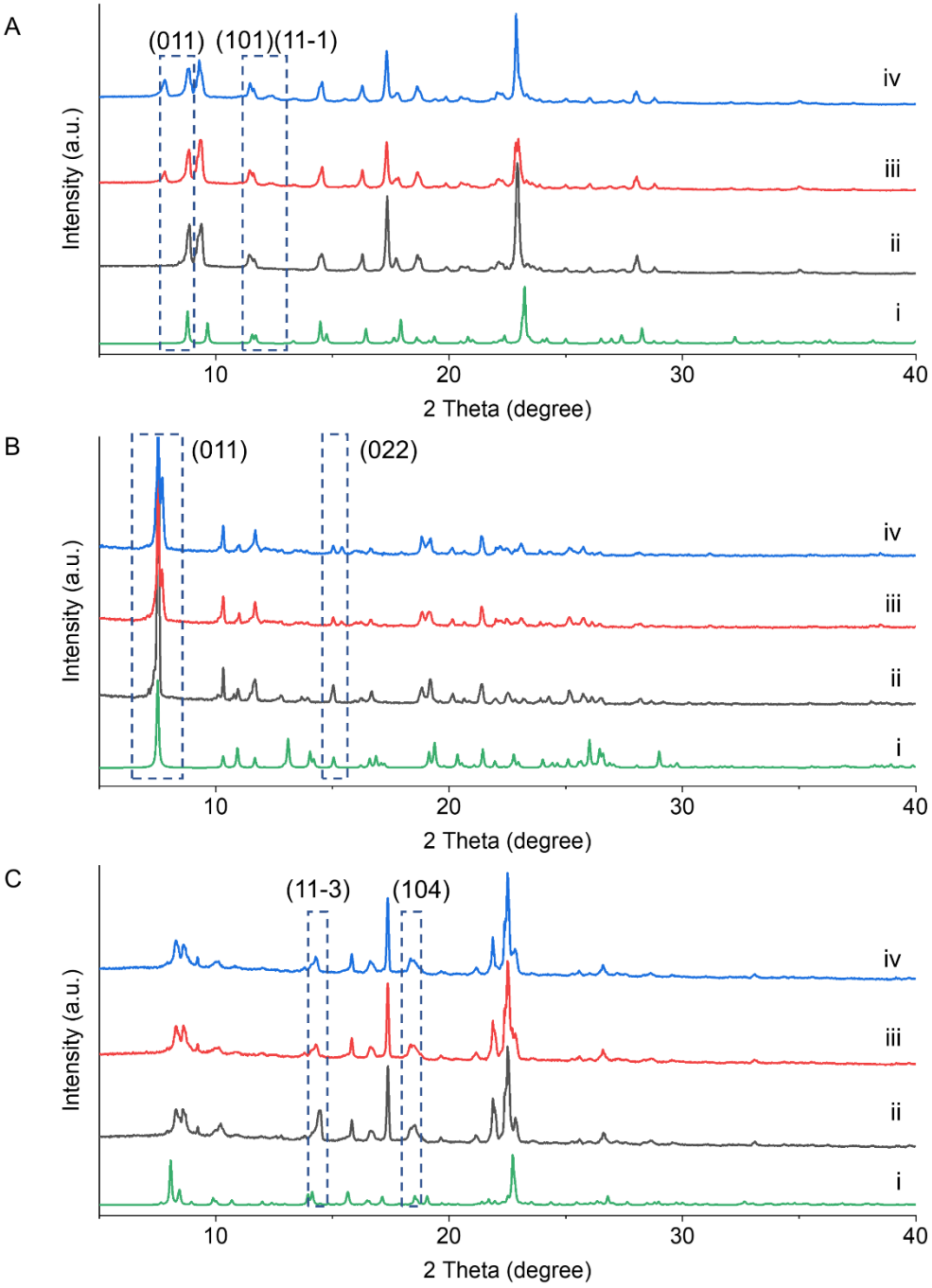

Figure S35. Simulated PXRD patterns (i) based on the single crystal data of **2FSPyL** (A), **3FSPyL** (B) and **2ClSPyL** (C) and PXRD patterns of the corresponding microcrystals before (ii) and after in-situ irradiation by 365 nm light for 1 min (iii) and 5 min (iv).

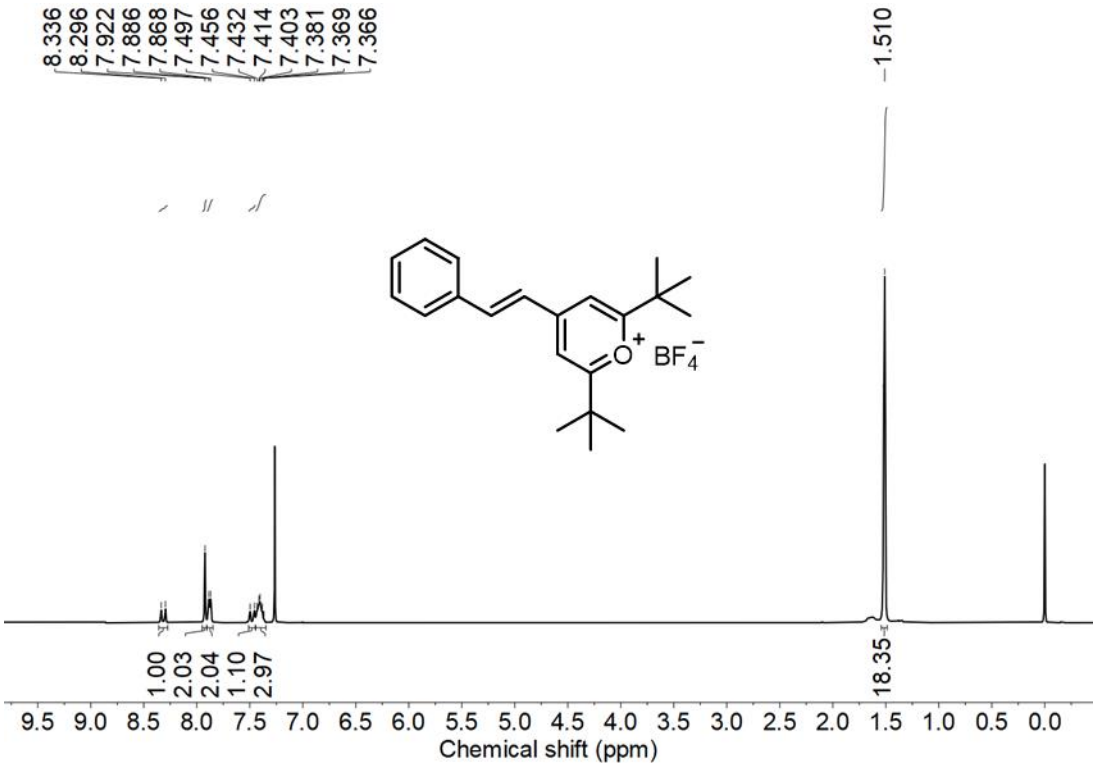

Figure S36. ^{1}H NMR spectrum of **SPyL** in $CDCl_3$ (400 MHz).

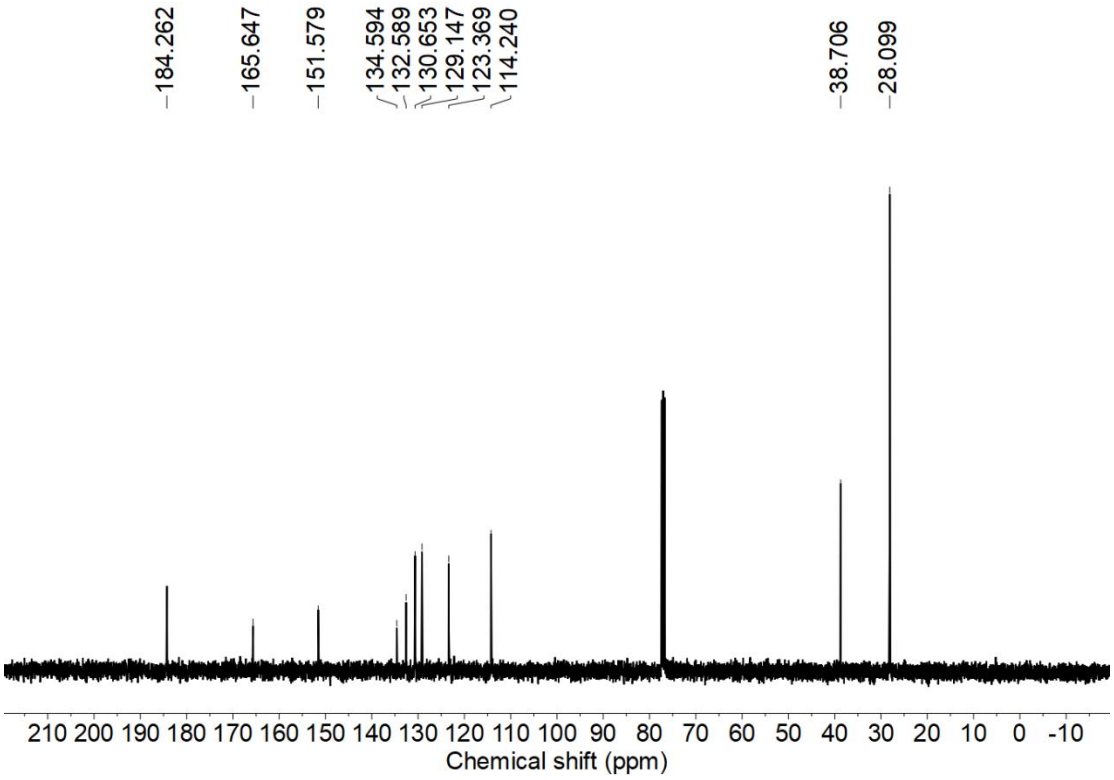

Figure S37. ^{13}C NMR spectrum of **SPyL** in $CDCl_3$ (100 MHz).

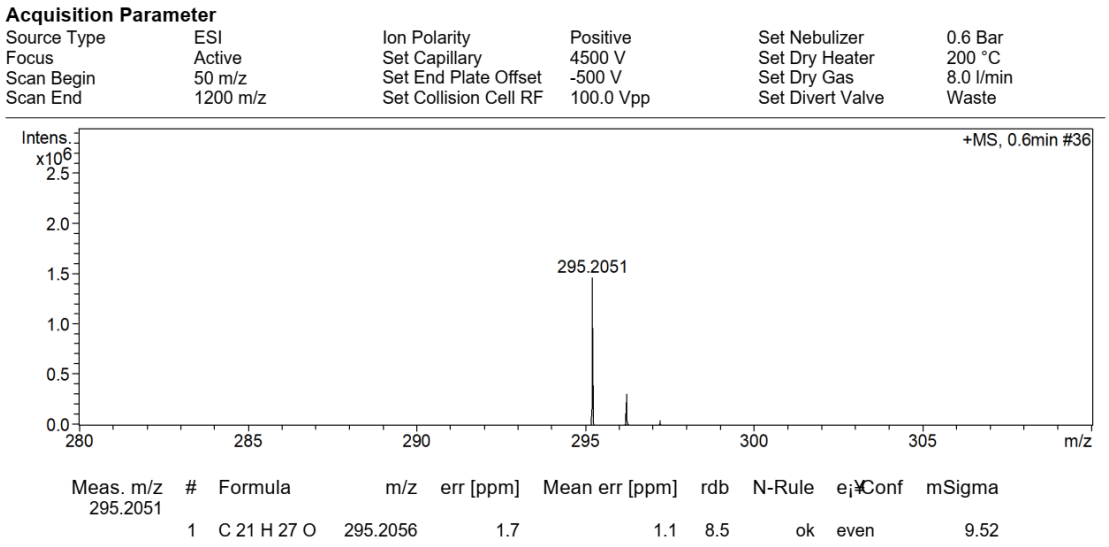

Figure S38. HRMS spectrum of **SPyL**.

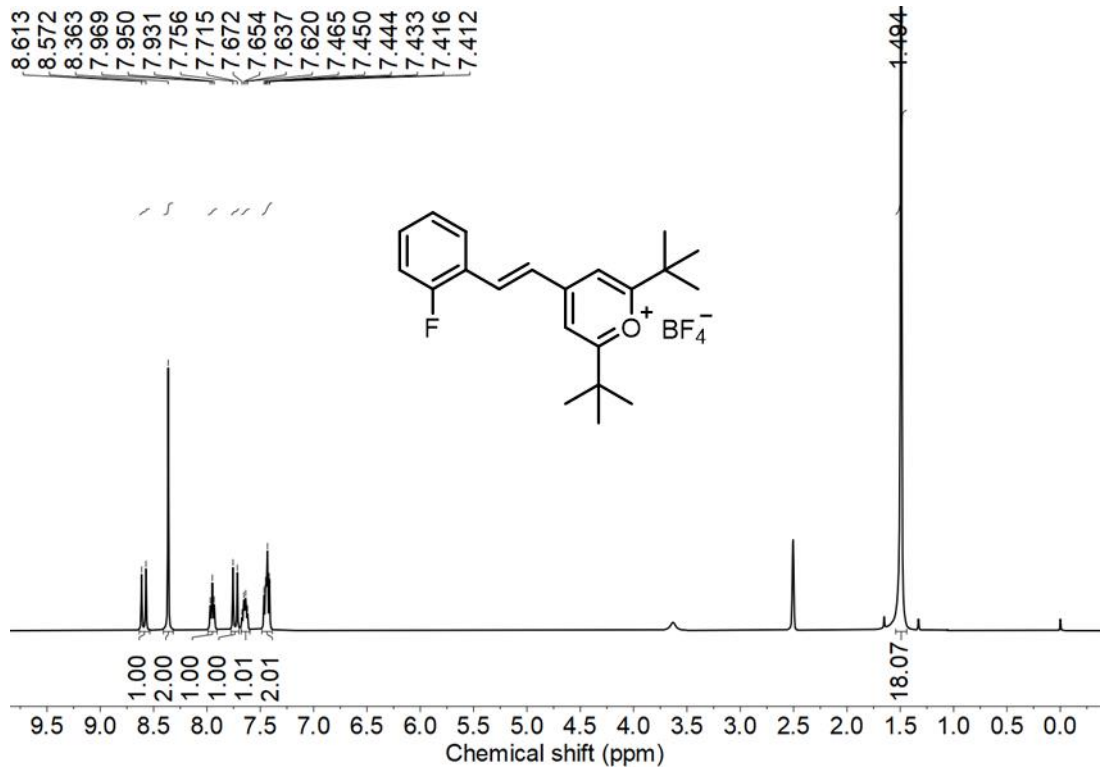

Figure S39. ^{1}H NMR spectrum of **2FSPyL** in DMSO-d_6 (400 MHz).

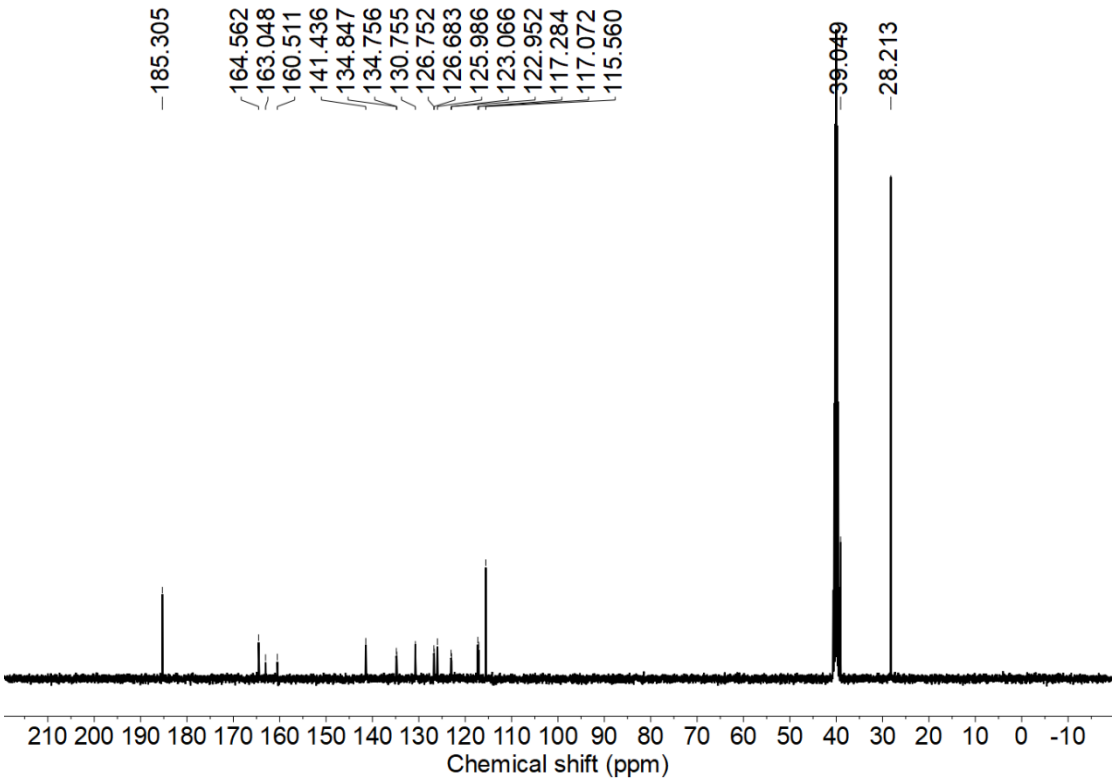

Figure S40. ^{13}C NMR spectrum of **2FSPyL** in DMSO-d_6 (100 MHz).

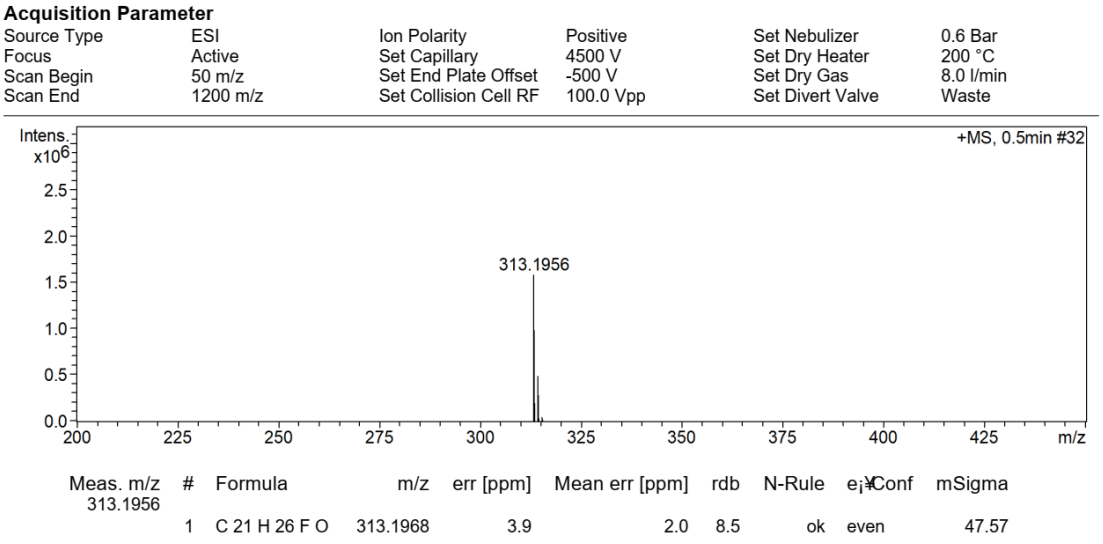

Figure S41. HRMS spectrum of **2FSPyL**.

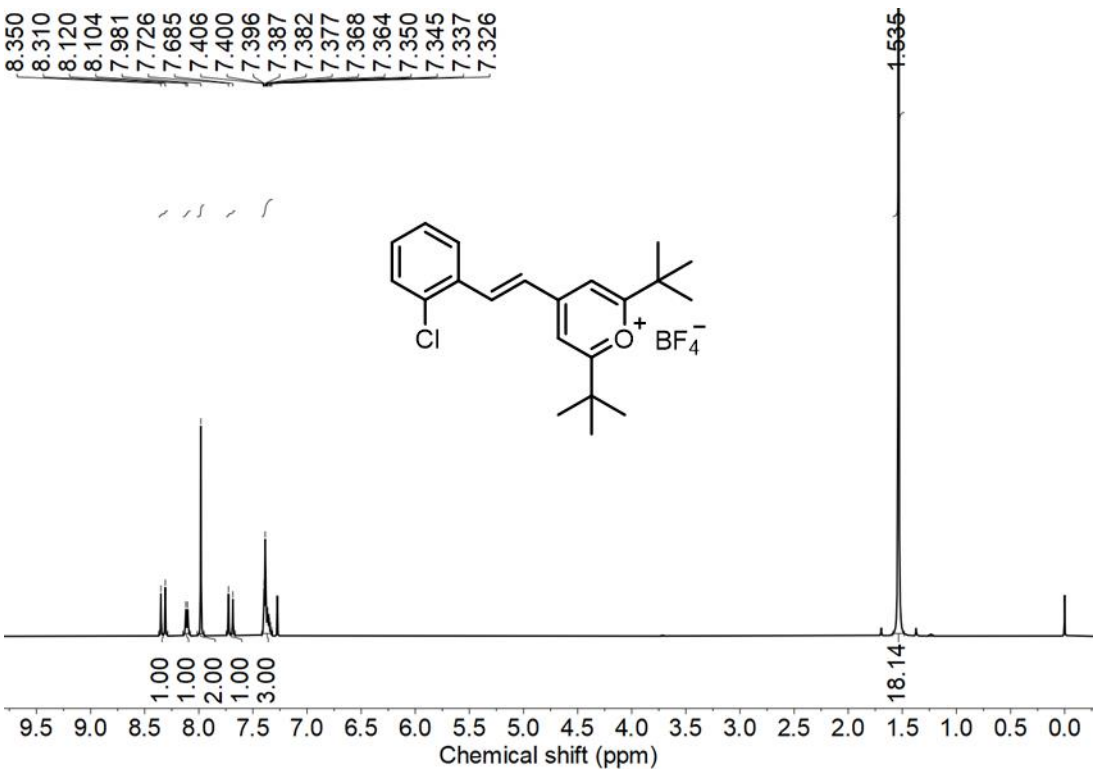

Figure S42. ^{1}H NMR spectrum of **2ClSPyL** in $CDCl_3$ (400 MHz).

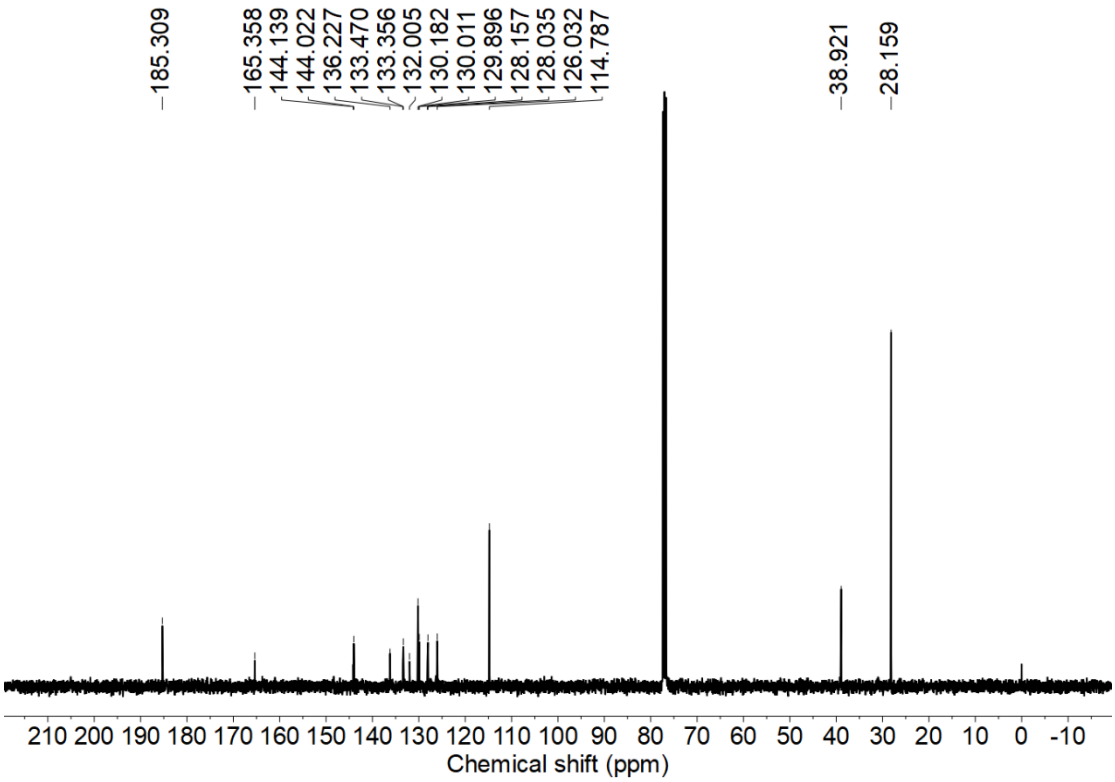

Figure S43. ^{13}C NMR spectrum of **2ClSPyL** in $CDCl_3$ (100 MHz).

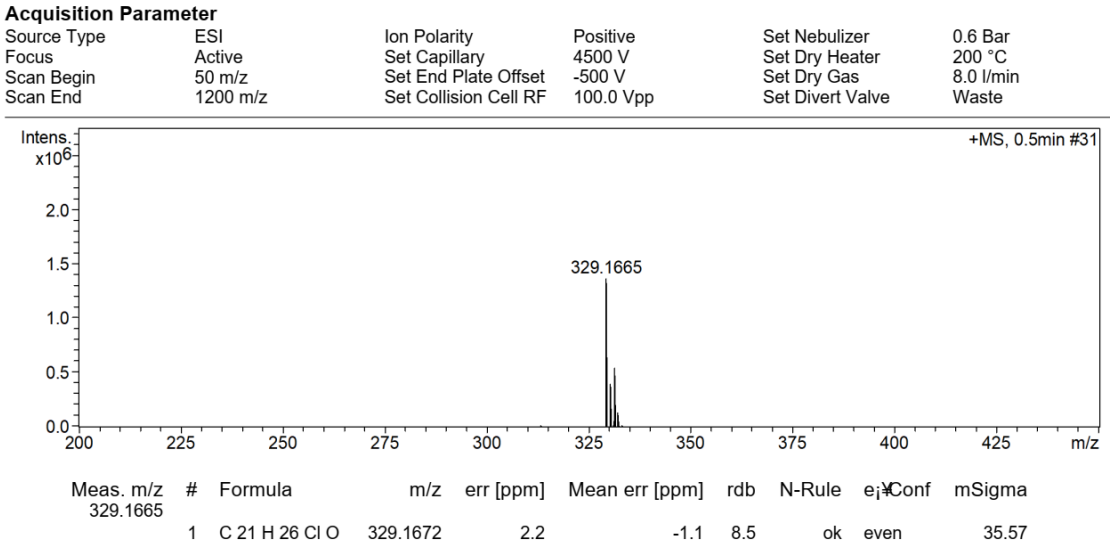

Figure S44. HRMS spectrum of **2ClSPyL**.

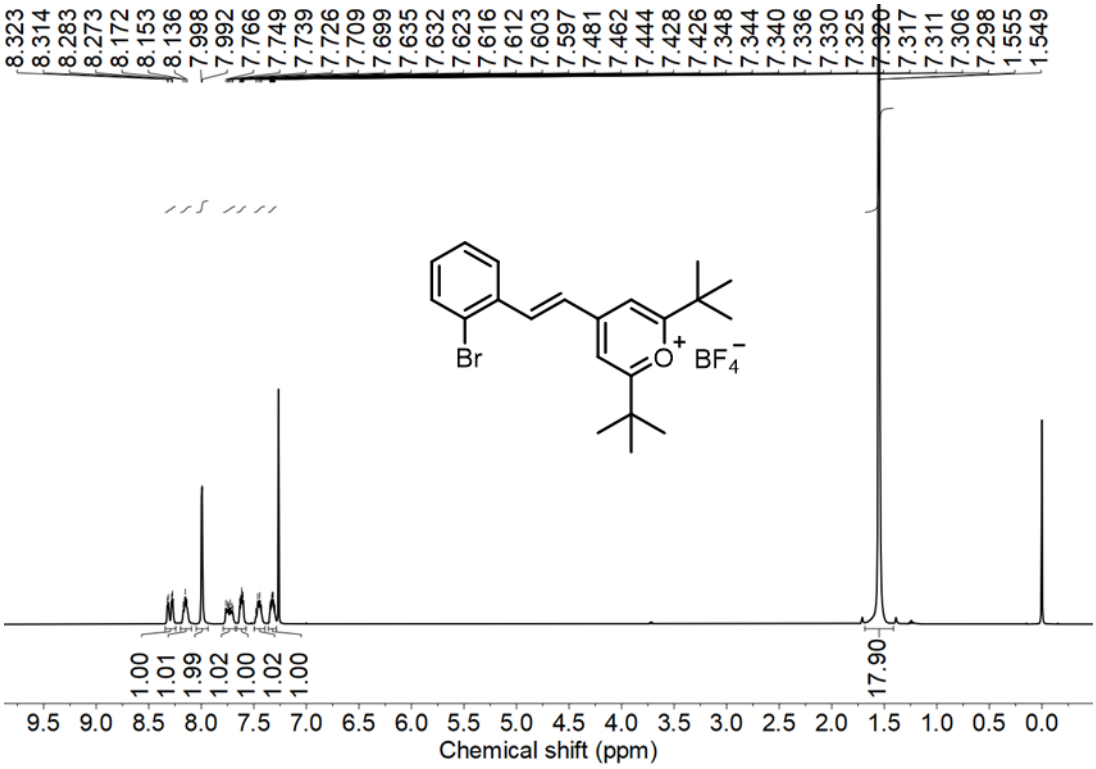

Figure S45. ^{1}H NMR spectrum of **2BrSPyL** in $CDCl_3$ (400 MHz).

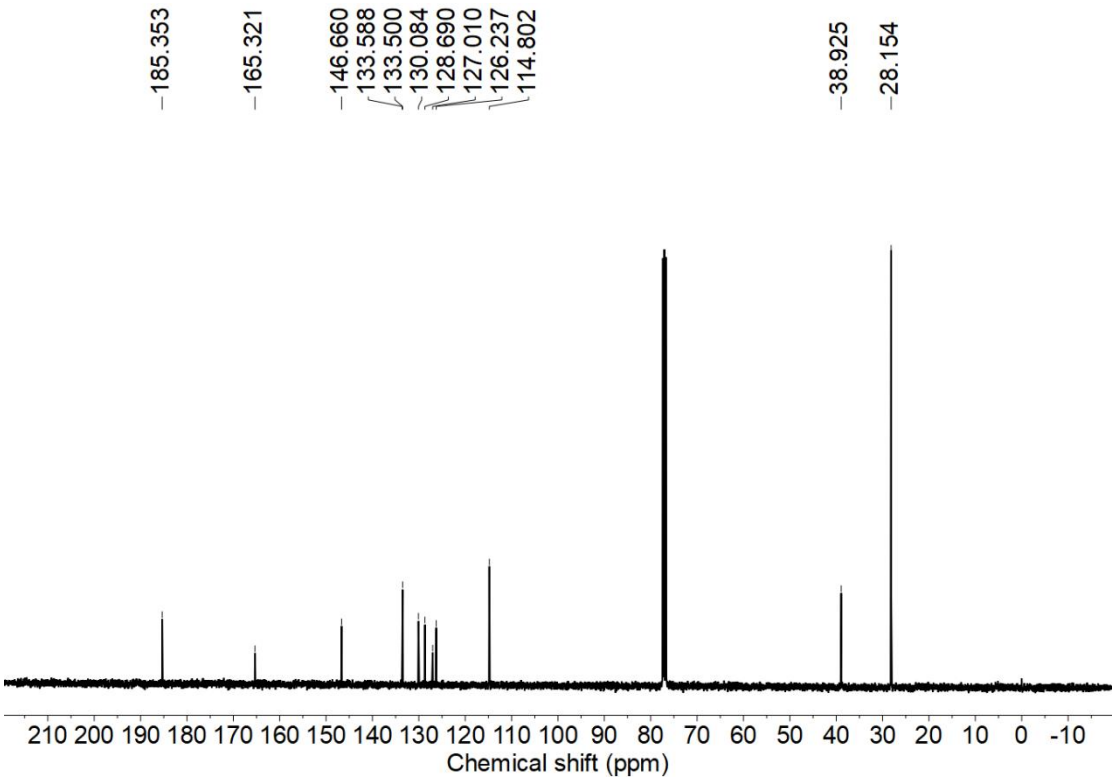

Figure S46. ^{13}C NMR spectrum of **2BrSPyL** in $CDCl_3$ (100 MHz).

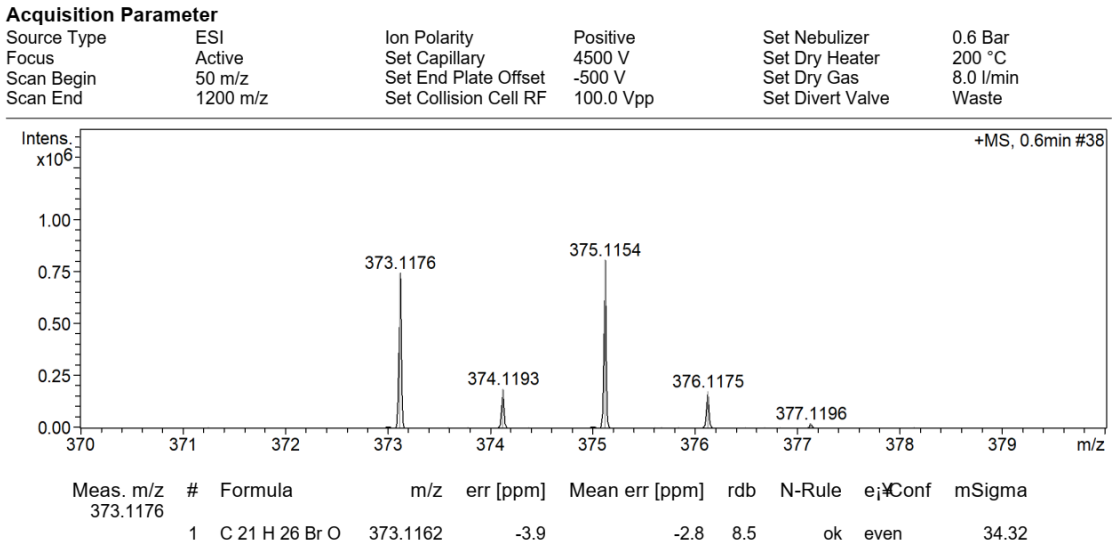

Figure S47. HRMS spectrum of **2BrSPyL**.

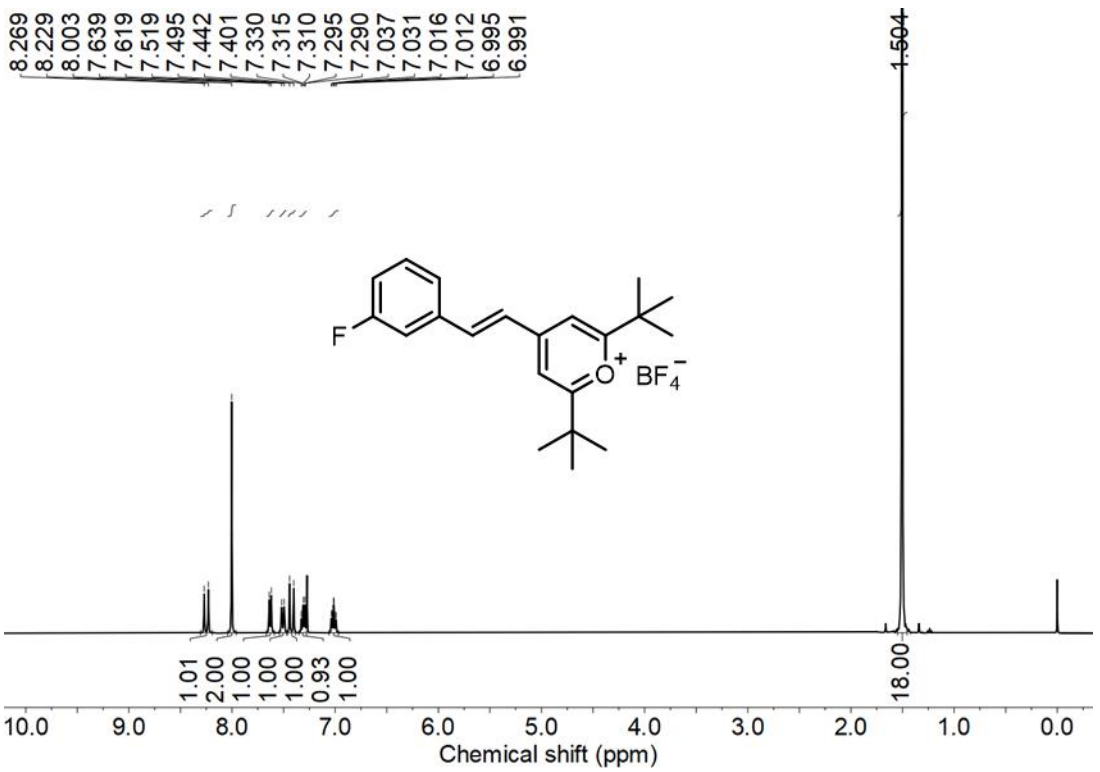

Figure S48. ^{1}H NMR spectrum of **3FSPyL** in $CDCl_3$ (400 MHz).

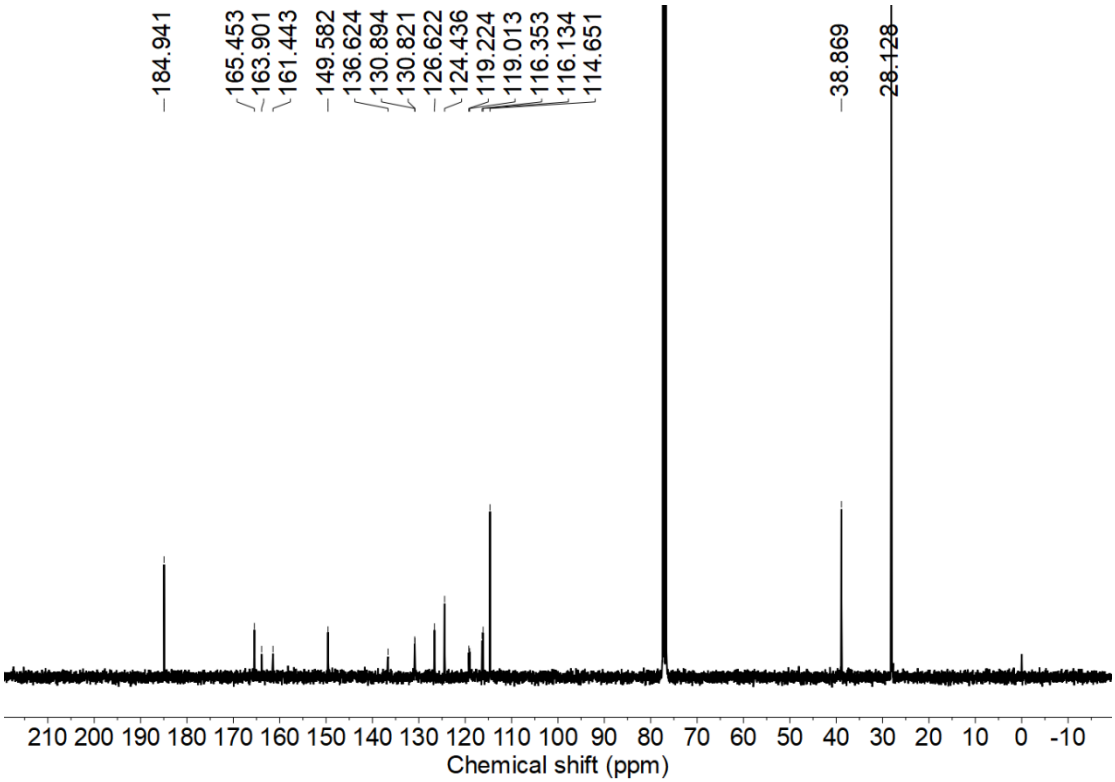

Figure S49. ^{13}C NMR spectrum of **3FSPyL** in $CDCl_3$ (100 MHz).

Acquisition Parameter

Source Type	ESI	Ion Polarity	Positive	Set Nebulizer	0.6 Bar
Focus	Active	Set Capillary	4500 V	Set Dry Heater	200 °C
Scan Begin	50 m/z	Set End Plate Offset	-500 V	Set Dry Gas	8.0 l/min
Scan End	1200 m/z	Set Collision Cell RF	100.0 Vpp	Set Divert Valve	Waste

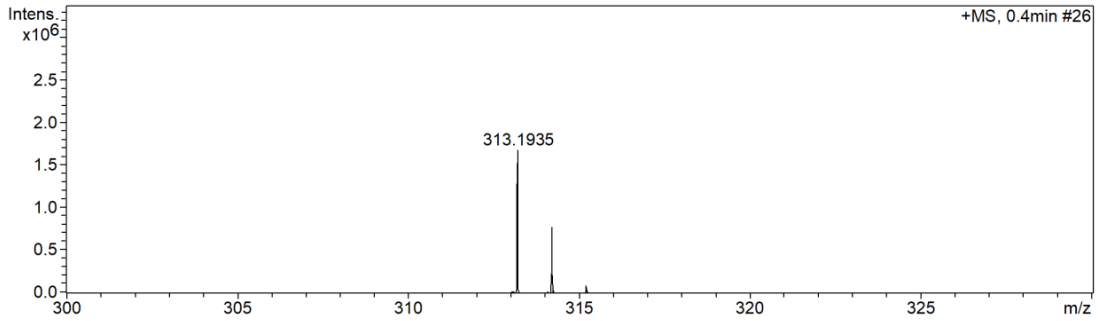

Meas. m/z	#	Formula	m/z	err [ppm]	Mean err [ppm]	rdb	N-Rule	e¡¥Conf	mSigma
313.1935									
	1	C 21 H 26 F O	313.1968	10.3	6.3	8.5	ok	even	134.04

Figure S50. HRMS spectrum of **3FSPyL**.

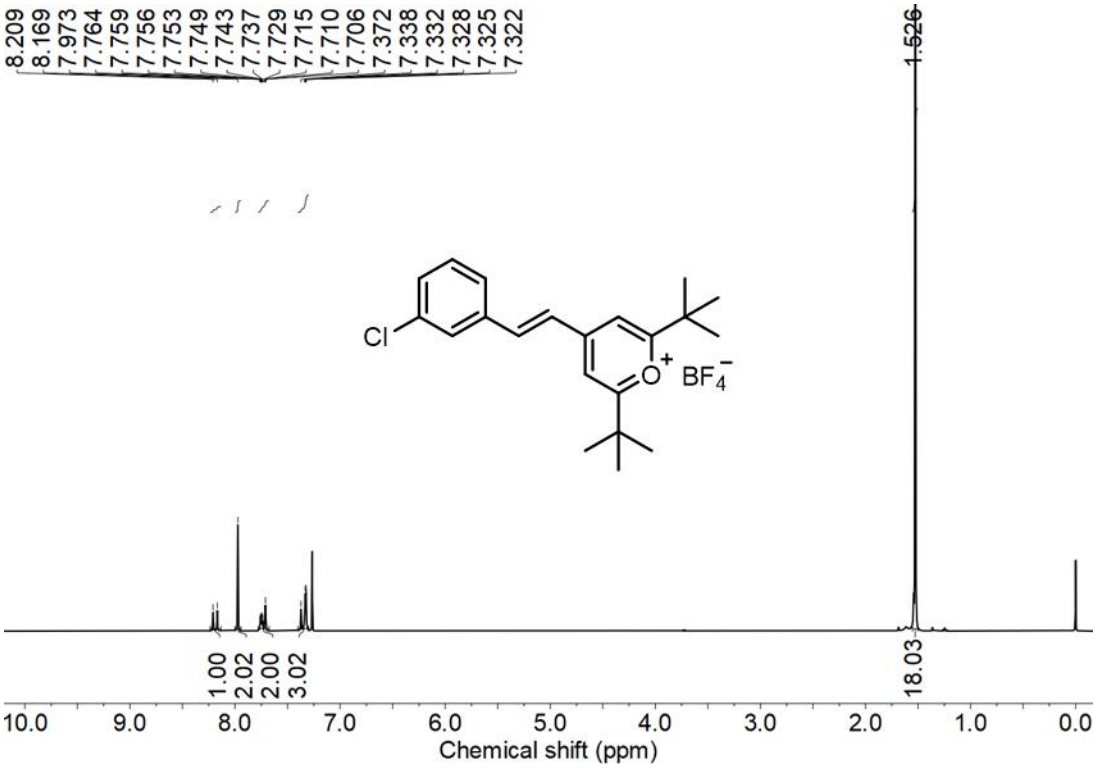

Figure S51. ^{1}H NMR spectrum of **3ClSPyL** in $CDCl_3$ (400 MHz).

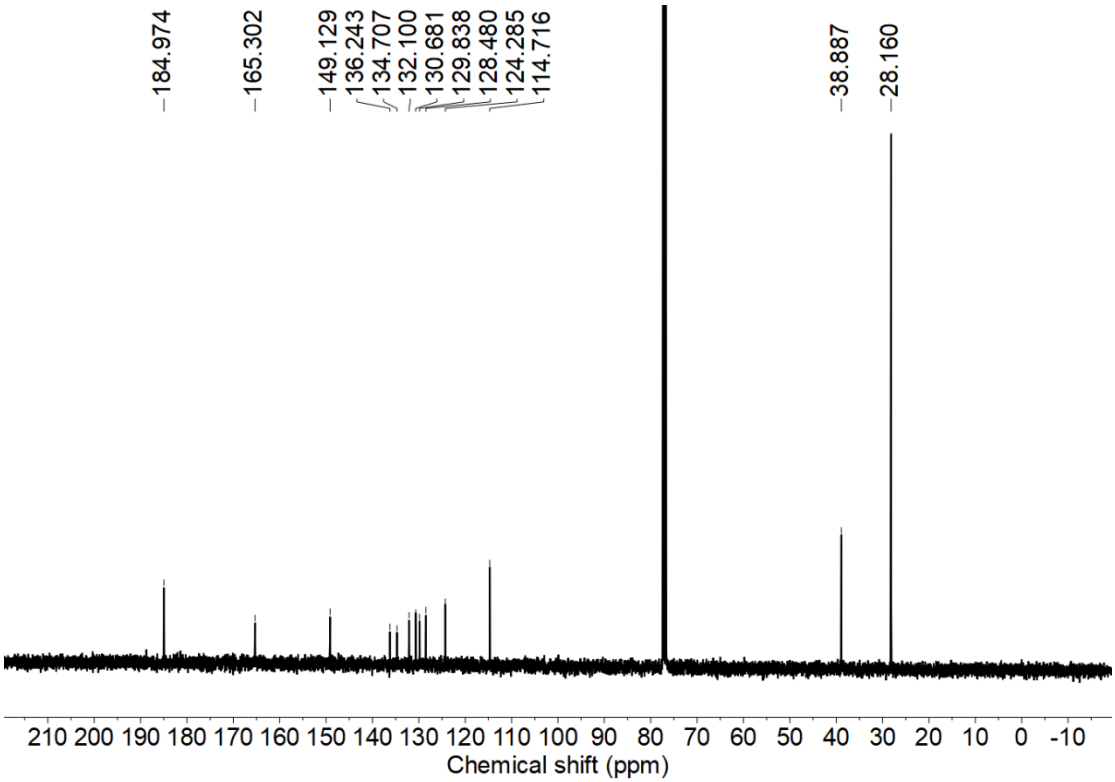

Figure S52. ^{13}C NMR spectrum of **3ClSPyL** in $CDCl_3$ (100 MHz).

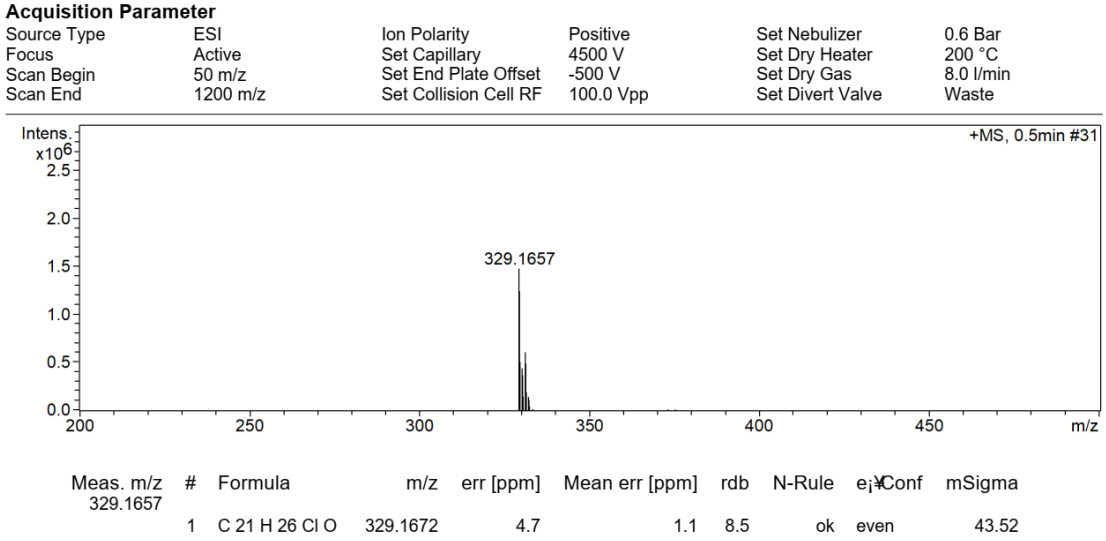

Figure S53. HRMS spectrum of **3ClSPyL**.

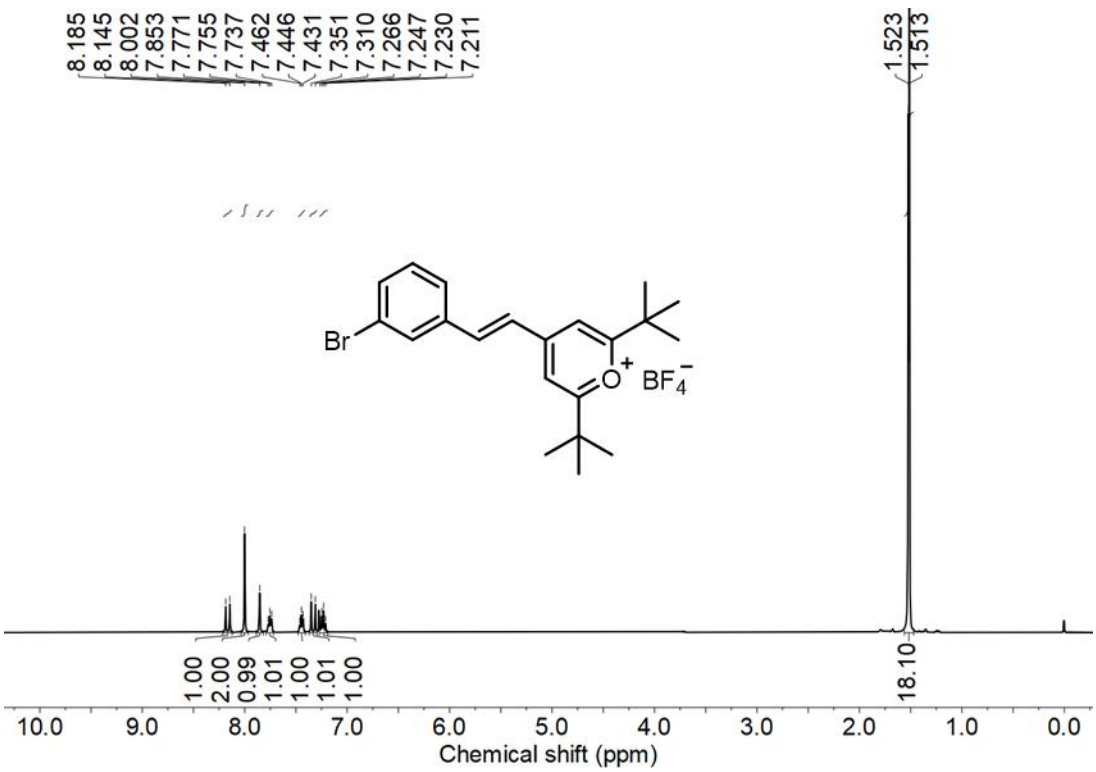

Figure S54. ^{1}H NMR spectrum of **3BrSPyL** in $CDCl_3$ (400 MHz).

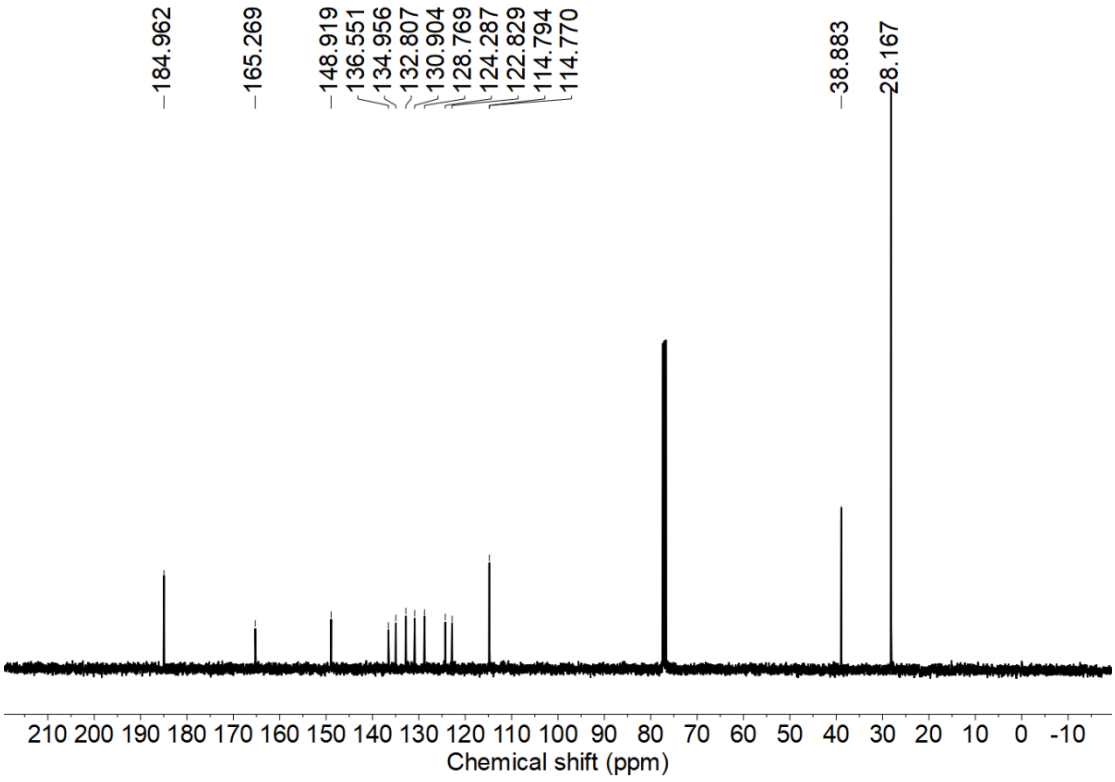

Figure S55. ^{13}C NMR spectrum of **3BrSPyL** in $CDCl_3$ (100 MHz).

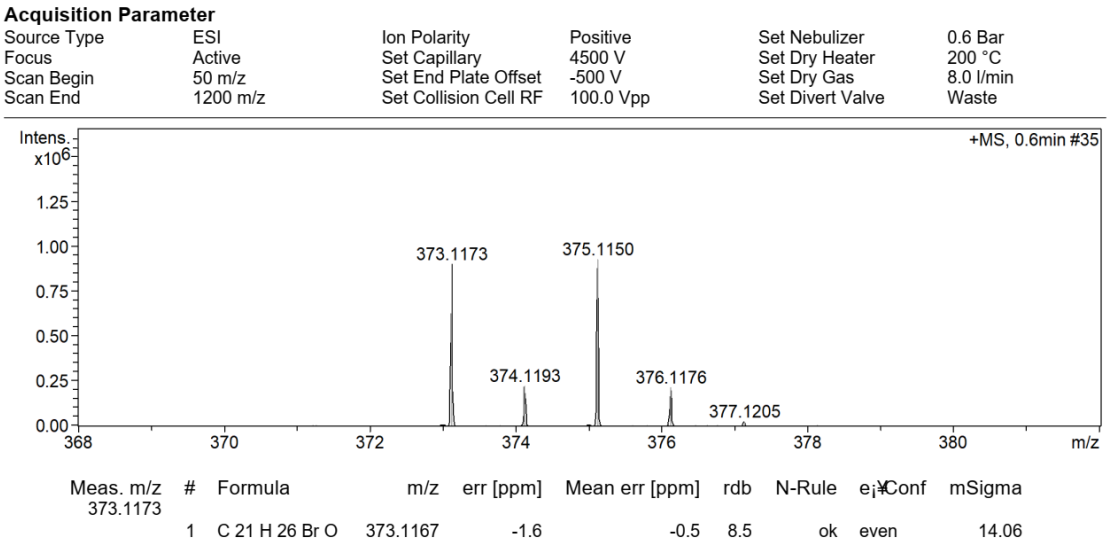

Figure S56. HRMS spectrum of **3BrSPyL**.

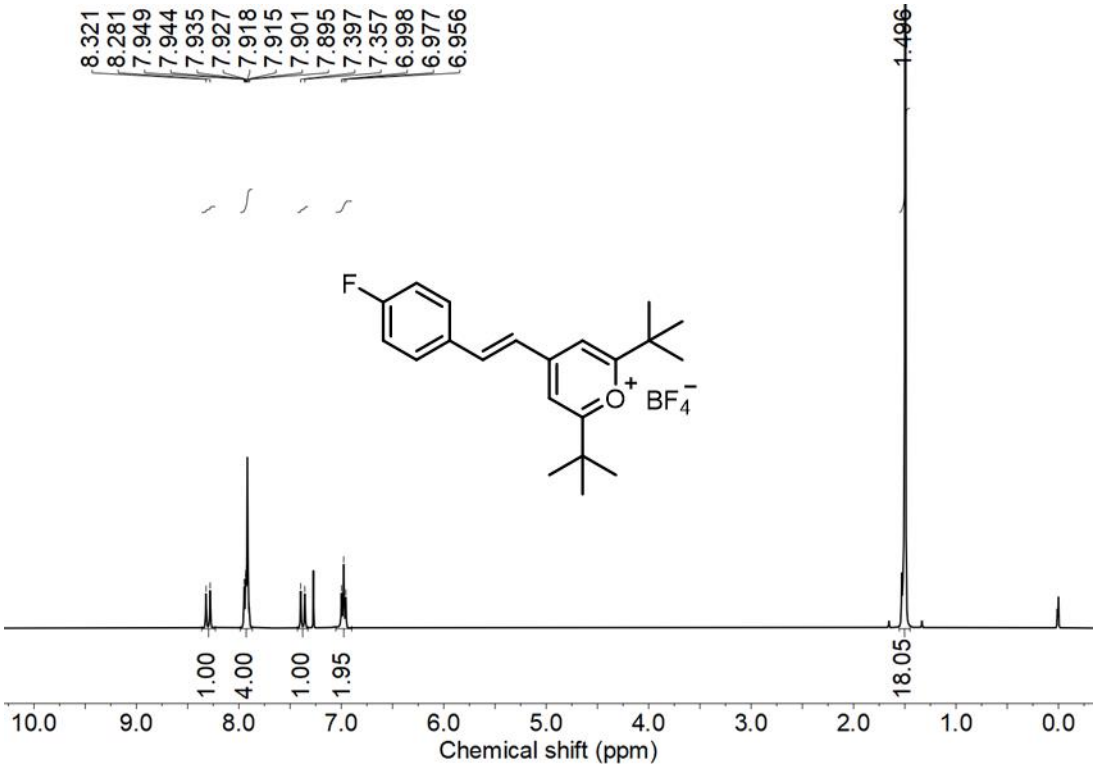

Figure S57. ^{1}H NMR spectrum of **4FSPyL** in $CDCl_3$ (400 MHz).

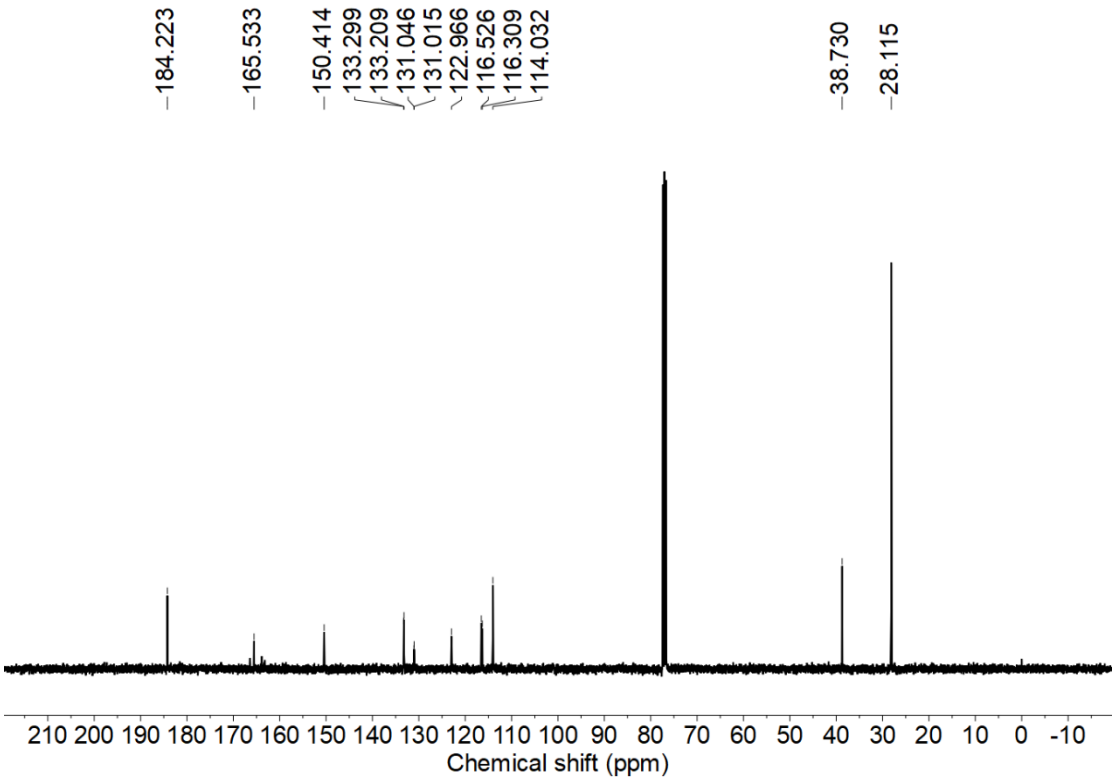

Figure S58. ^{13}C NMR spectrum of **4FSPyL** in $CDCl_3$ (100 MHz).

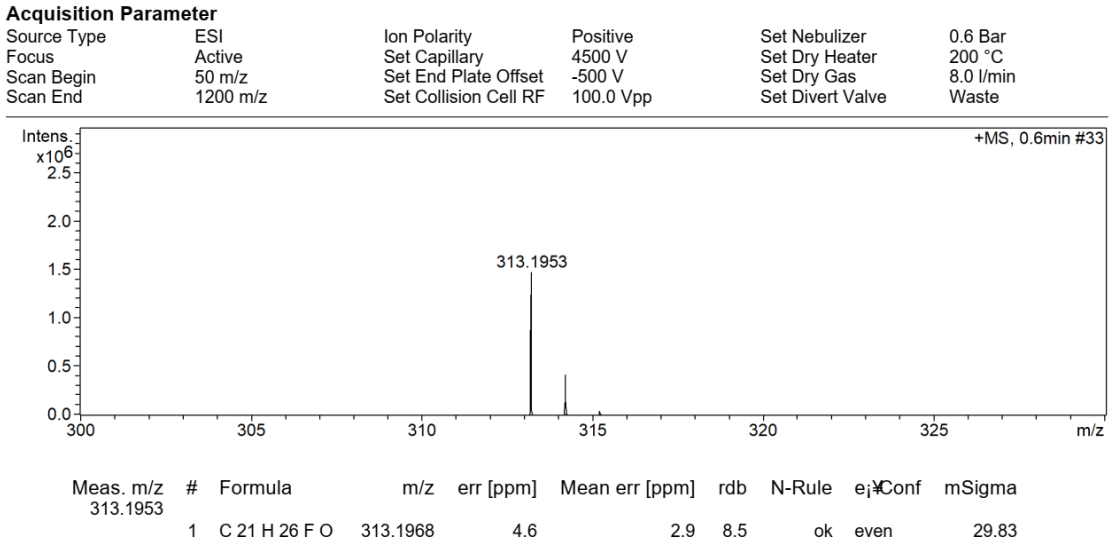

Figure S59. HRMS spectrum of **4FSPyL**.

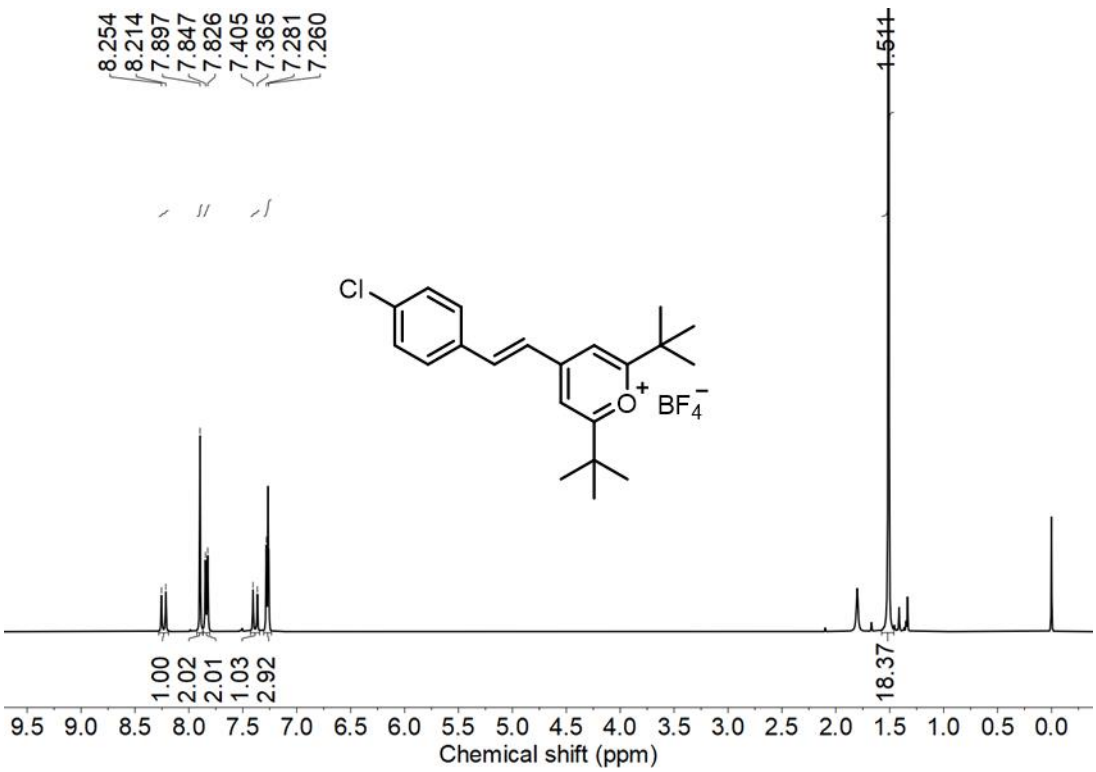

Figure S60. ^{1}H NMR spectrum of **4ClSPyL** in $CDCl_3$ (400 MHz).

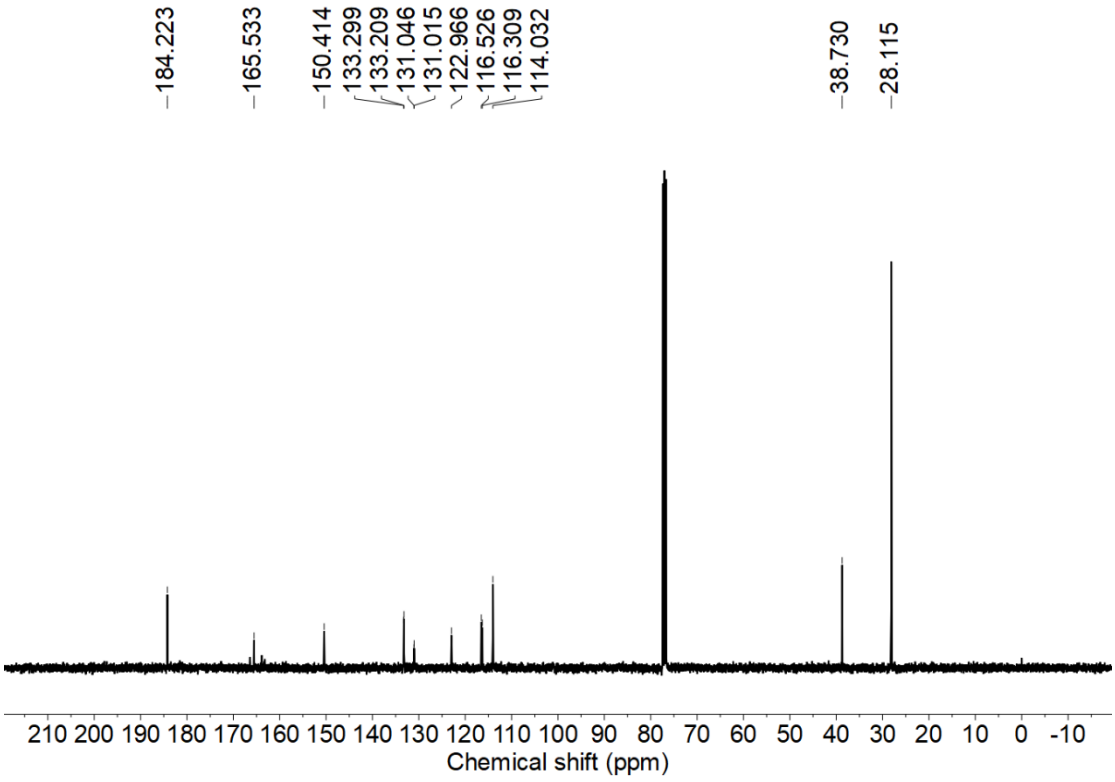

Figure S61. ^{13}C NMR spectrum of **4ClSPyL** in $CDCl_3$ (100 MHz).

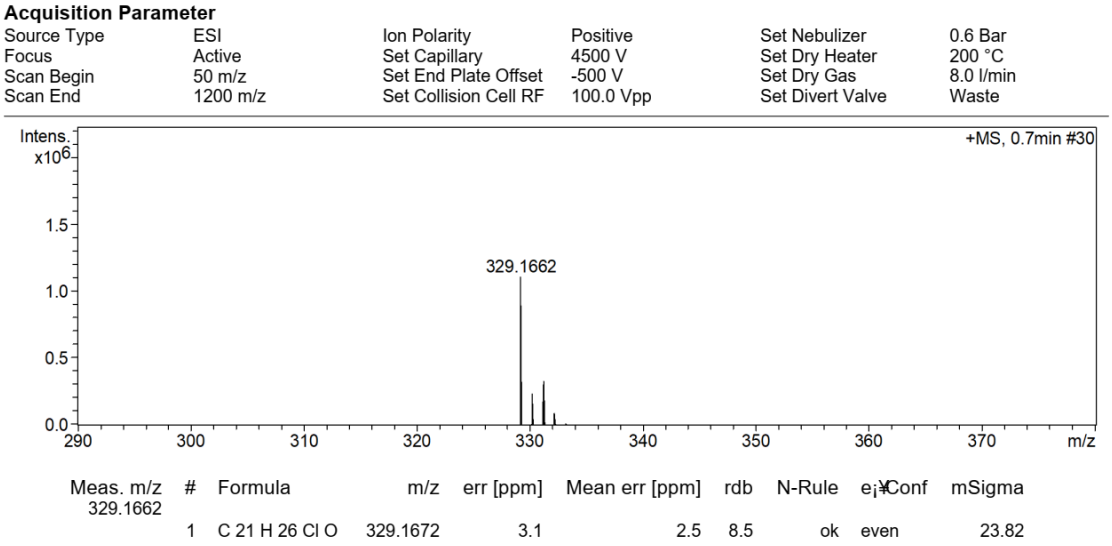

Figure S62. HRMS spectrum of **4ClSPyL**.

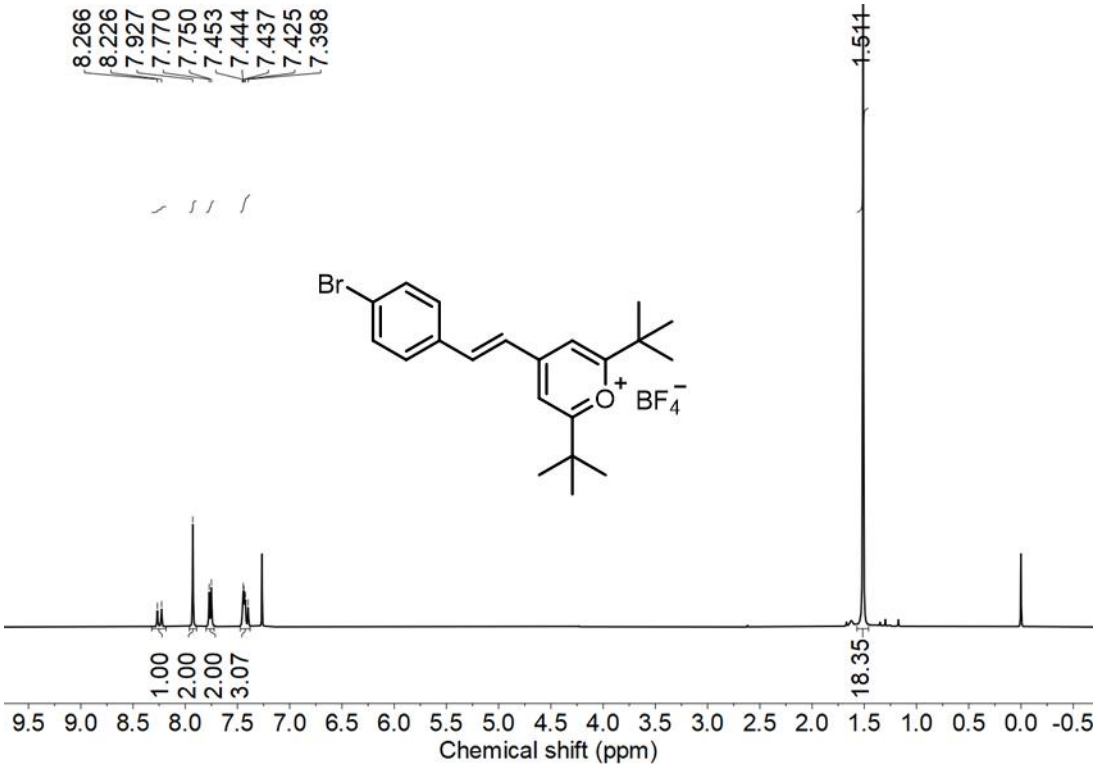

Figure S63. ^{1}H NMR spectrum of **4BrSPyL** in $CDCl_3$ (400 MHz).

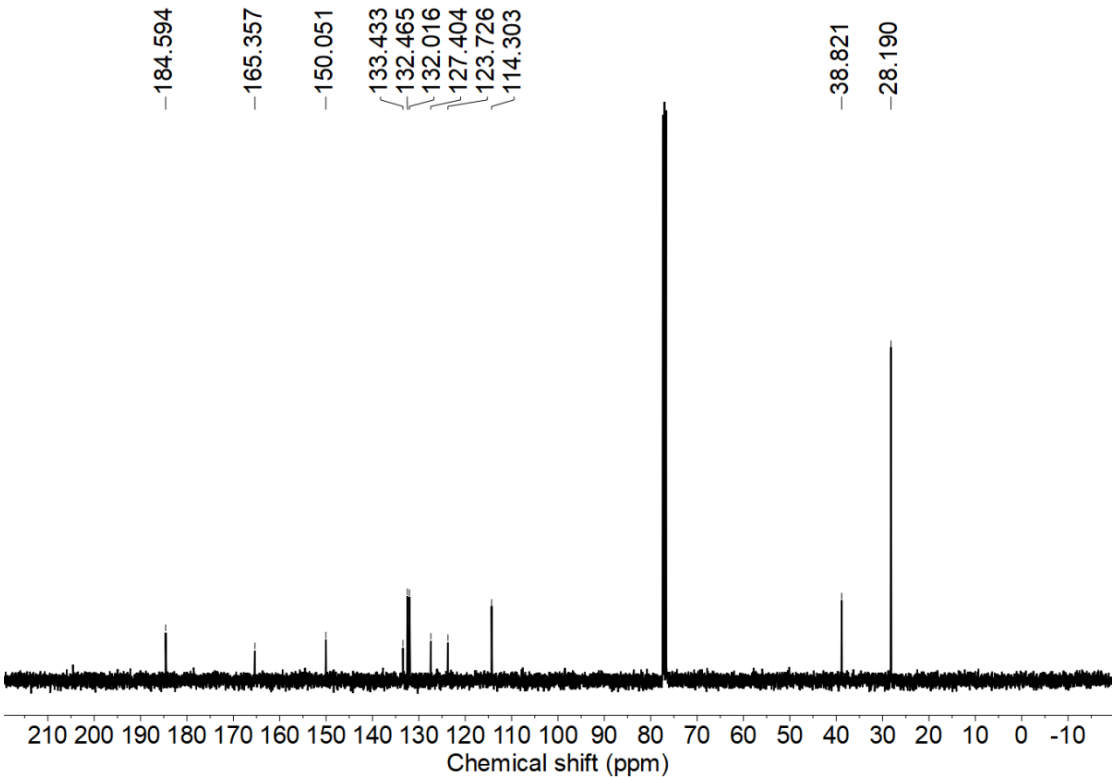

Figure S64. ^{13}C NMR spectrum of **4BrSPyL** in $CDCl_3$ (100 MHz).

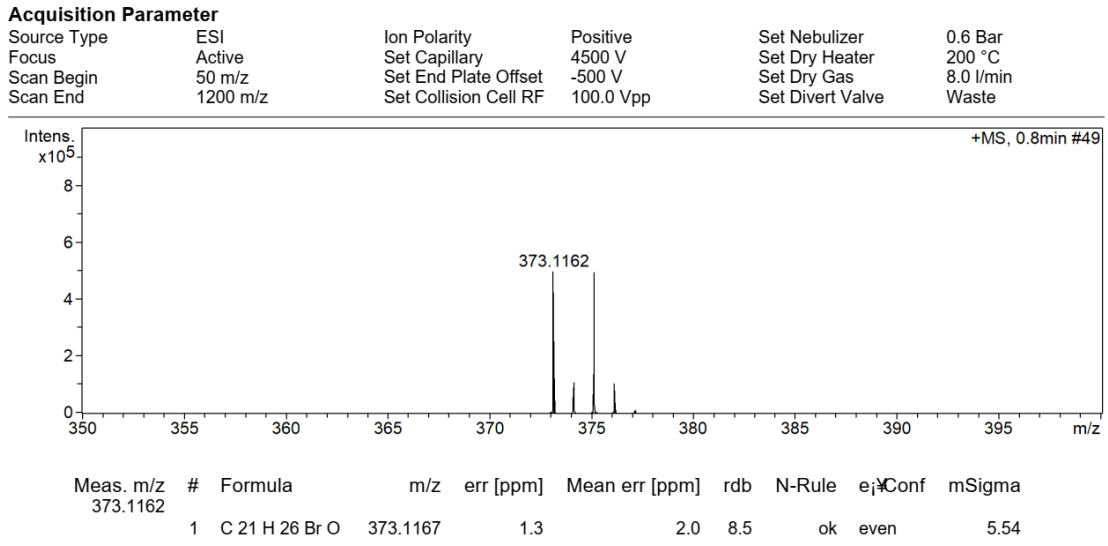

Figure S65. HRMS spectrum of **4BrSPyL**.

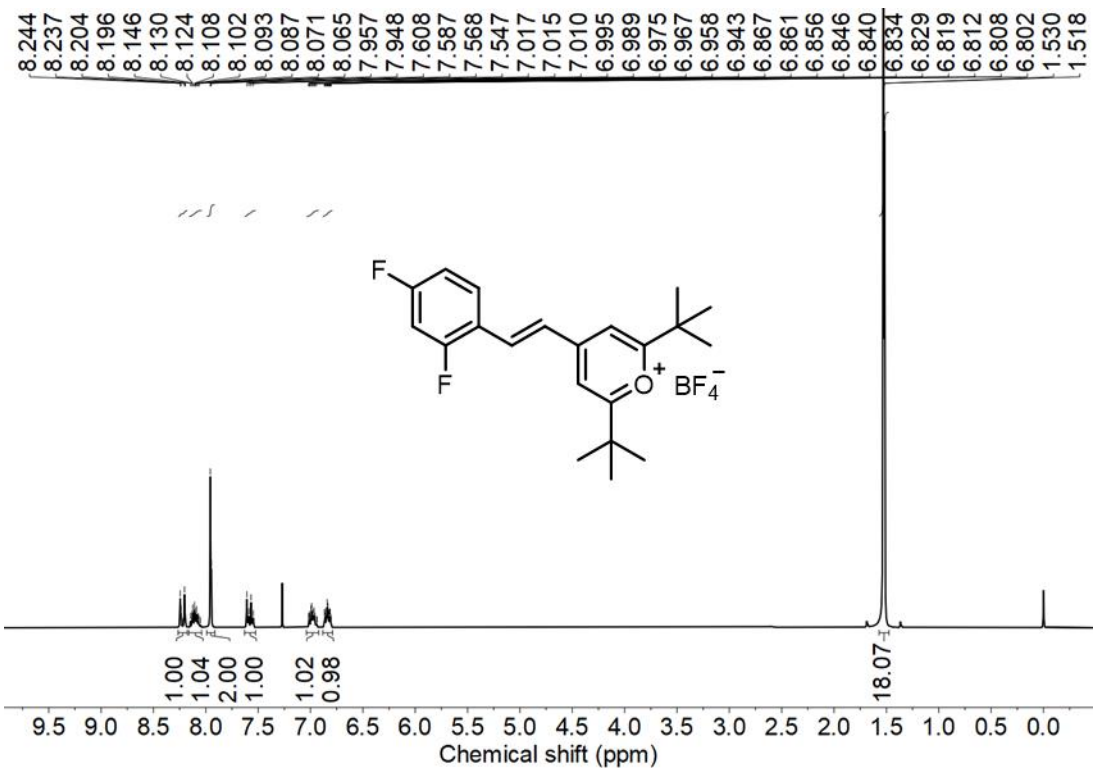

Figure S66. ^{1}H NMR spectrum of **24FSPyL** in $CDCl_3$ (400 MHz).

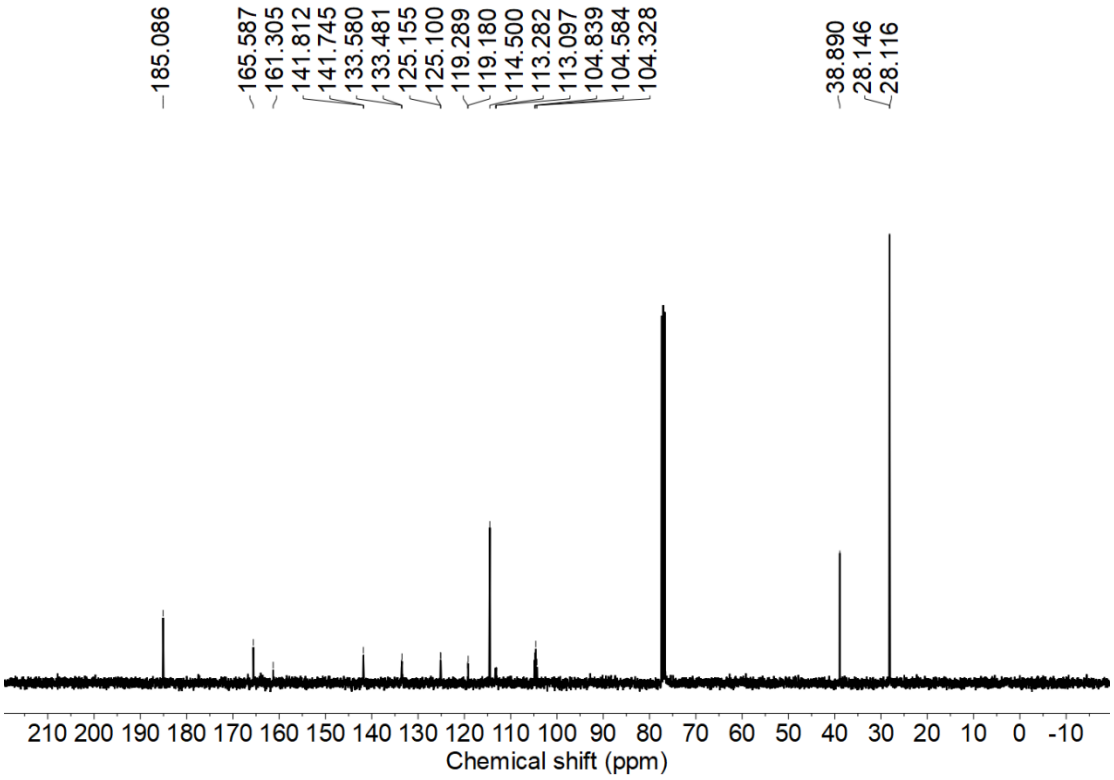

Figure S67. ^{13}C NMR spectrum of **24FSPyL** in $CDCl_3$ (100 MHz).

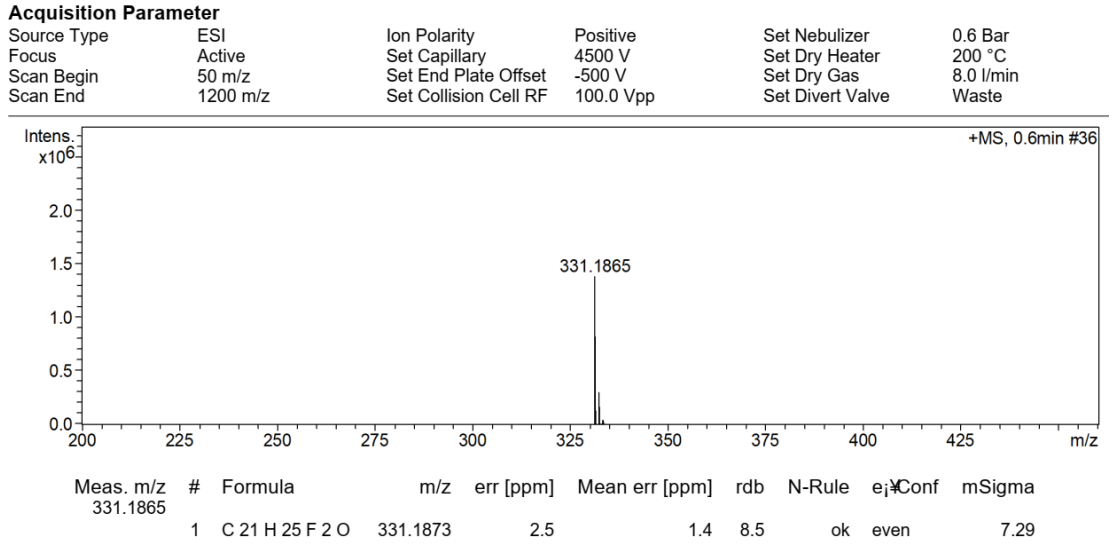

Figure S68. HRMS spectrum of **24FSPyL**.

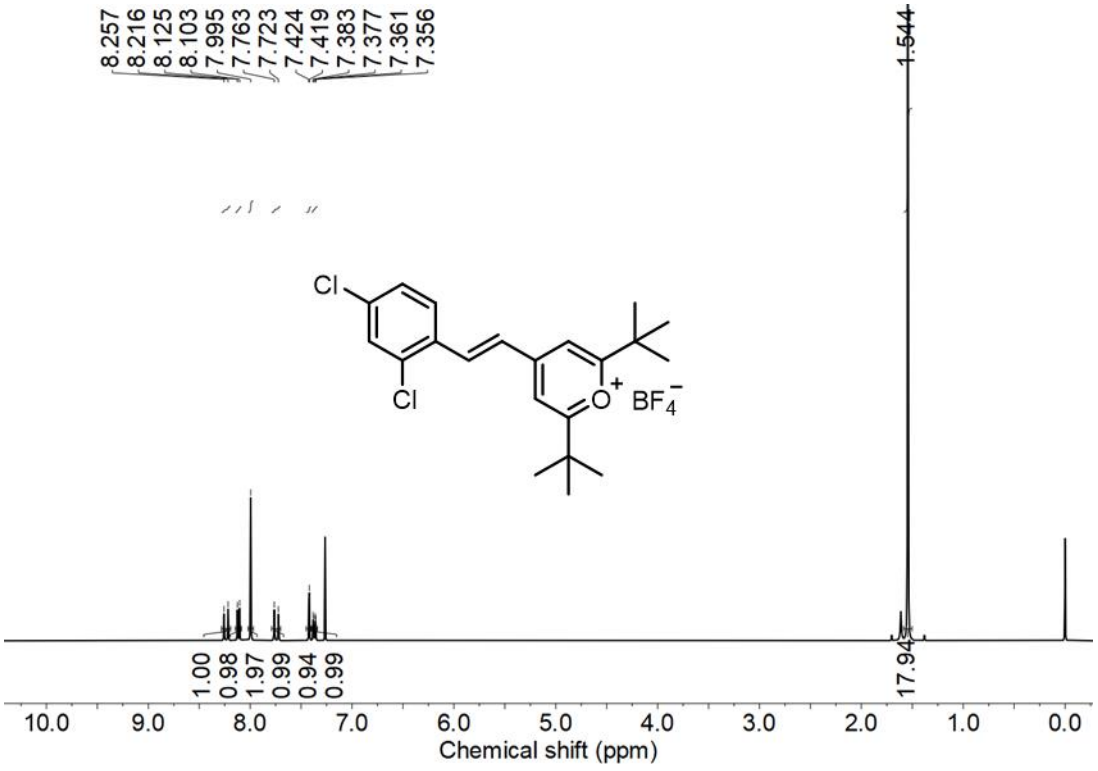

Figure S69. ^{1}H NMR spectrum of **24ClSPyL** in $CDCl_3$ (400 MHz).

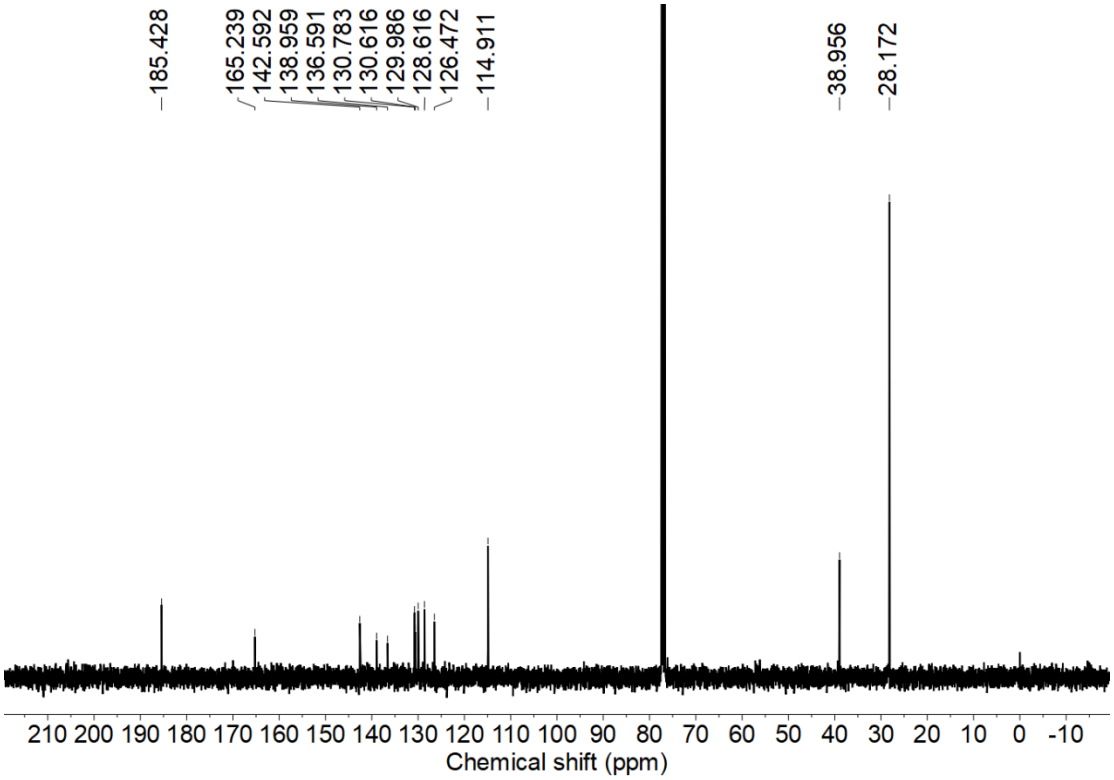

Figure S70. ^{13}C NMR spectrum of **24ClSPyL** in $CDCl_3$ (100 MHz).

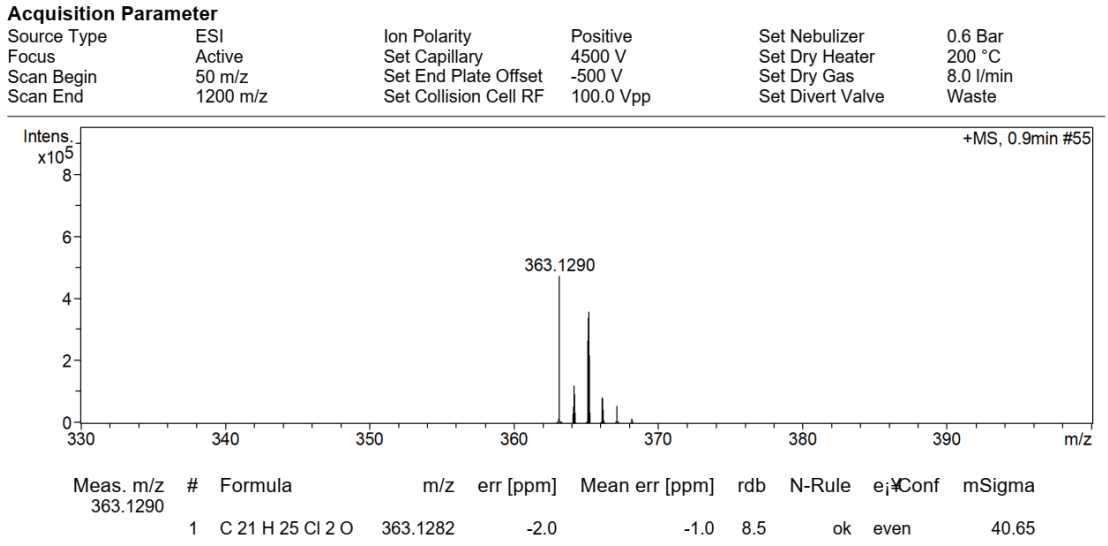

Figure S71. HRMS spectrum of **24ClSPyL**.

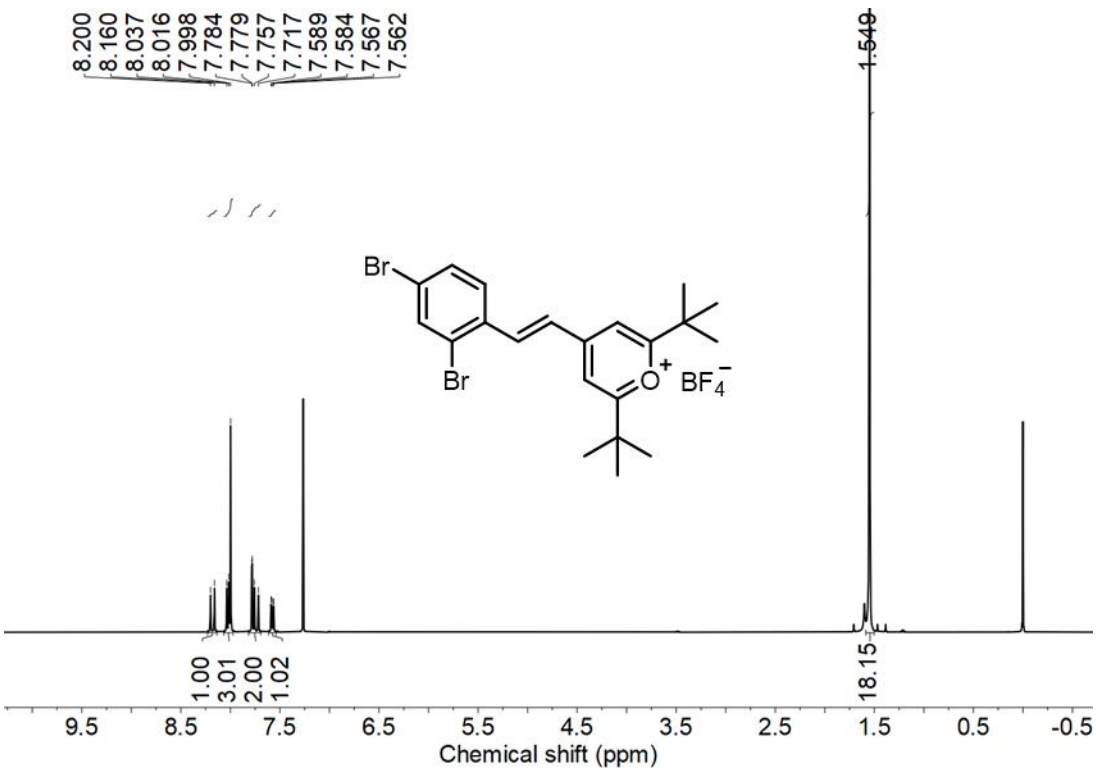

Figure S72. ^{1}H NMR spectrum of **24BrSPyL** in $CDCl_3$ (400 MHz).

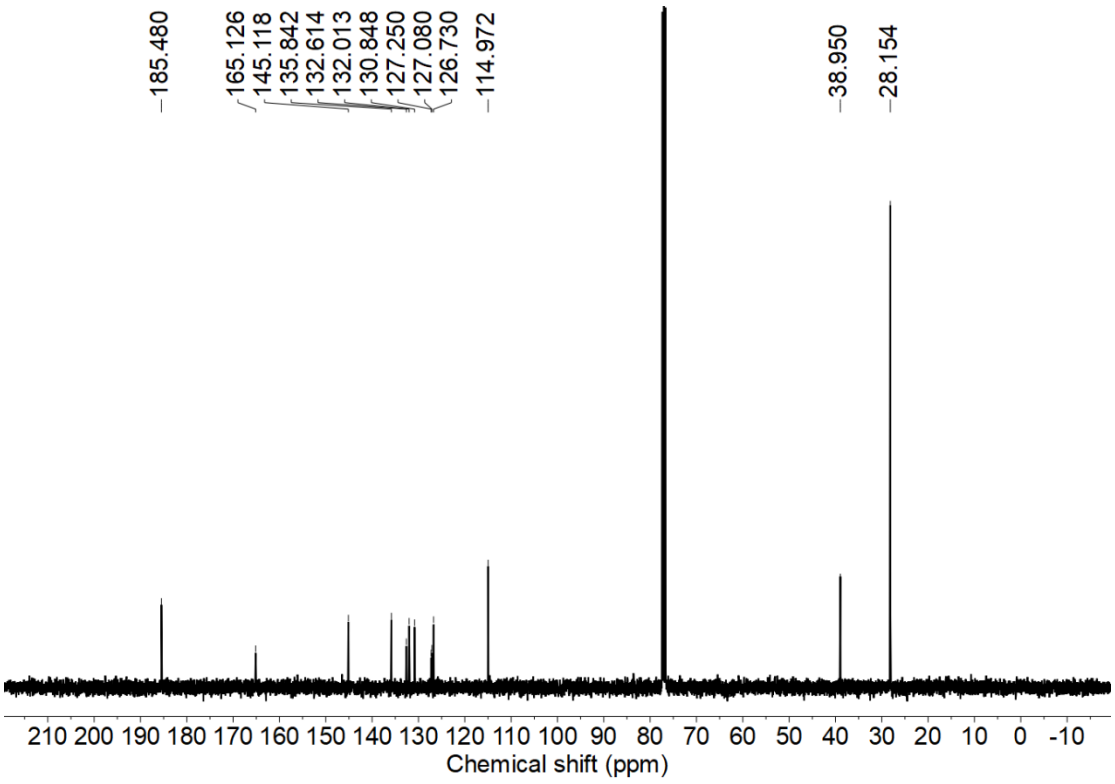

Figure S73. ^{13}C NMR spectrum of **24BrSPyL** in $CDCl_3$ (100 MHz).

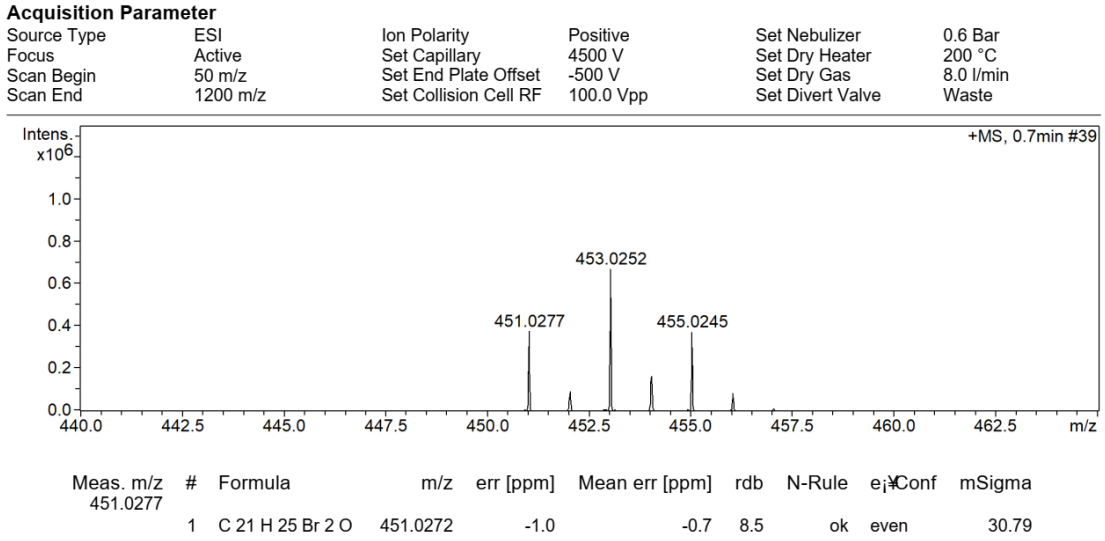

Figure S74. HRMS spectrum of **24BrSPyL**.

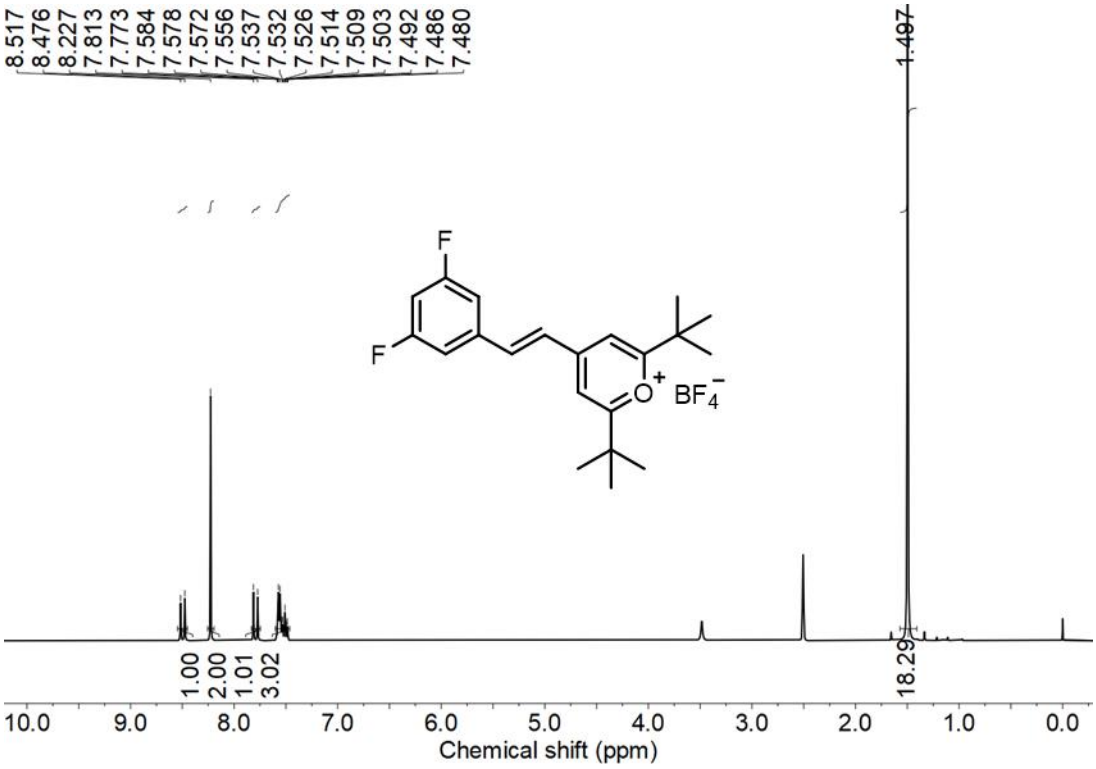

Figure S75. ^{1}H NMR spectrum of **35FSPyL** in DMSO-d_6 (400 MHz).

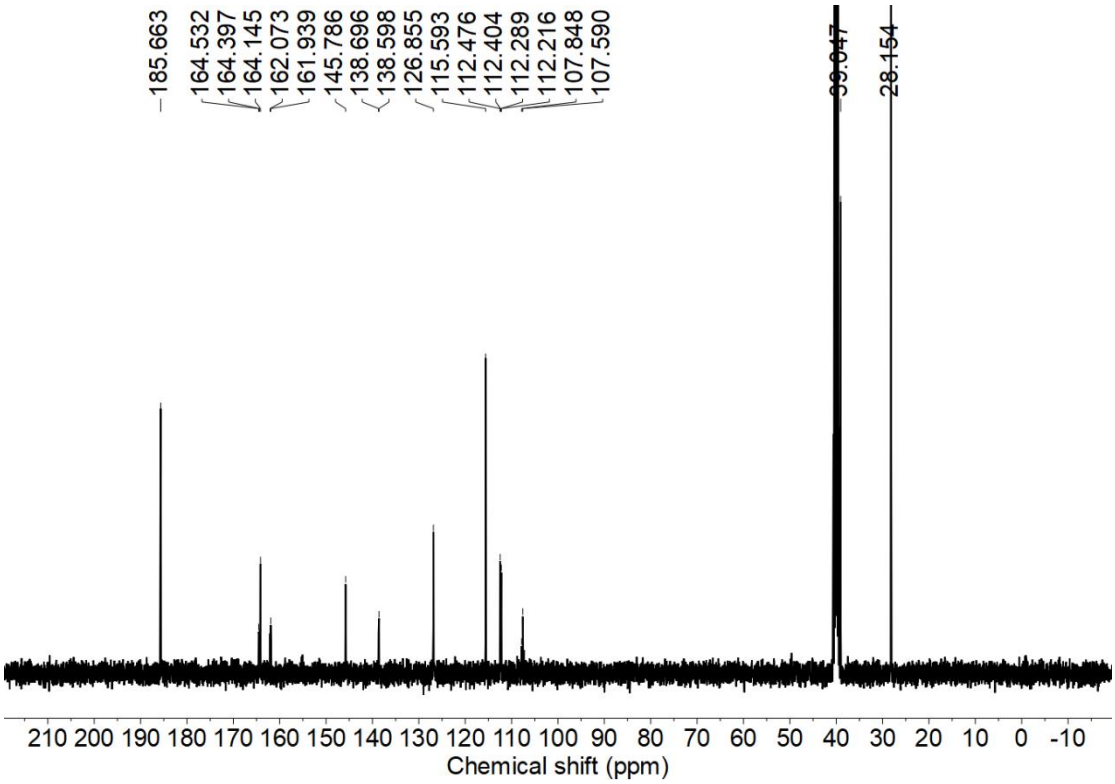

Figure S76. ^{13}C NMR spectrum of **35FSPyL** in DMSO-d_6 (100 MHz).

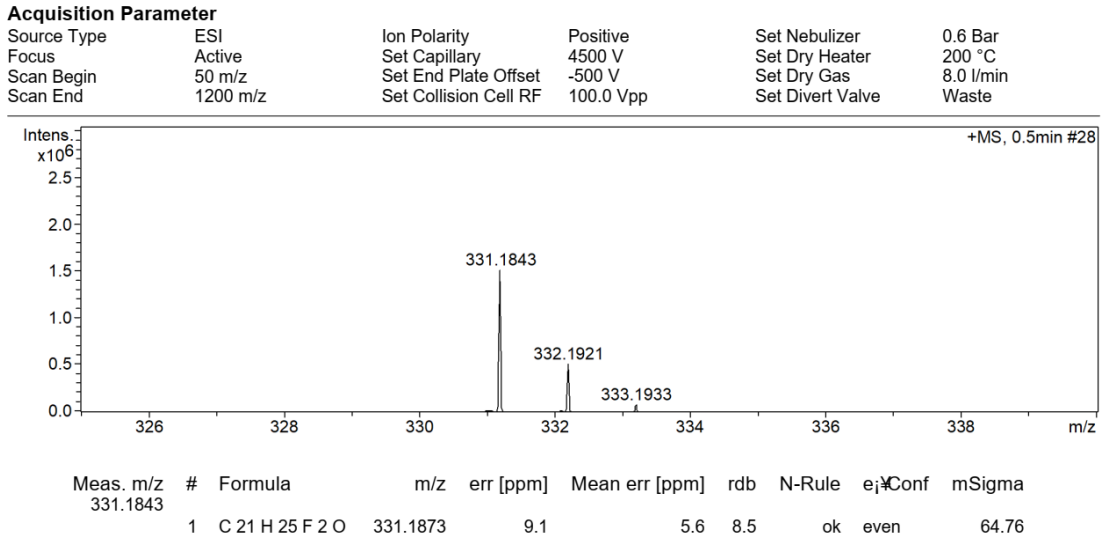

Figure S77. HRMS spectrum of **35FSPyL**.

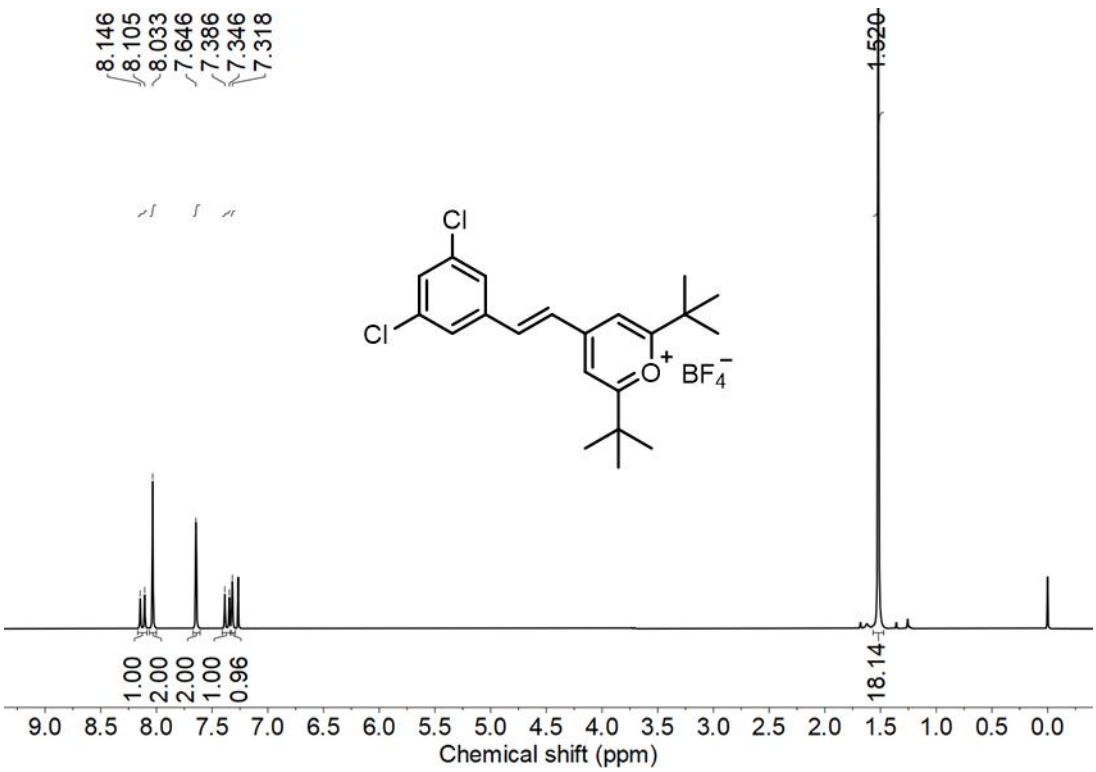

Figure S78. ^{1}H NMR spectrum of **35ClSPyL** in $CDCl_3$ (400 MHz).

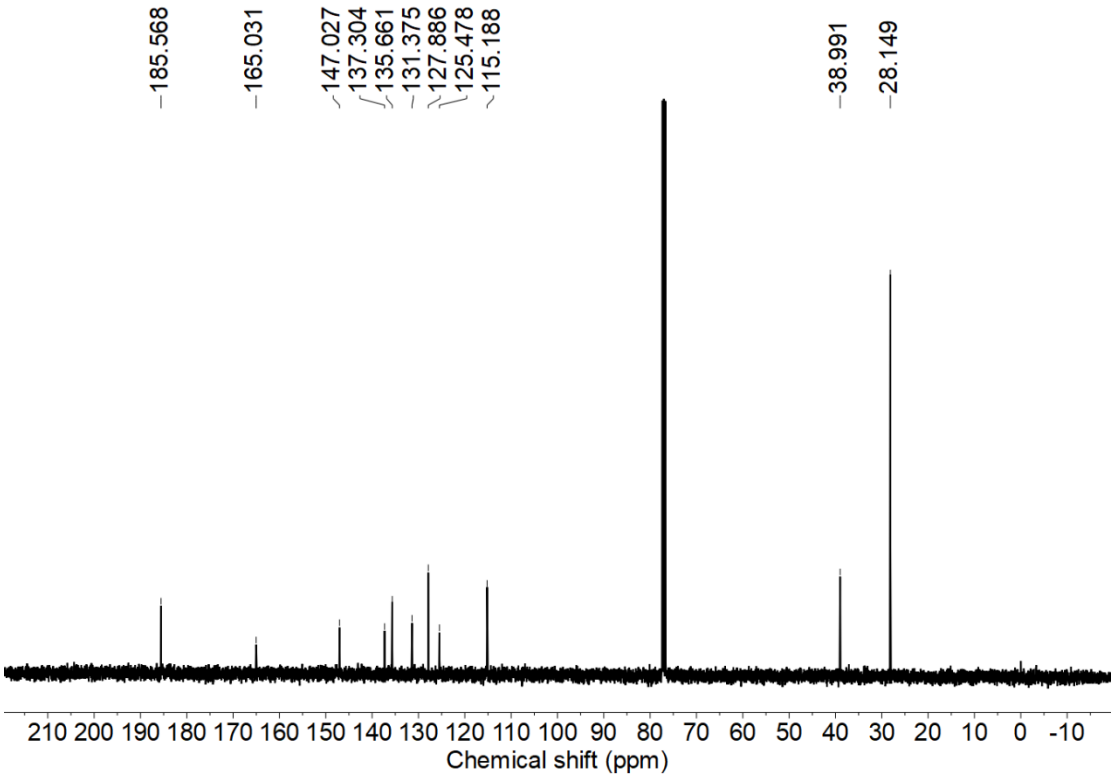

Figure S79. ^{13}C NMR spectrum of **35ClSPyL** in $CDCl_3$ (100 MHz).

Acquisition Parameter

Source Type	ESI	Ion Polarity	Positive	Set Nebulizer	0.6 Bar
Focus	Active	Set Capillary	4500 V	Set Dry Heater	200 °C
Scan Begin	50 m/z	Set End Plate Offset	-500 V	Set Dry Gas	8.0 l/min
Scan End	1200 m/z	Set Collision Cell RF	100.0 Vpp	Set Divert Valve	Waste

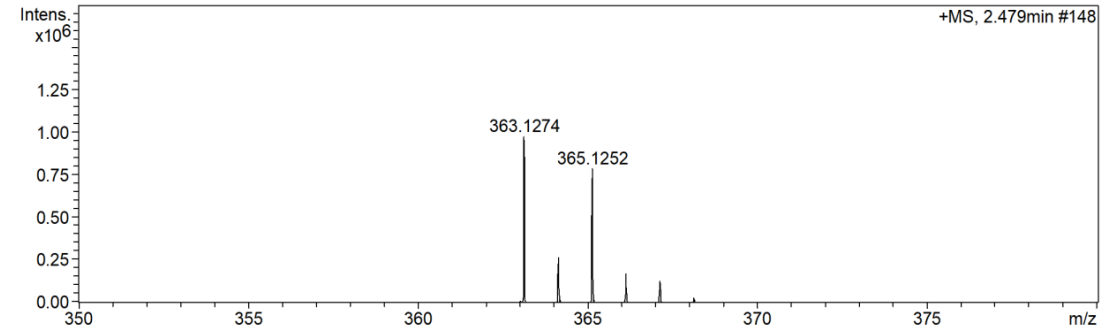

Meas. m/z	#	Formula	m/z	err [ppm]	Mean err [ppm]	rdb	N-Rule	e⁻ Conf	mSigma
363.1274									
	1	C 21 H 25 Cl 2 O	363.1277	0.9	1.0	8.5	ok	even	60.28
	2	C 22 H 20 Cl N 2 O	363.1259	-4.2	-2.7	13.5	ok	even	214.42

Figure S80. HRMS spectrum of **35ClSPyL**.

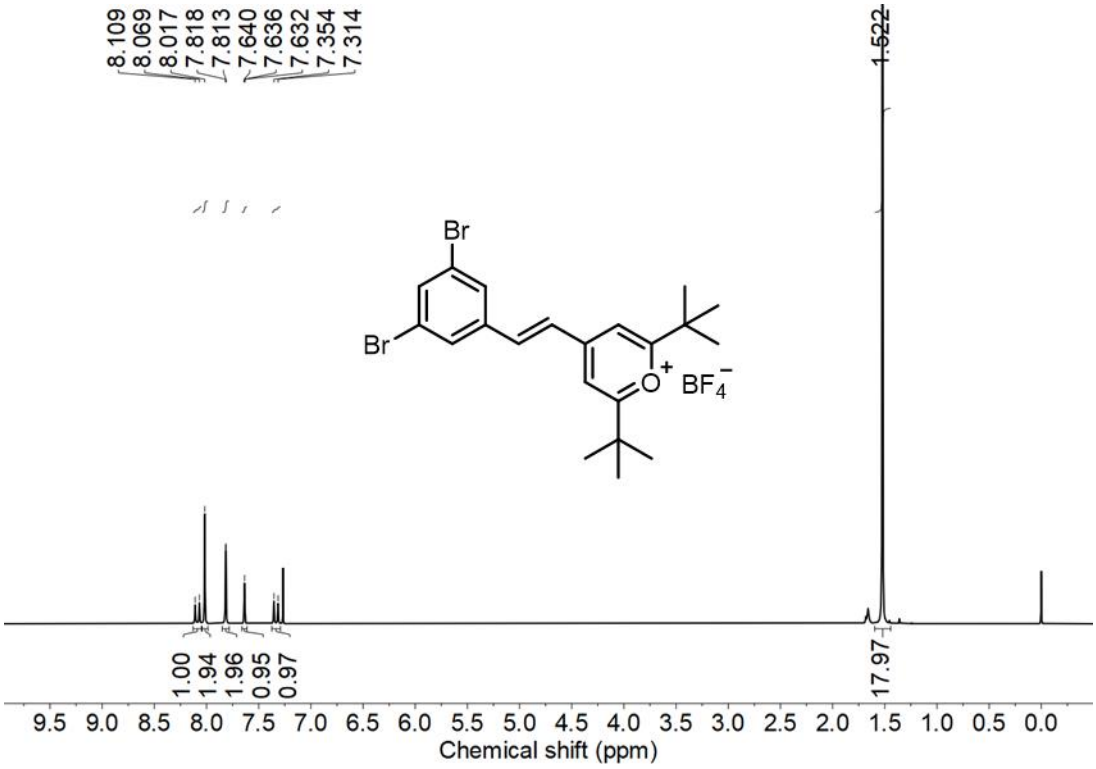

Figure S81. ^{1}H NMR spectrum of **35BrSPyL** in $CDCl_3$ (400 MHz).

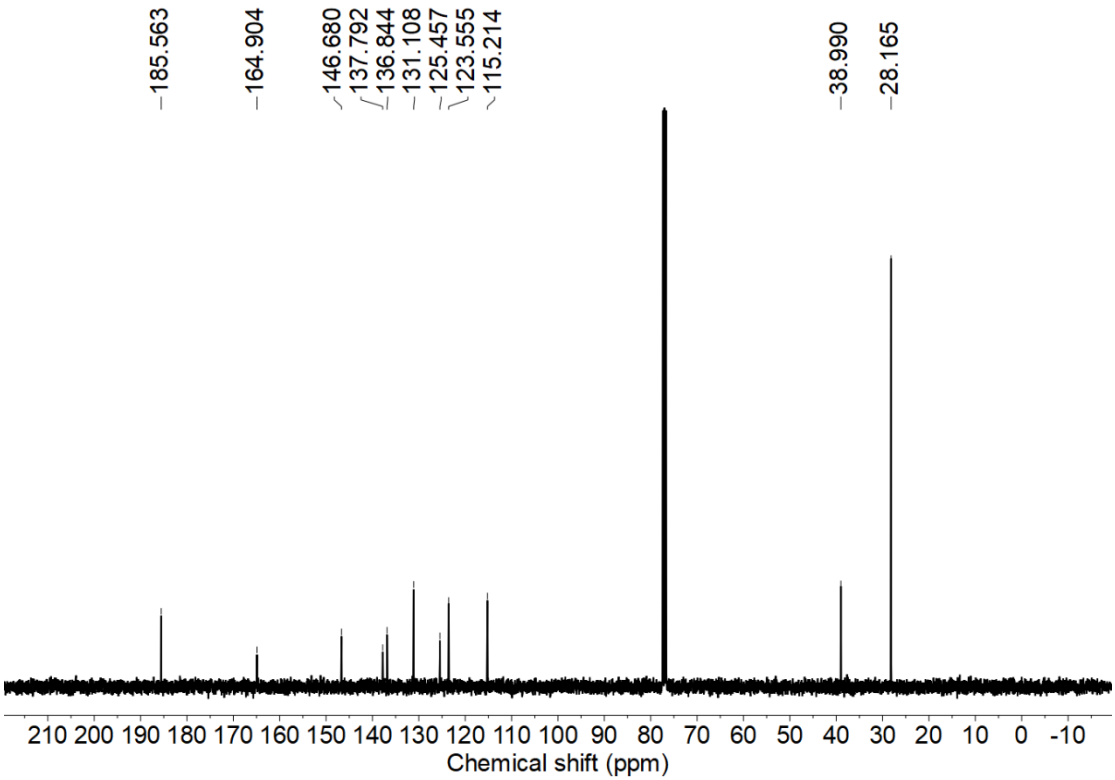

Figure S82. ^{13}C NMR spectrum of **35BrSPyL** in $CDCl_3$ (100 MHz).

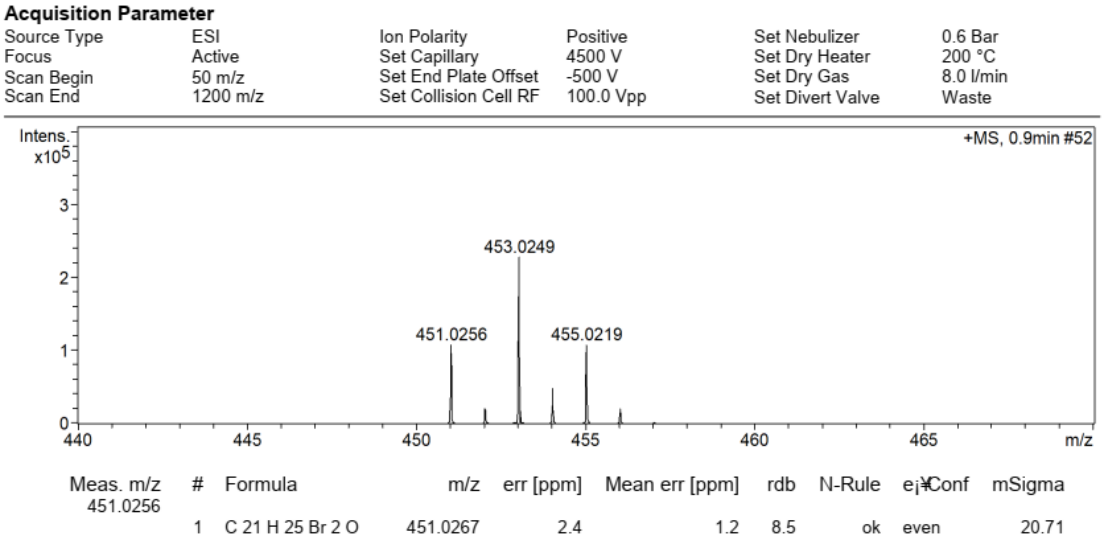

Figure S83. HRMS spectrum of **35BrSPyL**.

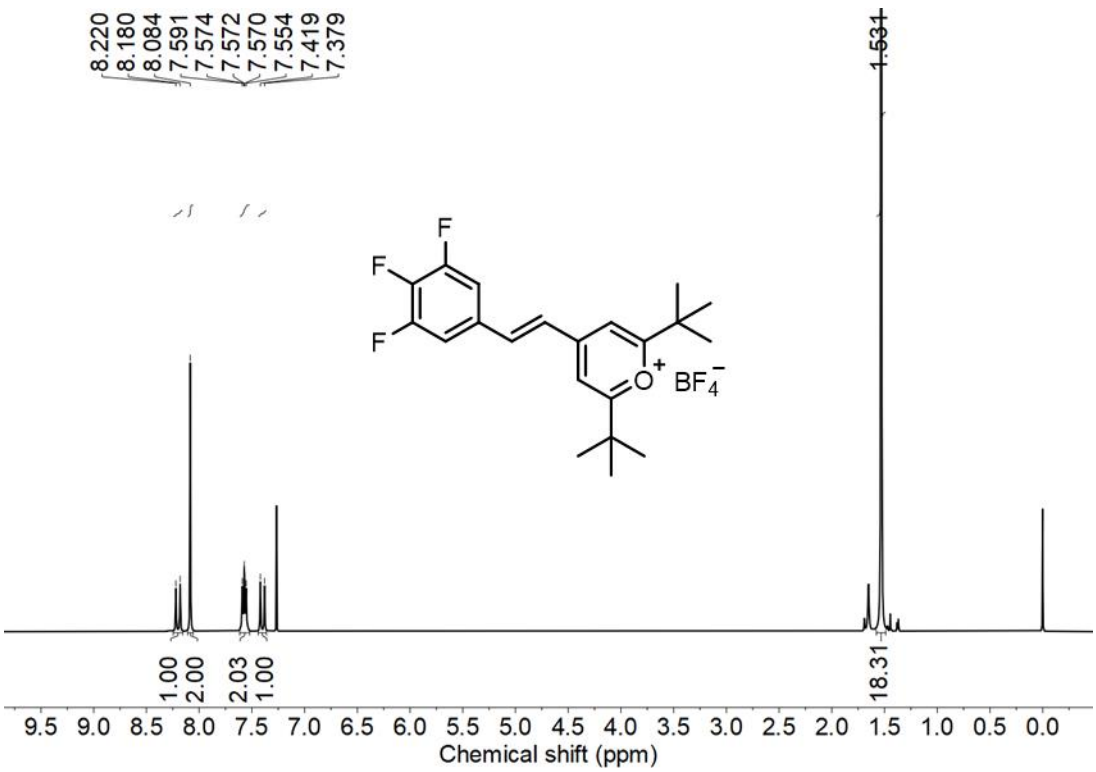

Figure S84. ^{1}H NMR spectrum of **345FSPyL** in $CDCl_3$ (400 MHz).

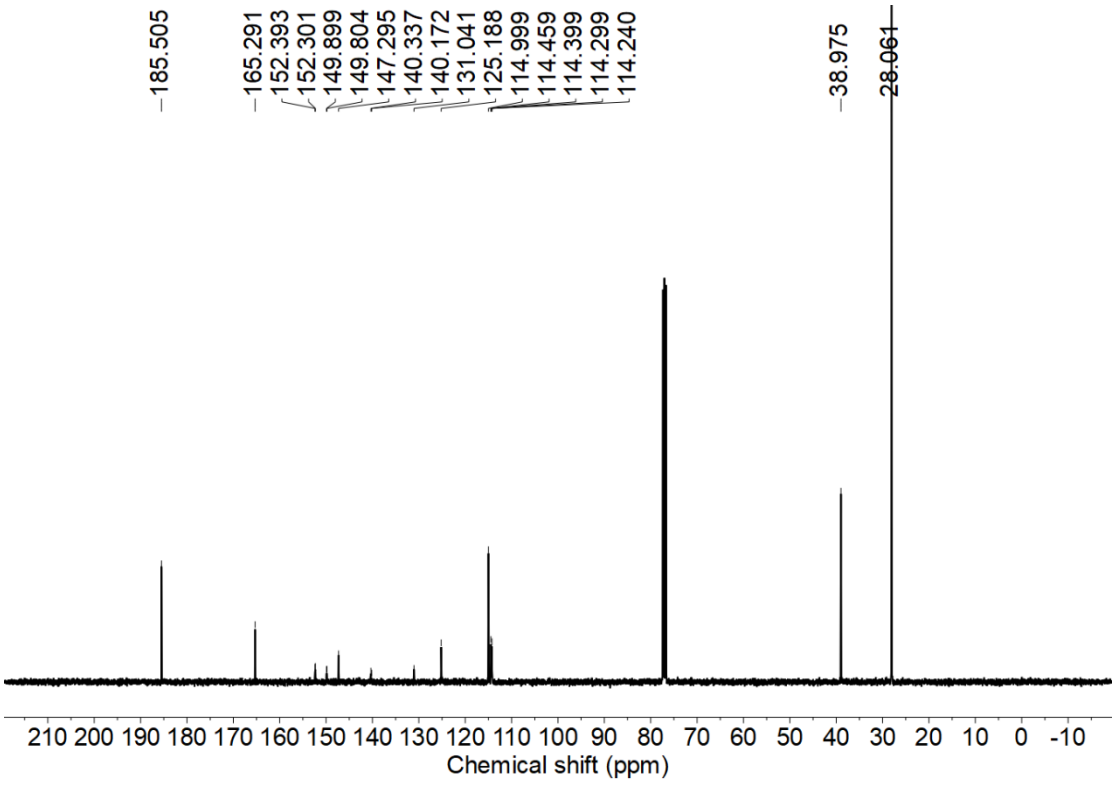

Figure S85. ^{13}C NMR spectrum of **345FSPyL** in $CDCl_3$ (100 MHz).

Acquisition Parameter

Source Type	ESI	Ion Polarity	Positive	Set Nebulizer	0.6 Bar
Focus	Active	Set Capillary	4500 V	Set Dry Heater	200 °C
Scan Begin	50 m/z	Set End Plate Offset	-500 V	Set Dry Gas	8.0 l/min
Scan End	1200 m/z	Set Collision Cell RF	100.0 Vpp	Set Divert Valve	Waste

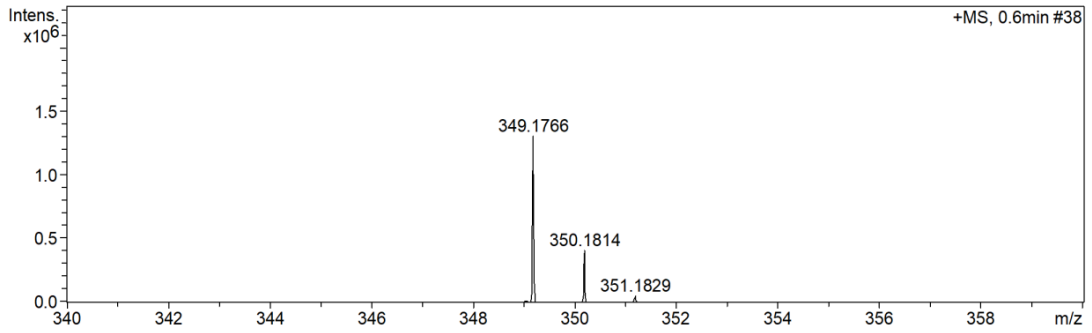

Meas. m/z	#	Formula	m/z	err [ppm]	Mean err [ppm]	rdb	N-Rule	e¡¥Conf	mSigma
349.1766									
	1	C 21 H 24 F 3 O	349.1774	2.3	1.3	8.5	ok	even	50.19

Figure S86. HRMS spectrum of **345FSPyL**.

References

[1] A. T. Balaban, *Org. Prep. Proced. Int.* **1977**, *9*, 125-130.
[2] R. Z. Lange, G. Hofer, T. Weber, A. D. Schlüter, *J. Am. Chem. Soc.* **2017**, *139*, 2053-2059.
[3] G. Sheldrick, *SHELXL-97, Program for the Refinement of Crystal Structures*, University of Göttingen: Göttingen, Germany, **1997**.
[4] J. D. H. Donnay, D. Harker, *Am. Mineral.* **1937**, *22*, 446-467.
[5] P. R. Spackman, M. J. Turner, J. J. McKinnon, S. K. Wolff, D. J. Grimwood, D. Jayatilaka, M. A. Spackman, *J. Appl. Crystallogr.* **2021**, *54*, 1006-1011.